Long-Term Evaluation of Water Transparency in Lake Malawi Using MERIS and Sentinel-3A Data

A Dissertation Submitted to
the Graduate School of Life and Environmental Sciences,
the University of Tsukuba
in Partial Fulfillment of the Requirements
for the Degree of Doctor of Philosophy
(Doctoral Program in Integrative Environment and Biomass Sciences)

Augusto Nunes Brito Vundo

Table of Contents

Abstract

Lake Malawi, with an area of 29,252 km^2, is the 3rd largest lake in Africa and the 9th largest in the world if the Aral Sea is excluded. The lake serves as an important water resource, providing economic, recreational and domestic uses for riparian countries. Lake Malawi has the largest number of indigenous fish species in the world, and thus conservation of the biodiversity in the lake is important. However, given the steady population growth of the riparian countries, and land use conversion from forests to agriculture in the watershed of the lake, water quality in Lake Malawi has been deteriorating. Therefore, routine monitoring of water quality is essential. However, financial and institutional constraints in Africa make for poor availability of in situ water quality data in most African lakes. In addition, in situ monitoring of a large lake such as Lake Malawi has spatial constraints, which makes it difficult to represent the characteristics of water quality across the entire lake. Therefore, the remote sensing technique should be considered as an effective method for providing water quality information on African lakes, especially for monitoring a big lake such as Lake Malawi. Secchi Disk Depth (SD) and chlorophyll-a (Chl-a) concentration are two main water quality parameters, which can be retrieved from remote sensing data.

In this study, Chapter 1 is about the general introduction including the explanation of the significance of the study and the existing methods for water quality parameter studies which can be used in Lake Malawi, followed by a review about previous studies on estimating water quality in Lake Malawi.

In Chapter 2, the performance of the two semi-analytical algorithms Doron11 and Lee15 were first compared, which can estimate SD from satellite data, in Lake Malawi. The results showed that even though the SD estimations from the two algorithms were highly correlated (with R^2 larger than 0.96) using the Medium Resolution Imaging Spectrometer (MERIS), the Lee15 algorithm outperformed the Doron11 in Lake Malawi with high estimation accuracy (RMSE = 1.17 m, MAPE

= 18.7%). It was then evaluated the water transparency in Lake Malawi using the SD values estimated from nine years of MERIS data (2003-2011) and one year of Ocean and Land Colour Instrument (OLCI) data 2017 with the Lee15 algorithm. Results showed that Lake Malawi maintained four water transparency levels throughout the study period (i.e., level 1: SD > 12 m; level 2: SD between 6-12 m; level 3: SD between 3-6 m; level 4: SD between 1.5-3 m). Level 1 and 2 water areas tended to shift or trade places depending on year or season. In contrast, level 3 and 4 water areas were relatively stable and constantly distributed along the southwestern and southern lakeshores. In general, Lake Malawi is dominated by waters with SD values larger than 6 m (more than 95% lake area). The transparency level was characterized by a gradient increase from the lakeshore to the pelagic zone.

In Chapter 3, first Chl-a from MERIS and OLCI data was estimated by using NASA's OC4E algorithm. And then Carlson's trophic state index (TSI) was modified to Lake Malawi by combining OC4E derived-Chl-a and Lee15 derived-SD to estimate the trophic levels of Lake Malawi. The results from the modified TSI show that Lake Malawi is still in the oligotrophic state, with a mean TSI value of 31 for both TSI derived from SD and from Chl-a throughout the study period. However, mesotrophic (with TSI values between 43-45), eutrophic (with TSI values between 56-59), and hypereutrophic (with TSI values between 76-87) waters were also found along the lake shore. Deviations between the TSI (Chl-a) and TSI (SD) demonstrated that light attenuation in Lake Malawi was dominated by algae especially in oligotrophic and mesotrophic waters TSI (Chl-a) ≈ TSI (SD). In contrast, the light attenuation in the eutrophic and hypereutrophic waters was mainly dominated by non-algae particles with TSI (Chl-a) < TSI (SD).

Finally, in Chapter 4 the general conclusions are made, and the limitations of the study are pointed out with indications of future studies.

List of Tables

List of Figures

List of Abbreviations

AMD	=	Absolute Mean Difference
AOP	=	Apparent Optical Property
ASTER	=	Advanced Spaceborne Thermal Emission and Reflection Radiometer
CDOM	=	Colored Dissolved Organic Matter
Chl-a	=	Chlorophyll-a
CI	=	Color Index
CMODIS	=	Chinese Moderate Resolution Imaging Spectrometer
C2R	=	Case-2 Regional
CZCS	=	Coastal Zone Color Scanner
ESA	=	European Space Agency
FR	=	Full Resolution
GDEM	=	Global Digital Elevation Model
IOCCG	=	International Ocean Colour Coordinating Group
IOP	=	Inherent Optical Property
MAPE	=	Mean Absolute Percent Error
MERIS	=	Medium Resolution Imaging Spectrometer
METI	=	Ministry of Economy, Trade, and Industry of Japan
MODIS	=	Moderate Resolution Imaging Spectroradiometer
NASA	=	National Aeronautics and Space Administration
OC4	=	Ocean Chlorophyll Four-band
OECD	=	Organization for Economic Cooperation and Development
OLCI	=	Ocean and Land Color Instrument
QAA	=	Quasi-Analytical Algorithm

RMD	=	Relative Mean Difference
RMSE	=	Root Mean Square Error
RR	=	Reduced Resolution
SD	=	Secchi Disk Depth
SeaWiFS	=	Sea-viewing Wide Field-of-view Sensor
SNAP	=	Sentinel Application Platform
TOA	=	Top of Atmosphere
TP	=	Total Phosphorus
TSI	=	Trophic State Index
TSM	=	Total Suspended Matter

Chapter 1 General Introduction

1.1. Significance of water quality studies in Lake Malawi

Lake Malawi, with an area of 29,252 km^2, is the 3rd largest lake in Africa and the 9th largest in the world if the Aral Sea is excluded (Lehner and Döll, 2004). The lake serves as an important water resource, providing economic, recreational and domestic uses for riparian countries (Bootsma and Hecky, 1993). In addition, the lake has the largest number of indigenous fish species in the world, and thus conservation of the biodiversity in the lake is important (Snoeks, 2000). However, given the steady population growth in the riparian countries, and land use conversion from forests to agriculture in the watershed, water quality in Lake Malawi has been deteriorating (Hecky et al., 2003; Chavula et al., 2009). Therefore, routine monitoring of water quality is essential. Worldwide, with the population increase, there is more and more pressure on the few available freshwater resources, resulting in poor management systems, pollution, excessive water withdrawal and other significant environmental problems (Haddeland et al., 2014). However, the process of water quality monitoring involves several aspects, from financial, institutional, technical and meteorological which are directly or indirectly linked to the existing water quality monitoring techniques.

1.2. Review on methods for water quality studies

Generally, two main techniques are used for monitoring water quality: (1) field survey by a boat; and (2) application of remote sensing data. Nevertheless, if field survey by boat is used as the main technique for regular monitoring, financial and institutional constraints in Africa make for poor availability of in situ water quality data in most African lakes (Ballatore et al., 2014). In

addition, in situ monitoring of a large lake such as Lake Malawi has spatial limitations, which makes it difficult to represent the characteristics of water quality across the entire lake. Therefore, the remote sensing technique should be considered as an effective method for providing water quality information on African lakes, especially for monitoring a big lake such as Lake Malawi (Dube et al., 2015; Ballatore et al., 2014). Remote sensing can be used as a complementary part of the field survey by boat as it offers synoptic, repetitive, consistent, cost-effective and comprehensive spatiotemporal views (Dube et al., 2015; Ballatore et al., 2014), especially in big lakes like Lake Malawi where the budget for field survey becomes a big obstacle for the adjacent developing countries.

Notwithstanding its spatial limitation, field survey by boat does have its merits. It can enable the measurement and evaluation of several parameters, and their vertical profile at several depths. On the contrary, it can be time-consuming, needs a lot of effort and work, and it is expensive in general. A major disadvantage of a field survey by boat is that it is time and space specific, considering that the water quality can change both spatially and temporally (Kiefer et al., 2015). Remote sensing shows more merits than demerits when compared to field survey by boat, for water quality studies in big lakes. But this does not mean that the field survey by boat should be replaced, discarded or put in the second plan. Although the importance of in situ measurement (field survey by boat) is recognized and emphasized, it is equally important to explore the potentiality of remote sensing as an effective method for monitoring water quality and its spatiotemporal changes (Kiefer et al., 2015; Chen et al., 2004). But remote sensing on its own cannot estimate and validate the same results, thus the need for the complementary part of a field survey by boat for ground truthing. It has been confirmed that the lack of in situ water measurements to validate remotely sensed water quality estimates is a major challenge in Sub-Saharan Africa (Ballatore et al., 2014).

There are two requirements for monitoring water quality by the remote sensing technique. First, a satellite sensor with ocean bands is desired. These include, for example, the Sea-viewing

Wide Field-of-view Sensor (SeaWiFS) and Moderate Resolution Imaging Spectroradiometer (MODIS) from the National Aeronautics and Space Administration (NASA), and the MEdium Resolution Imaging Spectrometer (MERIS) from the European Space Agency (ESA), refer to the International Ocean-Colour Coordinating Group (IOCCG). Compared to sensors for land applications, the ocean color sensors can provide remote sensing reflectance (R_{rs}) data with better temporal and spectral resolution, as well as higher radiative sensitivity, all of which are necessary for monitoring water quality (Mouw et al., 2015).

Second, an algorithm is needed for estimating water quality parameters from the R_{rs}. The algorithm can be either empirical or semi-analytical. Although empirical algorithms are easy to implement, in situ data for recalibration is always necessary, which limits their applicability to different lakes, especially those without available in situ data. In contrast, semi-analytical algorithms are based on a radiative transfer theory (or bio-optical model) with several secondary important empirical relationships under some assumptions, and thus do not require recalibration (Lee et al., 2002, 2015). In cases where there is a lack of enough in situ data such as in Lake Malawi, the application of a semi-analytical algorithm is the most practical and viable method for estimating water quality parameters.

Just the remote sensing data and the semi-analytical algorithm are not enough for water quality monitoring, the water quality parameter to be estimated needs to be defined as well, but unfortunately, only a certain number of water quality parameters can be estimated from remote sensing. The main water quality parameters that can be estimated from remote sensing data using the semi-analytical algorithms are Chlorophyll-a (Chl-a, Gitelson et al., 2008; Gilerson et al., 2010; Yang et al., 2011), Total Suspended Matter (TSM; Nechad et al., 2010), Colored Dissolved Organic Matter (CDOM, Yang et al., 2011), and Secchi Disk Depth (SD, Doron et al., 2011; Lee et al., 2015). As the SD estimation is based on an underwater visibility theory, and the SD value itself is an apparent optical property (AOP) of a water body just like R_{rs}, the relationship between SD and R_{rs} values can be considered more robust than those between other water quality

parameters and R_{rs} values. In addition, the SD value is easy to measure and like Chl-a, can be understood by the general public. Thus, SD has been widely used as an indicator for evaluating water quality (transparency or clarity) since the 1860s (Secchi, 1864) as well as one of the important parameters like Chl-a for calculating trophic state index (TSI), using Carlson's model (Carlson, 1977).

The currently standardized method to determine the water clarity has its history back to the nineteenth century and was coined after Pietro Angelo Secchi, published in 1865 (Wernand, 2010). This method is based on lowering a 30 centimeters black and white disk in a water body until it can no longer be seen.

There are two main semi-analytical algorithms for estimating SD values from remote sensing data. The first developed by Doron et al. (2011) is based on a classic underwater visibility theory that has been used for over 60 years (Duntley, 1952; hereafter referred to as 'Doron11'). The second semi-analytical algorithm was developed by Lee et al. (2015), based on a new underwater visibility theory proposed by the same authors in the same study (hereafter, 'Lee15'). Although Lee et al. (2015) pointed out some shortcomings in the classic theory, and later Lee et al. (2018) compared directly the relationship of Doron11 and Lee15 using a simulated dataset, and the results showed a coefficient of determination equal to 0.89 between the two estimates. However, the two algorithms have not been applied in practice to the same water body and compared to a common in situ measured SD values. Therefore, it was considered that there was not yet enough evidence to show which algorithm should be selected and applied in Lake Malawi for monitoring programs and government planning.

Several studies have explored the application of satellite data for retrieving SD in lakes (Alikas and Kratzer, 2017; Lee et al., 2015, 2016; Kratzer et al., 2008). MERIS has a good spatiotemporal, radiometric and spectral resolution (Matthews et al., 2010; Fukushima et al., 2016; Kiefer et al., 2015) for water quality monitoring including SD. The inclusion of satellite remote sensing products for monitoring water quality would substantially increase the

description of spatial, seasonal and long-term changes (Alikas and Kratzer, 2017).

As mentioned earlier, satellite data can also be used to estimate Chl-a concentration and provides spatial distribution. Hu et al. (2012) proposed an algorithm to estimate surface Chl-a concentration in global water for Chl-a $\leq$ 0.25 mg/m^3. The algorithm was based on a color index (CI), defined as the difference between R_{rs} in the green and a reference formed linearly between R_{rs} in the blue and red. O'Reilly et al. (1998) proposed an Ocean Chlorophyll Four-band (OC4 - 443, 490, 510, 555 nm) maximum ratio formulation algorithm, for Chl-a range between 0.019 and 32.79 mg/m^3. Although several Chl-a concentration algorithms have been developed, (Gitelson et al., 2011; Yang et al., 2011) within the OC4 series the OC4E (E denotes the code for MERIS sensor) NASA's MERIS standard Chl-a retrieval algorithm (https://oceancolor.gsfc.nasa.gov/atbd/chlor_a/) was applied to Lake Malawi.

Moreover, the results from both SD and Chl-a were further used for the estimation of the TSI which is an index that allows the identification of problems and pressure that a water body ecosystem faces (Cunha et al., 2013) and helps in the preparation for corrective actions. In Lake Malawi in particular, an objective and descriptive evaluation of its TSI is necessary.

Regardless of the existence of several classification models (Nawrocka and Kobos, 2011) no model is standardized to be applied in specific water bodies. Carlson (1977) developed a numerical and multiparameter TSI based on Chl-a, SD and Total Phosphorus (TP) which can independently estimate algal biomass. One of the biggest advantages of this index resides in the correlation of these parameters which allows the comparison of the different trophic levels from different lakes (Carlson, 1977) but Chl-a derived TSI is recommended for TSI evaluation. This versatile characteristic allows its application, combined or independently and helps in cases where only one water quality parameter is available. Consequently, the Carlson's TSI model was modified and applied to Lake Malawi as suggested by previous studies (Cunha et al., 2013; Salas and Martino, 1991; Cheng and Lei, 2001) and the deviations of the TSI were evaluated to assess the effects of different components in light attenuation in the water column.

1.3. Previous Studies on Estimating Water Quality in Lake Malawi

Only a small number of studies are available on water quality in Lake Malawi in general, and the existing ones focus on other aspects than water quality (Thompson et al., 1996; Schulthei et al., 2011; Weyl et al., 2010). Some studies have focused on the lake's water quality (Bootsma et al., 2003; Macuiane et al., 2016). However, none of these has experienced the application of remote sensing data for water quality estimation in Lake Malawi. The existing two extensive reviews about the application of remote sensing to African and Sub-Saharan African lakes showed that only a small number of studies related to remote sensing of water quality in African lakes are available (Ballatore et al., 2014; Dube et al., 2015) and none of them investigated SD spatiotemporal variability nor the TSI. Regardless of the few studies on water quality by using remote sensing, two studies for water quality monitoring have been conducted in Lake Malawi (Chavula et al., 2009; Odermatt et al., 2018) using remote sensing. The first study used AQUA/MODIS and TERRA/MODIS and in situ data to create an empirical algorithm to estimate Chl-a. The result showed a moderate relationship between in situ Chl-a concentration and values obtained from satellite imagery. They concluded that the results had potential application in monitoring the trophic state of Lake Malawi**.** The second study, using MERIS data from (2002-2012) produced a database of several water quality parameters from 340 lakes worldwide including Lake Malawi, and the final result was several monthly, yearly and 9-year average water quality parameters (Chl-a, total suspended matter, turbidity, colored dissolved organic matter, lake surface water temperature, cyanobacteria and floating vegetation maps), and the matchups were obtained from 24 lakes and reservoirs in a wide range (Odermatt et al., 2018).

In addition, a literature review was carried out on November 4th 2018 to investigate the number of studies done over Lake Malawi waters aiming at monitoring water quality. Table 1

shows a summary of the number of studies carried out in Lake Malawi, Lake Tanganyika, and Lake Victoria. The search was done based on the Web of Science Core Collection (1900-present) provided by Thomson Reuters. However, only a certain number of combinations is presented in Table 1. The number in parenthesis represents the search result for each combination of keywords.

Table 1. Available studies over Lake Malawi, Lake Tanganyika, and Lake Victoria.

Available Studies		
Lake Malawi	**Lake Tanganyika**	**Lake Victoria**
Word combination		
Lake Malawi (1,478)	Lake Tanganyika (1,621)	Lake Victoria (3,481)
Lake Malawi Reviews (70)	Lake Tanganyika Reviews (66)	Lake Victoria Reviews (168)
Lake Malawi Water Quality (28)	Lake Tanganyika Water Quality (41)	Lake Victoria Water Quality (197)
Lake Malawi Transparency (3)	Lake Tanganyika Transparency (12)	Lake Victoria Transparency (28)
Lake Malawi Secchi Disk Depth (0)	Lake Tanganyika Secchi Disk Depth (0)	Lake Victoria Secchi Disk Depth (2)
Lake Malawi SDD (0)	Lake Tanganyika SDD (0)	Lake Victoria SDD (1)
Lake Malawi Remote Sensing (11)	Lake Tanganyika Remote Sensing (14)	Lake Victoria Remote Sensing (53)
Lake Malawi Clarity (1)	Lake Tanganyika Clarity (3)	Lake Victoria Clarity (6)

Despite the numbers presented above, in Lake Malawi for example, only 3 studies were directly related to Lake Malawi remote sensing, and 1 for Lake Malawi transparency. The list of the search results does not really reflect the number of studies directly linked to the input word combination. It can be misleading if there is no deeper evaluation of the content listed in the search results.

From the information above and the two previous reviews, it was confirmed that Lake Malawi lacks applicability of remotely sensed data over its waters for water quality monitoring (SD and TSI). Previous studies have documented scientific research about Lake Malawi focusing on several topics including fisheries (Bootsma et al., 2003; Otu et al., 2011; Hamblin et al., 2003; Thompson et al., 1996; Munthali, 1997; Schulthei et al., 2011; McCullough et al., 2007; Weyl et al., 2010; Guildford and Hecky, 2000). However, all the above-mentioned studies are based on the field survey. Thus, three conclusions were drawn:

(i) There are very few studies applying remote sensing to estimate water quality from African lakes.

(ii) Only two studies have applied remote sensing to estimate water quality from Lake Malawi.

(iii) No study is available for estimating SD and TSI using Remote Sensing in Lake Malawi.

In consideration of the above, and the fact that few studies have comprehensively evaluated water quality in Lake Malawi (Chavula et al., 2009; Odermatt et al., 2018) using remote sensing the research objectives of the present study were defined.

1.4. Research objectives of this study

(1) To comprehensively compare the performance of the two semi-analytical algorithms (Doron11 and Lee15) in Lake Malawi;

(2) To obtain an overall evaluation of water transparency in Lake Malawi from MERIS and OLCI data;

(3) To estimate and assess the trophic state of Lake Malawi from MERIS and OLCI data.

Chapter 2 An overall evaluation of water transparency in Lake Malawi from MERIS and OLCI Data

2.1. Study Area: Lake Malawi/Niassa/Nyasa

Lake Malawi (09º 30'-14º 40' S, 33º 50' - 33º 36' E) is the southernmost lake in the Great Rift Valley, surrounded by Malawi, Mozambique, and Tanzania (Fig. 1). While the lake is also known as Niassa in Mozambique and Nyasa in Tanzania, internationally and scientifically it is known as Lake Malawi. It is about 560-km long and has a maximum width of about 75-87 km, an average depth of 292 m, and a maximum depth of 706 m. There are three seasons in the area surrounding the lake, determined by rainfall and temperature. They are the cool dry season (May-August), hot dry season (September-October), and warm wet season (November-April), with 95% of precipitation falling during the latter period (Fig. 2, Weyl et al., 2010). The majority of the lake's catchment is in Malawi, where the population has doubled in the past 25 years, with a 2.8% yearly increase over the last 10 years for a current total population of about 19 million. Most of the population relies directly on subsistence agriculture and fish for food, and the high population density is resulting in the expansion of subsistence agriculture to marginal land, including wetlands and steep hill slopes (Bootsma and Jorgensen, 2004). About 7% of the catchment area is within Mozambique, while approximately 25% lies within Tanzania; the remainder is in Malawi. Most of the rain falls along the lake's shore, which is dominated by flat land contrary to other regions of the basin. All three adjacent countries are developing, and subsistence agriculture is still vital to most of the population.

Figure 1 below shows the geographical location of the lake in Africa (a) and its basin including the neighboring countries (b). All three adjacent countries are developing, and

subsistence agriculture is still a core to most of the population. Rainfall and temperature generally have the same pattern. The data from Figure 2 was obtained from the World Bank Climate Portal on country historical [1] data referent to the monthly average rainfall and temperature for Malawi from 1991-2015.

Table 2 shows the basic physical characteristics of Lake Malawi, including its main inflow complemented by the data from Figure 1b. The lake has one outflow, the Shire River at its most south part (Fig. 1b).

Table 2. Physical characteristics of Lake Malawi.

Basic Characteristics	Value
Area	29,600 km^2 – 30,800 km^2
Depth	Max 704 – 785 m, average 290 – 426 m
Length	Max 505/ 603 km
Width	Max 87 km; average 50 – 60 km
Shoreline length	1500 km
Major inflow rivers	13
Outflow river	1
Residence time	140 years
Secchi depth (m)	12 - 20 m

Source: modified from Weyl et al. (2010)

1 http://sdwebx.worldbank.org/climateportal/

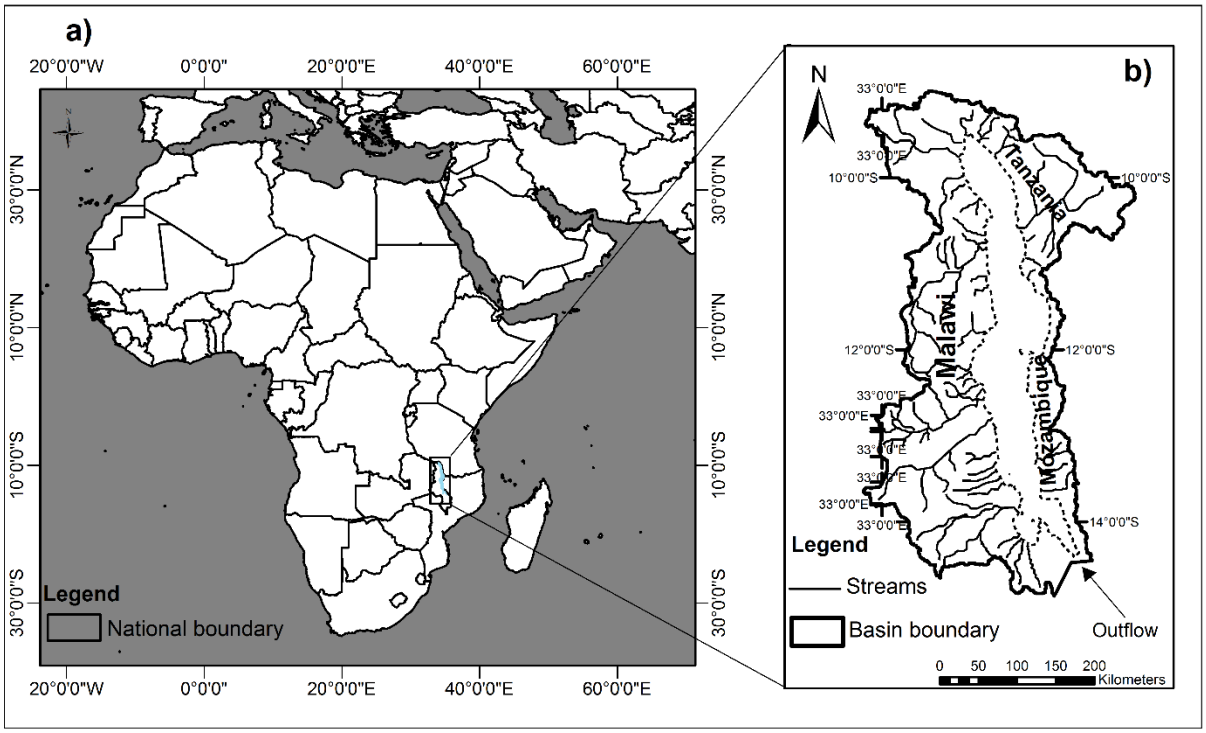

Source: modified from Hecky et al. (2003).

Figure 1. Location of Lake Malawi and its watershed; the lake includes 13 main inflows and only 1 outflow**, (**a) Geographical location of Lake Malawi (b) Lake Malawi basin including its adjacent countries namely Malawi, Mozambique, and Tanzania.

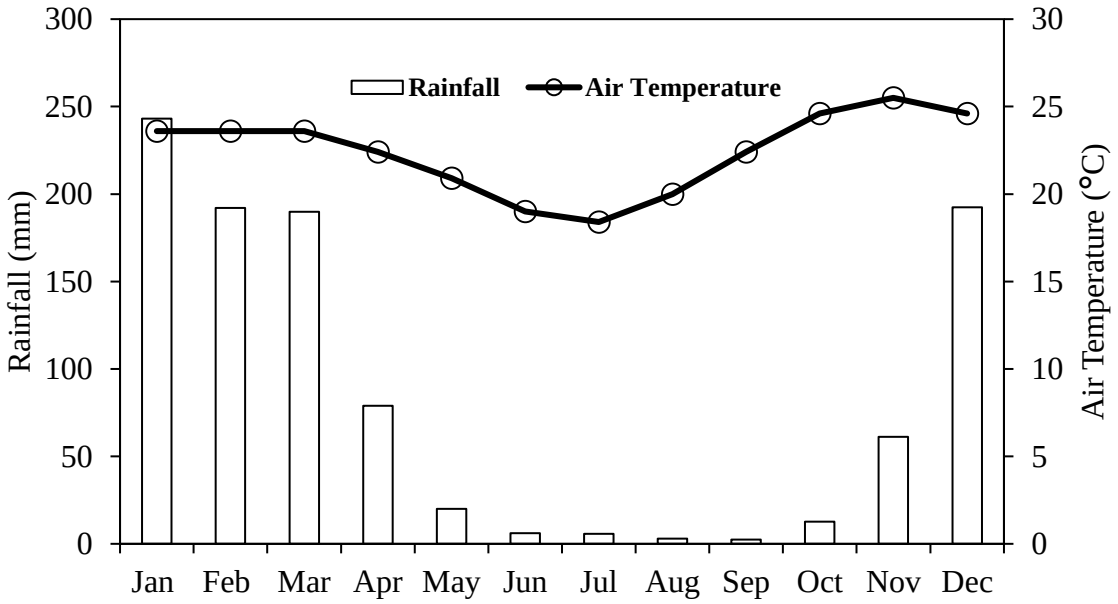

Figure 2. Monthly average temperature and rainfall in Malawi (1991-2015).

There are three seasons in Lake Malawi basin: the cool dry season (May-August), hot dry season (September-October), and warm wet season (November-April) in Lake Malawi basin. These two sets of data (rainfall and temperature) demonstrate the same temporal pattern.

Figure 3 shows the rainfall and temperature variation for the yearly data. The maximum rainfall during the study period was found in 2004 and minimum in 2005, but from 2006 to 2009 the precipitation stabilized, and there is no clear or sudden change in rainfall except for 2004 and 2005. However, it is important to remind that most of this rain falls in the first season (November-April), thus resulting in the destruction of infrastructures and probably an increase in runoff from the watershed to the lake, due to the lake's topographical characteristics as it is shown later in (Fig. 4).

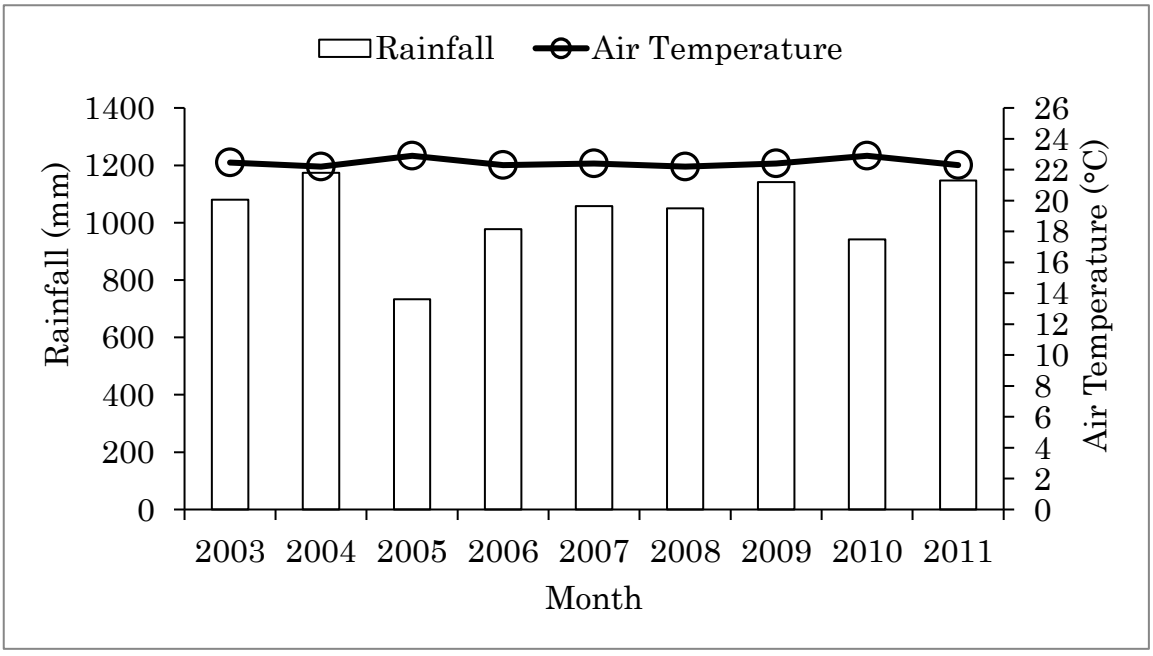

Figure 3. Yearly average air temperature and rainfall in Malawi from 2003 to 2011.

The topographical location of the lake and its surrounding are to be considered. Because Lake Malawi is in a valley, it is natural that most of the runoff from the watershed goes directly to the lake after a period of intense rainfall. From Figure 4, it is visible that the lake is

surrounded by highland in the northern, western and eastern region. The western region has a higher elevation than the eastern region. However, the region along the shore has lower elevation when compared to other regions. The combination of rivers, precipitation, air temperature, elevation, and land use/cover can provide important information about the aspects related to water quality in Lake Malawi. Lake Malawi is enclosed by most of the biggest cities in Malawi including the capital city Lilongwe represented by the red dot on the map from Figure 4.

Land use/cover maps from 2003 and 2017 show that there was a change during this period (Fig. 5). Most of these changes can be identified in places where there is agglomeration of people, such as the southwest part of the lake. The changes are from savanna to mixed forest, crop, and grasslands to crop. These changes in the basin are linked to anthropogenic activities.

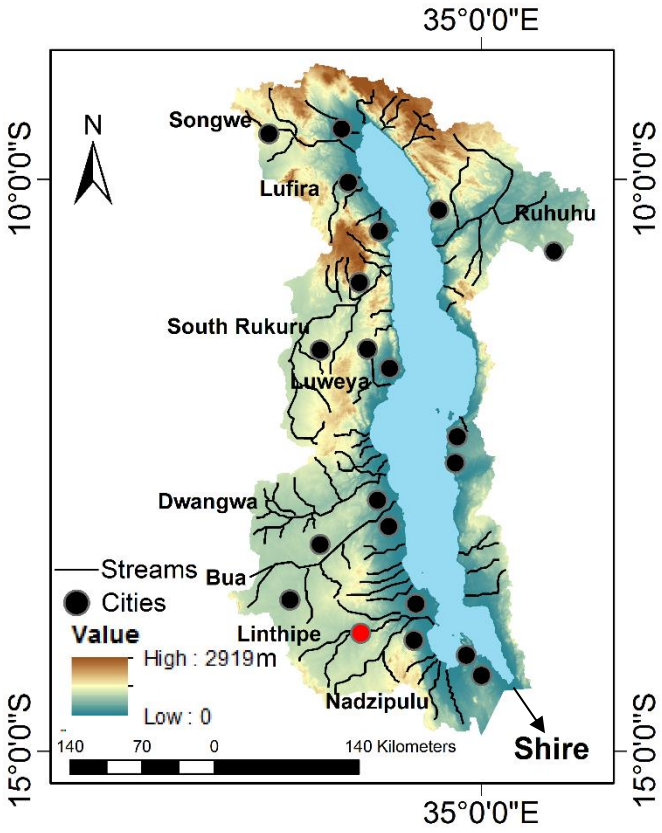

Source: ASTER GDEM a product of METI and NASA.

Figure 4. Elevation data in the basin showing low elevation along the shore contrasting with the high land in other areas.

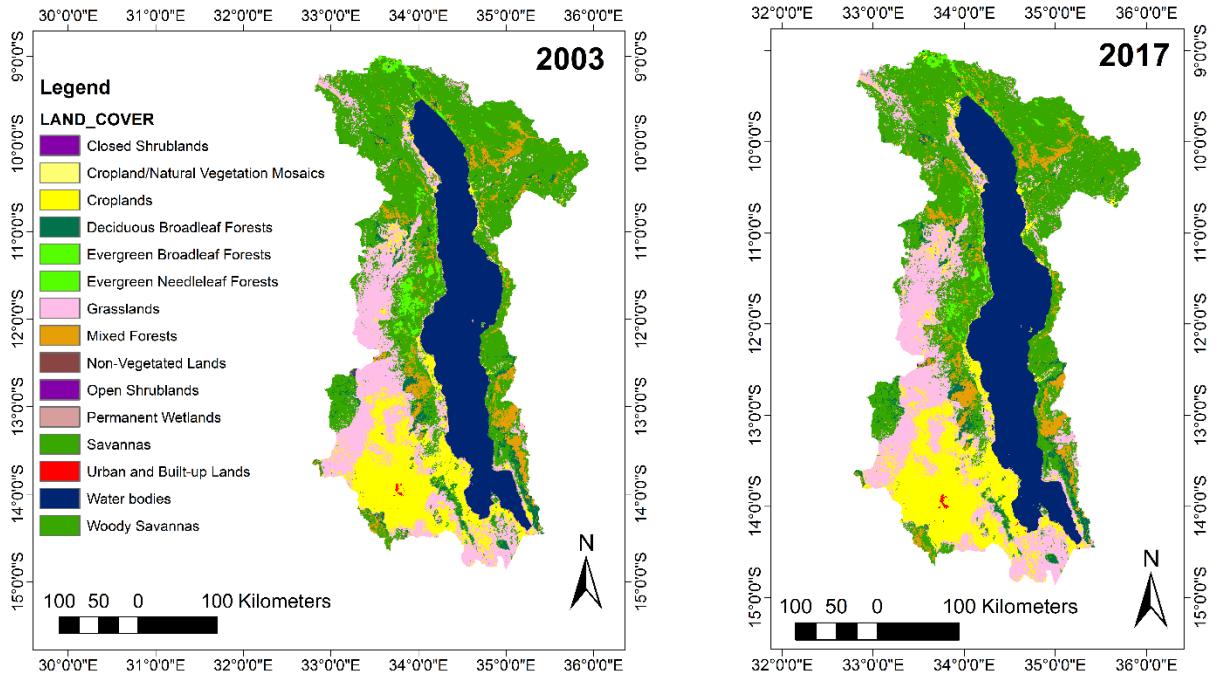

Source: NASA Land Data Products_L3_Global 500m (University of Maryland).

Figure 5. Land Use/Cover in Lake Malawi basin for 2003 and 2017.

2.2. Datasets

The ocean color sensors have a long history that can be traced back to the period between 1978-1986 when the Coastal Zone Color Scanner (CZCS) sensor was launched and terminated its mission. Due to its limitations, this sensor was later replaced by several other ocean color sensors such as the Chinese Moderate Resolution Imaging Spectrometer (CMODIS), onboard the 'Shenzhou-3' spaceship, followed by the Global Imager (GLI), MERIS, SeaWiFS and more recently OLCI. IOCCG [2] provides more detailed information for several missions and instruments.

[2] http://ioccg.org/resources/missions-instruments/historical-ocean-colour-sensors/

2.2.1. Satellite data collection and pre-processing: Envisat/MERIS and Sentinel-3/OLCI Data

MERIS was launched by the ESA onboard its polar-orbiting Envisat Earth Observation Satellite. It was primarily dedicated to Ocean Color Observations and has in the past broadened its scope of objectives to atmospheric and land surface related studies. It has a high spectral and radiometric resolution and a dual spatial resolution, Full Resolution (FR) data at 300 m on-ground resolution at a sub-satellite point which is mainly required in coastal zones and over land. Reduced Resolution (RR) data at 1200 m on-ground resolution at a sub-satellite point which is intended for large-scale studies. Oceanographic and atmospheric investigations require global Earth coverage within three days. The global mission of MERIS has a major contribution to scientific projects which seek to understand the role of the oceans and ocean productivity in the climate system through observations of watercolor and is furthering the ability to forecast change through models. Secondary, objectives of the MERIS mission is directed to the understanding of atmospheric parameters associated with clouds, water vapor and aerosols in addition to land surface parameters, vegetation processes. MERIS was designed to acquire 15 spectral bands in the 390-1040 nanometer range of the electromagnetic spectrum. The instrument had the capability to change its band position width and gain throughout its lifetime. In accordance with the mission goals and priorities of this instrument, Table 3 shows the 15 spectral bands from MERIS and other additional 6 bands from which encompasses the OLCI [3].

The OLCI is an optical instrument used to provide data continuity for ENVISAT's MERIS. OLCI is a push-broom imaging spectrometer that measures solar radiation reflected by the Earth, at a ground spatial resolution of 300 m, in 21 spectral bands. Because it is an instrument prepared to provide data continuity for MERIS, it was used in this study to expand the range of temporal

[3] https://earth.esa.int/web/guest/missions/esa-operational-eo-missions/envisat/instruments/meris/design

coverage of the study. Although the main purpose of OLCI was to give continuity to the MERIS legacy, some improvements have been made to this new satellite sensor such as a new channel at 1.02 μm which was included to improve atmospheric and aerosol correction capabilities. Additional channels in the O_2A absorption line (764.4 nm and 767.5 nm, adding to the existing channel at 761.25 nm) were included for improved cloud top pressure (height) and an additional channel at 940 nm in the H_2O absorption region, to improve water vapor retrieval. A channel at 673 nm has been added for improved chlorophyll fluorescence measurement (ESA, Standard Document Date: 13th January 2017, Issue: 1.1, Rev 1) [4]. The primary objective of OLCI to which was designed was to screen the ocean and land surface to collect information related to biology (e.g. phenology of marine and terrestrial biomass). Among other applicability are marine monitoring, net primary production estimates, and others. A total of 274 OLCI images were downloaded from [5], for the year 2017 and finally 261 were used for the subsequent application. The monthly distribution of OLCI data depended highly on the cloud cover. In this study 12 to 26 images were downloaded for each month. Despite this number of images, the spatial coverage was relatively low, resulting in low monthly lake area coverage. Figure 6 shows the number of OLCI images used. The shaded bands in Table 3 are the new bands which were not available in MERIS.

4 https://sentinel.esa.int

5 https://scihub.copernicus.eu/s3/#/home

Table 3. Band characteristics of MERIS and OLCI Sensor data.

Band No	Band Center (nm)	Band Width (nm)	Potential Application
Oa 1	400	15	Aerosol correction, improved water constituent retrieval
Oa 2	412.5	10	Yellow substance and detrital pigments
Oa 3	442.5	10	Chl absorption ma, biogeochemistry, vegetation
Oa 4	490	10	High Chl, other pigments
Oa 5	510	10	Chl, sediment, turbidity, red tide
Oa 6	560	10	Chlorophyll reference (Chl minimum)
Oa 7	620	10	Sediment loading
Oa 8	665	10	Chl (2nd Chl abs. max.) sediment, yellow substance/vegetation
Oa 9	673.75	7.5	For improved fluorescence retrieval and to better account for smile together with the bands 666 and 680
Oa 10	681.25	7.5	Chl fluorescence peak, red edge
Oa 11	708.75	10	Chl fluorescence baseline, red edge transition
Oa 12	753.75	7.5	O2 absorption/clouds, vegetation
Oa 13	761. 25	2.5	O2 absorption band /aerosol correction
Oa 14	764. 375	3.75	Atmospheric Correction
Oa 15	767. 5	2.5	O2A used for cloud top pressure, fluorescence over land
Oa 16	778.75	15	Atmos. corr/Aerosol corr
Oa 17	865	20	Atmos. corr/Aerosol corr, clouds, pixel co-registration
Oa 18	885	10	Water vapor absorption reference band. Common reference band/Vegetation monitoring
Oa 19	900	10	Water vapor absorption/vegetation monitoring (max. reflectance)
Oa 20	940	20	Water vapor absorption, atmos./aerosol corr.
Oa 21	1020	40	Atmos./aerosol corr.

Source[6]

6 https://earth.esa.int/web/guest/missions/esa-operational-eo-missions/envisat/instruments/meris/design

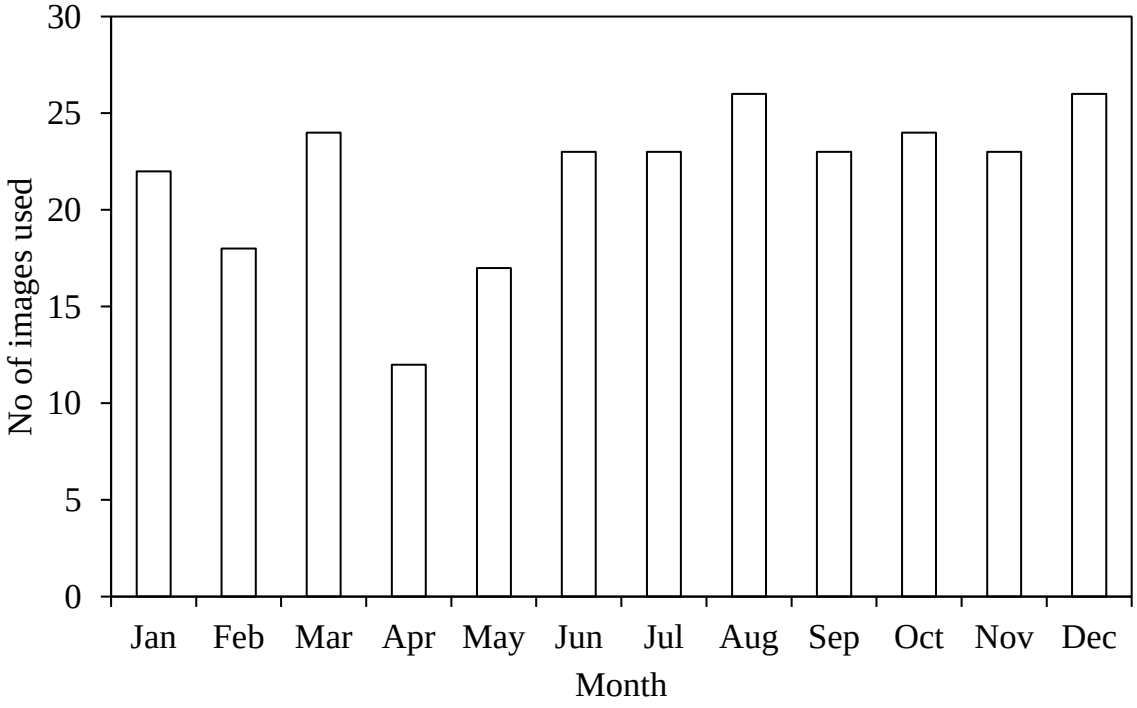

Figure 6. Temporal availability of OLCI dataset used in this study from January to December in 2017.

A set of 1658 MERIS L1b FR images covering the study area were downloaded from the ESA[7], from 2003-2012. These data were subset to the lake's basin area to reduce their size. After removing cloud-contaminated images, only 822 images from Jan. 20, 2003 to Dec. 30, 2011, were used, of which 338 images covered just half or more of the lake area. Table 4 summarizes the MERIS sensor data used in this study based on their temporal availability and pixel quality.

[7] http://merisfrs-merci-ds.eo.esa.int/merci

Table 4. Temporal availability of MERIS images used in this study from January to December.

	Year									
Month	2003	2004	2005	2006	2007	2008	2009	2010	2011	Total
Jan	2	9	4	10	2	2	5	2	4	40
Feb	1	7	2	6	2	5	4	1	3	31
Mar	2	1	6	10	8	6	2	4	4	43
Apr	3	1	3	8	9	10	6	11	6	57
May	3	1	11	11	16	13	11	11	7	84
Jun	10	0	15	14	13	13	11	10	13	99
Jul	4	1	14	13	12	11	8	9	10	82
Aug	10	3	12	14	13	15	9	13	12	101
Sep	12	3	14	12	11	14	7	11	8	92
Oct	7	1	13	6	12	12	8	6	7	72
Nov	10	2	11	7	12	8	5	7	7	69
Dec	9	5	8	6	5	5	3	5	6	52
Subtotal	73	34	113	117	115	114	79	90	87	822

The optical signal received by a satellite sensor is generally contaminated with several atmospheric particles. In total, the signal received by the top of atmosphere reflectance is a sum of the reflectance from Rayleigh scattering $\rho_r(\lambda)$, the reflectance from the sum of aerosol scattering and the interaction between Rayleigh and aerosol scattering $[\rho_a(\lambda) + \rho_{ra}(\lambda)]$, the diffuse transmittances of the atmospheric column $t(\lambda)$, and the water-leaving reflectance $\rho_w(\lambda)$ (Gordon and Wang, 1994).

The contributions to the top-of-the-atmosphere (TOA) radiance measured by a satellite come from several sources, from the solar radiance scattered by the atmospheric molecules and

aerosols, Sun and sky radiance reflected by the sea surface and from the water-leaving radiance [8]. Thus, for the estimation of any quantity of water quality parameters several steps must be followed. Figure 7 shows the schematic process of signal transmittance and interaction between the satellite and the water surface.

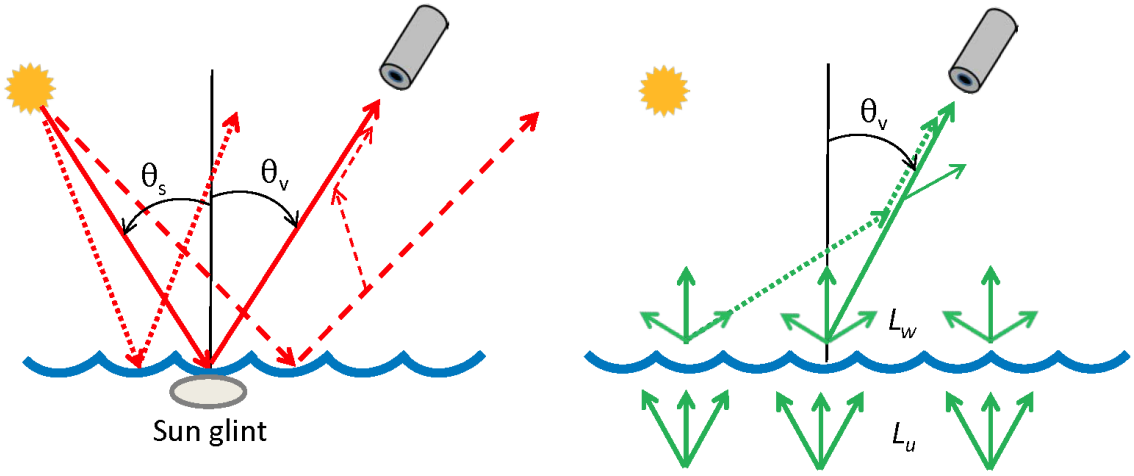

Figure 7. Left panel: Illustration of Sun glint as seen from the TOA, which is described by a direct transmittance. Right panel: Illustration of water-leaving radiance as seen from the TOA, which is described by a diffuse transmittance [9].

Where L_w is the water leaving radiance and L_u the upwelling radiance. Currently, there are several mechanisms for atmospheric correction, and they include those aimed at either clear or turbid waters. More details about atmospheric correction algorithms can be found in (Jaelani et al., 2013). Some of these atmospheric correction algorithms are embedded in software packages which are free of charge such as BEAMVISAT and they are based on neural network (NN) techniques (Doerffer and Schiller, 2007, 2008). The NN generally requires MERIS L1b TOA radiances as input to output atmospherically corrected water leaving reflectance at 12 bands. Because OLCI has similar characteristics of MERIS it was processed by using a new software

8 http://www.oceanopticsbook.info/view/atmospheric_correction/atmospheric_transmittances
9 http://www.oceanopticsbook.info/view/atmospheric_correction/atmospheric_transmittances

designed to follow up the legacy of BEAMVISAT, i.e. the Sentinel Application Platform (SNAP). SNAP is a software package aimed at replacing the BEAMVISAT software for the processing of OLCI data, but they can still be used simultaneously, and SNAP contains similar functions of BEAMVISAT including the atmospheric correction algorithms.

Among the existing atmospheric correction algorithms, the Case-2 regional processor (C2R) was chosen to carry out the atmospheric correction for both data, MERIS and OLCI. The C2R was chosen because (1) it has been tested over a wide range of atmospheric parameters (aerosol optical properties), and (2) it provides atmospheric correction, smile correction, land masking through its land detection, cloud and ice invalid pixels, and other flags for filtering the data (Doerffer and Schiller, 2008; Koponen et al., 2008; Doerffer and Brockmann, 2014). It is essential that atmospheric correction is performed on each satellite image to remove the atmospheric contributions and adjust for atmospheric attenuation of the water leaving radiance signal (Steissberg et al., 2010). The C2R processor uses a neural network which is trained with simulated R_{rs} spectra. About 30,000 spectra are used to cover a large range from case 1 and case 2 waters as well as different observation and solar angles (IOCCG, 2006).

To further avoid a possible influence from the bottom reflectance caused by the pixels along the shoreline, a 600-m buffer was generated to mask these pixels. After SD estimations, the daily SD values were aggregated into monthly (average 10-year SD values in each month) and yearly (average 12-months in each year) datasets.

2.2.2. In Situ Data Collection

The in situ measured SD values used in this study and applied to MERIS data were measured in 2007, Figure 8 shows the sampling locations. The SD values were measured along a 10-km South-North transect. The transect included one station (KGC) at the center of the cage farm (fish cages deployed in 2004 for fish aquaculture), 4 stations at the South (CS1-CS4) and 4 stations at the North of the fish cage farm (CN1-CN4). The distance between two stations was controlled to be at least 1 km away (Gondwe et al., 2011). The name of stations and the number of in situ SD measurements for each station including the minimum and maximum SD values are summarized in Table 5.

Although Malawi, Mozambique, and Tanzania have some research institutes focused on Lake Malawi studies, they investigate more about fish species and fish catch quantity, a little being done on the water quality (Guildford and Hecky, 2000). The available studies on water quality are mostly done by external researchers (Gondwe et al., 2011; Macuiane et al., 2016) who are not part of the research institutions and the studies are for academic purposes. The in situ data was used for comparison with the remotely sensed estimations through a validation process to check the performance of the two semi-analytical algorithms independently. Below is the location of the sampling stations.

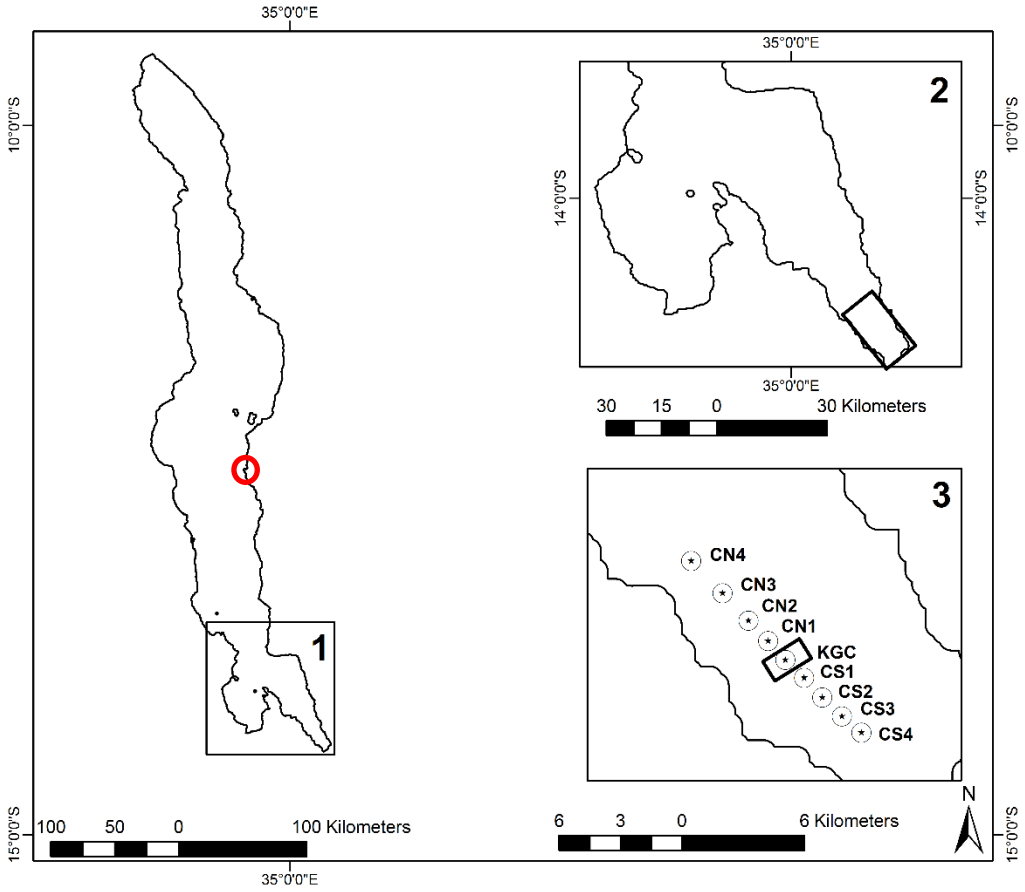

Source: modified from Gondwe et al. (2011).

Figure 8. Sampling locations in the southeast arm of Lake Malawi. KGC represents the center of the fish cage farm, CN1-CN4 represents four sampling stations in the North of KGC, and CS1-CS4 represents four sampling stations in the South of KGC, and the red circle is the sampling location for the data used in 2017.

The in situ data for 2017 was measured on December 6th. This set of data was measured from the Mozambican side of the lake, a total of 10 sampling sites. The image from Figure 9 shows the sampling location of the data used for validation of the OLCI sensor results. The 2017 sampling locations are relatively close to the shore because it was possible to measure a reasonably wider range when compared to sampling made only in the center of the lake as it does not provide a dynamic range of water quality change. The other factor influencing the amount and location was the weather condition which changed unexpectedly.

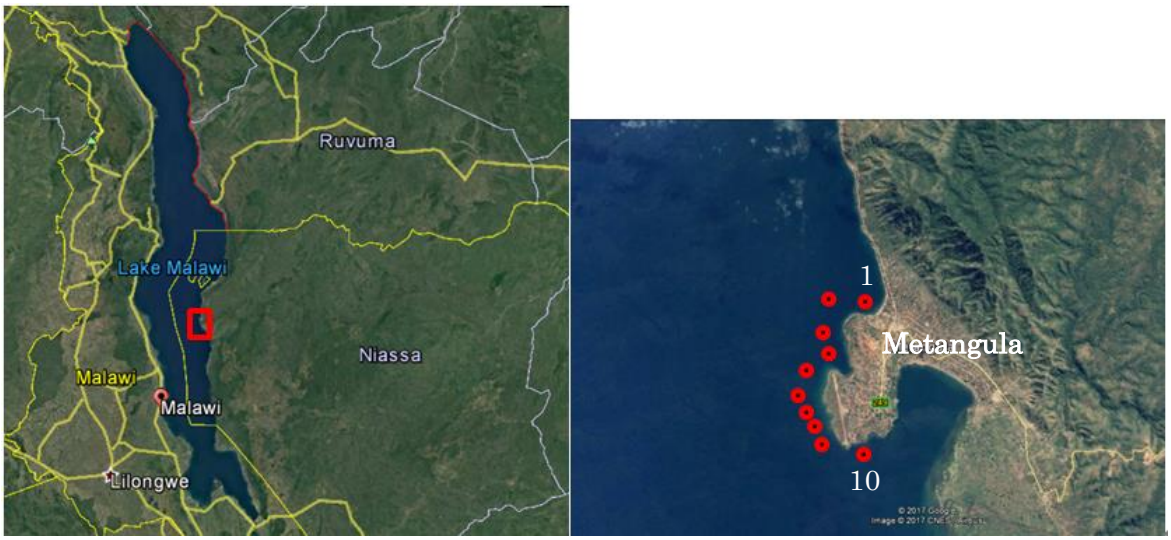

Source: Google Earth

Figure 9. Sampling locations for the 2017 validation data in Metangula, the red dots represent each location where sampling was carried out from North to South.

The SD measured from the lake varied from 11.0 to 14.2. The sampling from 2017 was done in Metangula where a Fisheries Research Institute – Niassa Branch (Instituto de Investigação Pesqueira_Delegação de Niassa) is located. The sampling was done with the support of the staff from the institute. Figure 10-11 below show all the process, from preparation, departure and the sampling.

Figure 10. Sampling location, (A) the vision of the lake high from the road (B) vehicle being washed in the lake, small boats and people bathing, washing clothes and dishes in the lake, (C) the staff of the institute and the boat owners, (D) one of the boat owners trying to remove the anchor from the depths of the lake.

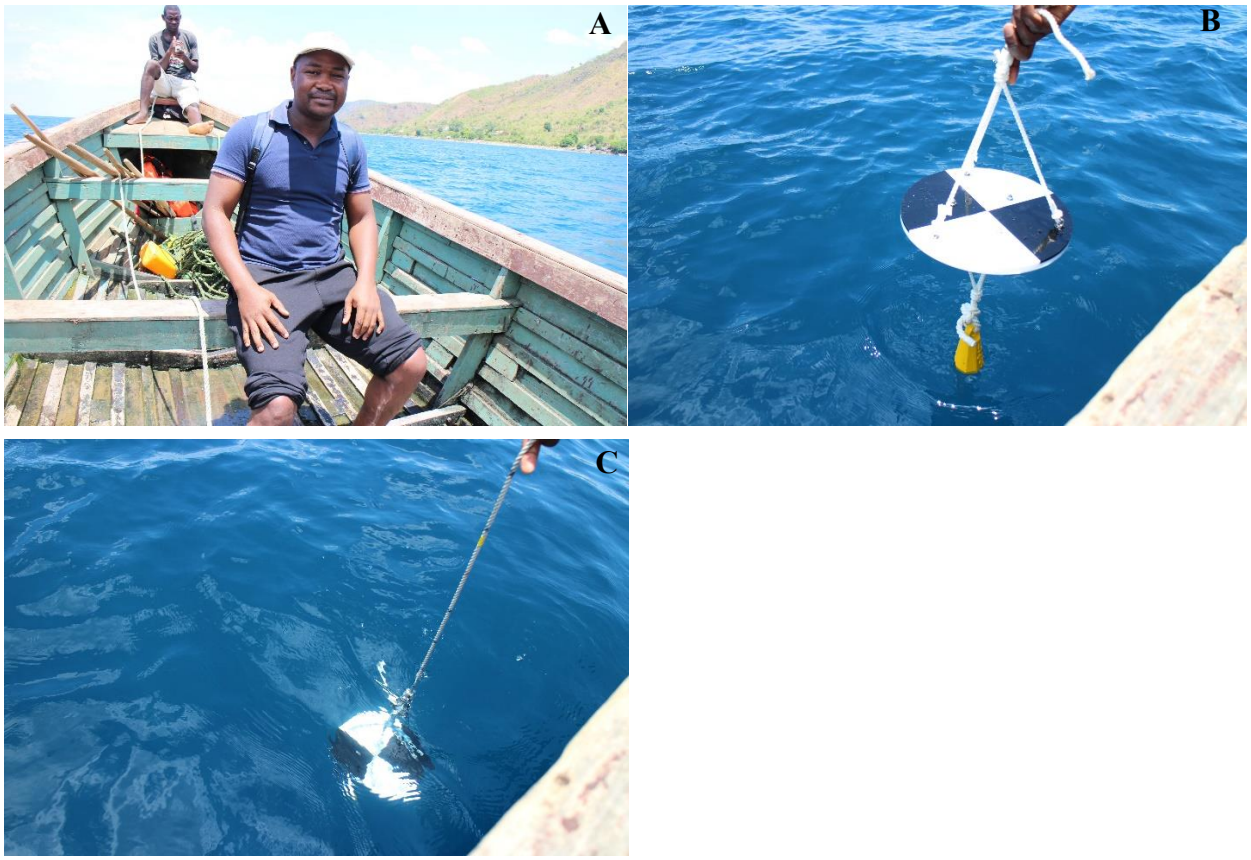

Figure 11. Sampling location, (A) departure to the sampling sites, (B) and (C) sampling in the first station.

Table 5. Stations and number of in situ SD measurements used for validation, including minimum and maximum values.

Station	No of SD measurements	Min–Max (m)	Sampling Time (Monthly)
CS4	20	2.8 – 9.6	
CS3	15	2.1 – 10.0	
CS2	21	2.4 – 10.2	except for Jul. and Aug.
CS1	14	2.8 – 11.1	
KGC	33	2.9 – 9.6	except for Jan. and Aug.
CN1	15	3.5 – 9.6	
CN2	22	2.9 – 9.0	except for Apr., Jul. and
CN3	14	3.0 –12.3	Aug.
CN4	19	3.9 –12.2	
In total	173	2.1–12.3	

KGC represents the center of the cage farm, CN1-CN4 represents 4 sampling stations in the North of KGC, and CS1-CS4 represents 4 sampling stations in the South of KGC (Gondwe et al., 2011). The total (min-max) is the range of the entire data.

2.3. The two Semi-Analytical Algorithms for estimating Secchi Disk Depth from Satellite Data

Two main semi-analytical algorithms are currently being used by researchers to retrieve SD from several water bodies based on remotely sensed data. For Doron et al. (2011), SD is determined by the beam attenuation coefficient c (m^{-1}), and the vertical diffuse attenuation coefficient, K_d (m^{-1}), whereas for Lee et al. (2015) it is determined by K_d (m^{-1}), in the transparent window of the water body.

2.3.1. Doron11 Algorithm

The algorithm from Doron et al. (2011) was used to estimate SD. This algorithm focuses on the semi-analytical retrieval of the Inherent Optical Properties (IOPs), total absorption a (m^{-1}) and backscattering coefficients b_b (m^{-1}) from reflectance at two wavelengths, λ_1, and λ_2 in the visible (490 and 560 nm) region. This algorithm was validated using a wide range of coincident satellite estimates including from MERIS sensor. The comparison between SD retrieved from remotely sensed data and in situ measurements generated coefficients of determination between 0.54 and 0.60, depending on the sensor. Therefore, following the algorithm from Doron et al. (2011), the first steps were carried out. Because the remotely sensed radiances from MERIS/OLCI had already been converted into R_{rs}, the next step was to convert them into irradiance reflectance. Thus, the following equations were used:

$$\mathrm{Rrs}(0^+,\lambda) = \frac{\mathrm{nLw}\,(0^+,\lambda)}{\bar{F}_{0(\lambda)}} \quad (1)$$

$$\rho_{w\,(0^+,\lambda,\theta,\phi)} = \frac{\pi \mathrm{nLw}\,(0^+,\lambda)}{\bar{F}_{0(\lambda)}} = \pi \mathrm{Rrs}(0^+,\lambda) \quad (2)$$

Because the final goal was to calculate the irradiance reflectance just below the surface (R), the following equation was applied:

$$R = \frac{Q\rho_w}{\pi\Re_0 + Q\bar{r}\rho_w} \quad (3)$$

where Q = 4, $\Re_0 = 0.529$ and $\bar{r}$ = 0.48; Consequently, R (490) and R (560) were obtained from Eq. (3). Knowing the values of R (490) and R (560), it was then calculated the backscattering coefficient at the reference wavelength b_b (490) and the absorption at the same wavelength a (490), using Eqs. (4-7) and in the end Eq. (8) was used to calculate the vertical diffuse attenuation coefficient, K_d (m^{-1}). Note that in Eq. (6) b_{bw} is the backscattering coefficient of pure water obtained from Zhang et al. (2009).

The average ratio ($B_{490-560}$) of the scattering coefficient at 490 and 560 nm was equal to 1.003 (dimensionless) and the proportionality factor ($\alpha_{490-560}$) between the residual absorption at 490 and 560 nm equal to 0.323 equally (dimensionless).

$$N = -B_{490-560}\, b_{bw}(560) + B_{490-560}\, \frac{a_w(560)}{f(560)}\, R(560) + \alpha_{490-560} B_{490-560}\, \frac{f(490)}{f(560)}\, \frac{R(560)}{R(490)}\, b_{bw(490)} - \alpha_{490-560} B_{490-560} \frac{R(560)}{f(560)}\, a_w(490) \quad (4)$$

$$D = 1 - \alpha_{490-560} B_{490-560} \frac{f(490)}{f(560)}\, \frac{R\,(560)}{R\,(490)} \quad (5)$$

$$b_b(490) = b_{bw}(490) + \frac{N}{D} \quad (6)$$

$$a(490) = \frac{f(490) b_b\,(490)}{R\,(490)} \quad (7)$$

The value for the proportionality factor f (λ) = 0.335 at both wavelength 490 and 560 nm, (Doron et al., 2011); and a_w (490) and (560) from Pope and Fry (1997).

K_d(490) can be estimated from a(490) and b_b(490) using the following equation (Lee et al., 2013):

$$K_d(\lambda) = (1 + 0.005\times\theta_s)\times a(\lambda) + (1\text{-}0.265\times(b_{bw}(\lambda)/b_b(\lambda)))\times 4.259\times(1 - 0.52e^{-10.8\times a(\lambda)}) \times b_b(\lambda) \quad (8)$$

where (θ_s) represents the solar zenith angle in degree, and b_{bw} has been described above (Zhang et al., 2009). Eq. (8) was used by both Doron11 and Lee15, having as input their respective *a* and b_b calculated independently.

Once the diffuse attenuation coefficient was calculated, then Eq. (9) was used to calculate the particulate backscattering coefficient $b_{bp(490)}$, at the reference wavelength, Eq. (10) particulate scattering coefficient $b_p(490)$, and Eq. (11) for the scattering coefficient for pure water $b_w(490)$, in the end, the beam attenuation coefficient c (490) was calculated using Eq. (12):

$$b_{bp(490)} = b_{b490} - b_{bw490} \quad (9)$$

$$b_p(490) = \frac{b_{bp(490)}}{-0.0310+0.0503\tanh\left(\frac{b_{bp(490)}+0.00686}{0.00820}\right)} \quad (10)$$

$$b_w(490) = b_{bw}(490)/0.5 \quad (11)$$

$$c(490) = a(490) + b_p(490) + b_w(490) \quad (12)$$

after obtaining K_d (490) and c (490), the visual photopic vertical diffuse attenuation coefficient of the medium $K_d(v)$ and the visual photopic beam attenuation coefficient c(v) both in (m^{-1}),

$(K_d(v) + c(v))$ was calculated using:

$$X = K_d(490) + c(490) \quad (13)$$

an important notice is that in equation (14) the "+" signal before "0.0467" was used as noted by Lee et al. (2018) instead of "-" in Doron et al. (2007, 2011).

$$(K_d(v) + c(v)) = 0.0989X^2 + 0.8879X + 0.0467 \quad (14)$$

where X represents $K_d(490) + c(490)$, which are the vertical diffuse attenuation coefficient and beam attenuation coefficient at a wavelength of 490 nm, respectively. The $c(490)$ can be further obtained from the sum of the total absorption coefficient and total scattering coefficient at 490 nm (i.e., a(490) and b(490); a(490) and the total backscattering coefficient at 490 nm (i.e., $b_b(490)$) can be calculated using Eqs. (11-12) in (Doron et al., 2011). The b(490) can be calculated from the sum of the particle scattering coefficient (Eq. 9 in Doron et al., 2007) and the scattering coefficient of pure water at a wavelength of 490 nm.

Finally, using Eq. (15), SD from Doron11 was calculated as follows:

$$SD = \frac{ln(\frac{C_0}{C_{min}})}{K_d(v) + c(v)} \quad , \quad ln(C_o/C_{min}) = \Gamma \quad (15)$$

where the inherent contrast between the disk and background water reflectance (C_o) is expressed as:

$$C_o = \frac{R_{SD} - R_\infty}{R_\infty} \quad (16)$$

The reflectance of the Secchi disk, R_{SD} = 0.82 based on Tyler (1968), R_∞ equal to irradiance reflectance just below the surface at 490 nm, and the minimum apparent contrast perceivable by the human eye (C_{min} = 0.0066).

2.3.2. Lee15 Algorithm

Lee et al. (2015) proposed a new mechanistic algorithm based on the underwater visibility theory. The new algorithm relies on the diffuse attenuation coefficients (K_d) at a wavelength corresponding to the maximum transparency for such interpretation. This algorithm was also validated by using data covering an extensive range of water types including oceanic, coastal, and inland, the results of SD showed excellent performance ranging from 1 to 30 m without regional tuning of any parameter. For the new algorithm, a and b_b were firstly calculated from the quasi-analytical algorithm in its most recent version (QAAv6).

The quasi-analytical algorithm was introduced by Lee et al. (2002), and the main objective was to retrieve absorption and backscattering coefficients, as well as absorption coefficients of phytoplankton pigments and gelbstoff. From its introduction, it has been modified into several versions including 4, 5 and more recently 6. Because it was designed for optically deep waters as input and applied to oceanic and coastal waters, some studies have proposed new alternatives, Yang et al. (2013) enhanced the QAAv5 to retrieve inherent optical properties IOPs for turbid inland waters based on the bandwidths of MERIS and the results indicated that the enhanced QAA had the potential to accurately retrieve the IOPs from MERIS Sensor observations for inland waters. Rodrigues et al. (2017) tested the applicability of Lee's algorithm, by using QAAv5 to retrieve a and b_b in an oligo-to mesotrophic reservoir in Brazil. They found that the results from (step 1) in their paper subsequently affected the performance of step 2 and 3. Because step 1 is mainly QAAv5, they then proposed a modified version of QAAv5 (QAA_{R17}) and evaluated its performance. The results showed an improvement of K_d and SD. This conclusion denotes that a and b_b are key elements in the calculation of SD. Lee et al. (2016) modified the QAA by verifying the representative wavelengths of Landsat-8 bands in the visible domain, as well as absorption and backscattering coefficients of pure water for these bands to be applied in the model of Lee et al. (2015). Once modified and applied to Landsat-8 data

high-spatial-resolution map of water clarity were produced. Table 6 describes the steps used to the calculation of *a* and b_b as it was applied in this study.

Table 6. Steps of the quasi-analytical algorithm version 6.

Step	QAAv6	
0	$r_{rs}(\lambda) = \mathrm{Rrs}(\lambda)/(0.52 + 1.7\mathrm{Rrs}(\lambda))$	
1	$u(\lambda) = \frac{-g_0 + \sqrt{(g_0)^2 + 4g_1 * r_{rs}(\lambda)}}{2g_1}$, where $g_0 = 0.089$ and $g_1 = 0.1245$	
2	**IF R_{rs} (670) < 0.0015 sr^{-1} (QAAv5)**	**(else)**
3	$\chi = \log\left(\frac{r_{rs}(443) + r_{rs}(490)}{r_{rs}(55x) + 5\frac{r_{rs}(670)}{r_{rs}(490)} r_{rs}(670)}\right)$ $a(\lambda_0) = a(55x) = a_w(\lambda_0) + 10^{h0+h1x+h2x^2}$	$a(\lambda_0) = a(670) = a_w(670) + 0.39\left(\frac{\mathrm{Rrs}(670)}{\mathrm{Rrs}(443) + \mathrm{Rrs}(490)}\right)^{1.14}$
4	$b_{bp}(\lambda_0) = b_{bp}(55x) = \frac{u(\lambda_0) * a(\lambda_0)}{1 - u(\lambda_0)} - b_{bw}(55x)$	$b_{bp}(\lambda_0) = b_{bp}(670) = \frac{u(\lambda_0) * a(\lambda_0)}{1 - u(\lambda_0)} - b_{bw}(670)$
5	$\eta = 2.0\left(1 - 1.2\exp\left(-0.9\frac{r_{rs}(443)}{r_{rs}(55x)}\right)\right)$	
6	$b_{bp}(\lambda) = b_{bp}(\lambda_0)\left(\frac{\lambda_0}{\lambda}\right)^{\eta}$	

The absorption and total backscattering coefficients are then calculated as:

$$a(\lambda) = \left(1 - u(\lambda)\right)\left(b_{bw}(\lambda) + b_{bp}(\lambda)\right)/u(\lambda) \quad (17)$$

$$b_b(\lambda) = b_{bw}(\lambda) + b_{bp}(\lambda) \quad (18)$$

Similarly, after calculating a and b_b from QAAv6, and K_d (λ), SD from Lee15 was calculated using Eq. (19):

$$\mathrm{SD} = \frac{1}{2.5\mathrm{Min}\left(K_d(443,490,510,560,620,665)\right)} \ln\left(\frac{\left|0.14 - \mathrm{R}_{\mathrm{rs}}^{\mathrm{pc}}\right|}{\mathrm{C}_{\mathrm{t}}^{\mathrm{r}}}\right) \quad (19)$$

where $\mathrm{R}_{\mathrm{rs}}^{\mathrm{pc}}$ is the $\mathrm{R_{rs}}$ corresponding to the wavelength with the minimum K_d, and $\mathrm{C}_{\mathrm{t}}^{\mathrm{r}}$ is the contrast threshold of the human eye in radiance reflectance (= 0.013 $\mathrm{sr^{-1}}$). Min (K_d(443, 490, 510, 560, 620, 665) is the K_d at MERIS/OLCI visible bands with a minimum value. The K_d at a given band can be estimated from a and b_b at the same band using Eq. (8) above. In the Lee15 algorithm, the total absorption coefficient a and total backscattering coefficient b_b were estimated from $\mathrm{R_{rs}}$ using the sixth version of the quasi-analytical algorithm (QAAv6).

2.4. Definition of Transparency Levels and Accuracy Assessment

The Organization for Economic Cooperation and Development (OECD, 1982) classification system was used to define water transparency levels in Lake Malawi. In all, there are five transparency levels according to thresholds of SD values (OECD, 1982), which were also linked to trophic states of a water body (Table 7). This classification system was established to provide guidance on water to OECD members and non-OEDC member countries.

Table 7. Transparency level definition according to thresholds of SD values in OECD (1982).

Trophic Category	Secchi Depth (m)	Transparency Level
Ultra-oligotrophic	>12	1
Oligotrophic	6 - 12	2
Mesotrophic	3 - 6	3
Eutrophic	1.5 - 3	4
Hyper-eutrophic	<1.5	5

In Table 7, the trophic categories from (OECD, 1982) are directly linked to the SD and water transparency levels. Because SD is related to light penetration in the water column and not productivity, only transparency levels are evaluated, and categorized from level 1 to 5. These transparency levels are graded from the clearest to the most turbid water in the lake. Before the definition of water transparency levels, the results were evaluated for their accuracy.

Thus, the following indexs were used: the Root mean square error (RMSE), Mean absolute percent error (MAPE), and Bias to evaluate the performance of the two semi-analytical algorithms. These error measurement indexs are defined as follows:

$$\text{RMSE} = \sqrt{\frac{\sum_{i=1}^{N}(X_{est,i} - X_{meas,i})^2}{N}} \quad (20)$$

$$\text{MAPE} = \frac{1}{N}\sum_{i=1}^{N}\left|\frac{X_{est,i} - X_{meas,i}}{X_{meas,i}}\right| \times 100\% \quad (21)$$

$$\text{Bias} = \frac{\sum(X_{est,i} - X_{meas,i})}{N}, \quad (22)$$

where X_{est} is the estimated SD value, X_{meas} is the corresponding in situ measured SD value, and N is the number of SD pairs.

In order to avoid possible influence of any radiometric error and because the water surface is always in movement depending on the wind speed, it was used a 3×3 pixel, window size for the sensor pixel to be compared to the in situ data.

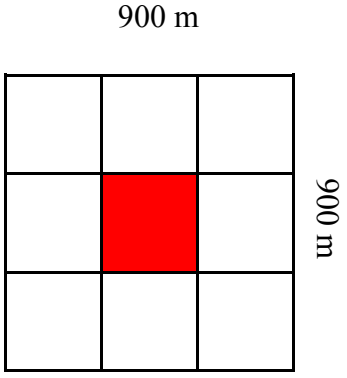

The central pixel is taken as the representing value to be compared with the in situ measured data.

2.5. Results

2.5.1. Comparison of Doron11 and Lee15 in Lake Malawi

Spatially the two SD algorithms depict similarities regarding their distribution. An increase of SD from the shore to the center of the lake is visible in both results. The gradual increase is most visible in areas such as the West shore of the lake, southern and northern parts. The center of the lake is generally clear, as well as most of the East shore except for the southern region where both sides have a similar pattern of low SD. The southern part has lower depths than the northern, and it is the region where the only outlet of the lake is located. Figure 12 shows the spatial distribution of SD estimated from both algorithms. From the distribution maps and comparing the two algorithm results, SD from Doron11 > Lee15. From the maps of Lee15, the northern region shows low SD like the West and South parts of the lake. The Central and East parts are the clearest in terms of SD distribution. In 2004 the northern region shows the lowest SD when compared to other years within the study period. Because Doron11 estimated higher values, the same pattern could not be observed, but in the same year (2004), Doron11 also shows the lowest SD in the northern region. The West and South parts of the lake do also show low SD, though less expressive if compared with the results from Lee15. Doron11 shows a clearer result in almost all the regions of the lake as most of the SD is equal or above 13 m while Lee15 shows lower SD values in similar areas. The upwelling in Lake Malawi is more expressive at the South end of the lake, and the cool surface horizontal gradient is maintained by the upwelling of cooler deeper water (Hamblin et al., 2003). The upwelling can also occasionally bring nutrients to the surface waters, thus enabling the increase in productivity and decrease in SD.

The results from both Doron11 and Lee15 show higher values in 2017 when compared to other years. Despite having similar band configuration, and same pre-processing procedures it the result from OLCI yields higher values when compared to the results from MERIS sensor.

However, it is still early to generalize such a difference between the products from both sensors. Only one year of OLCI was used, against 9 years from MERIS, thus making it a biased comparison and suggesting that further investigation is needed. For the first time in the study period values greater than 30 m were found in the lake in 2017.

2003	2004	2005
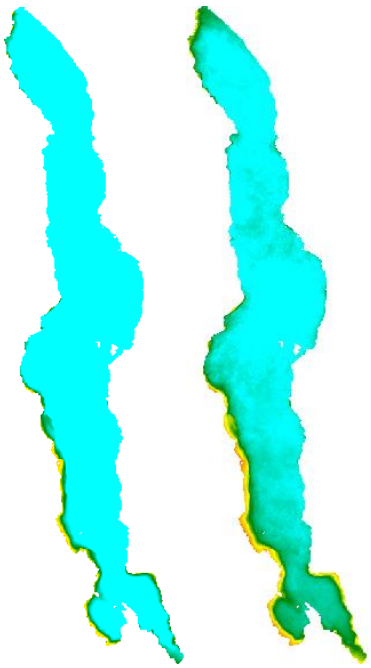	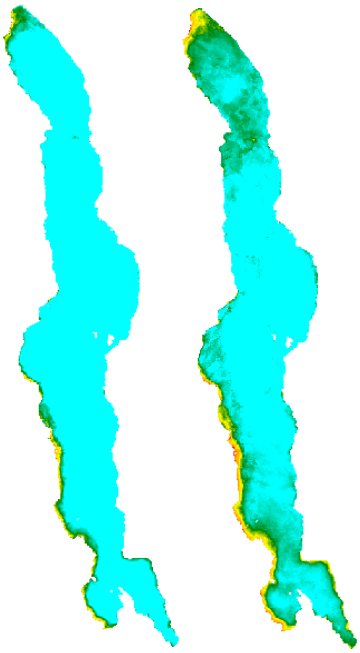	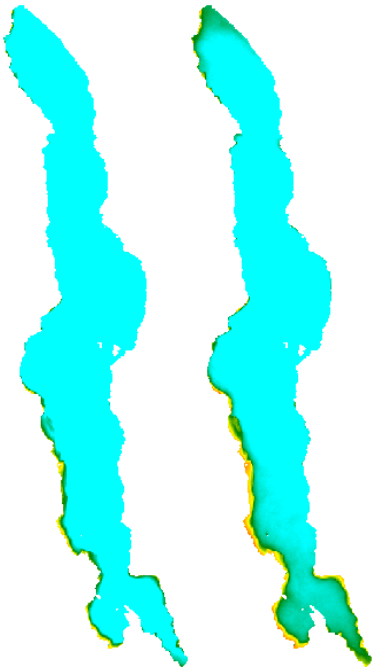
2006	**2007**	**2008**
	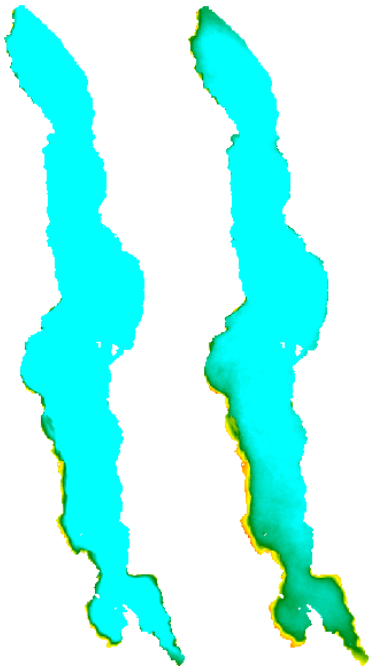	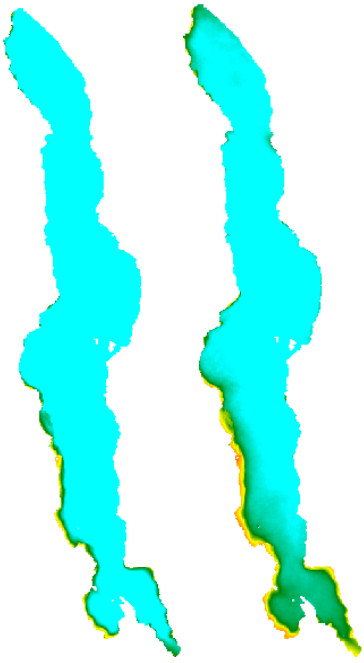

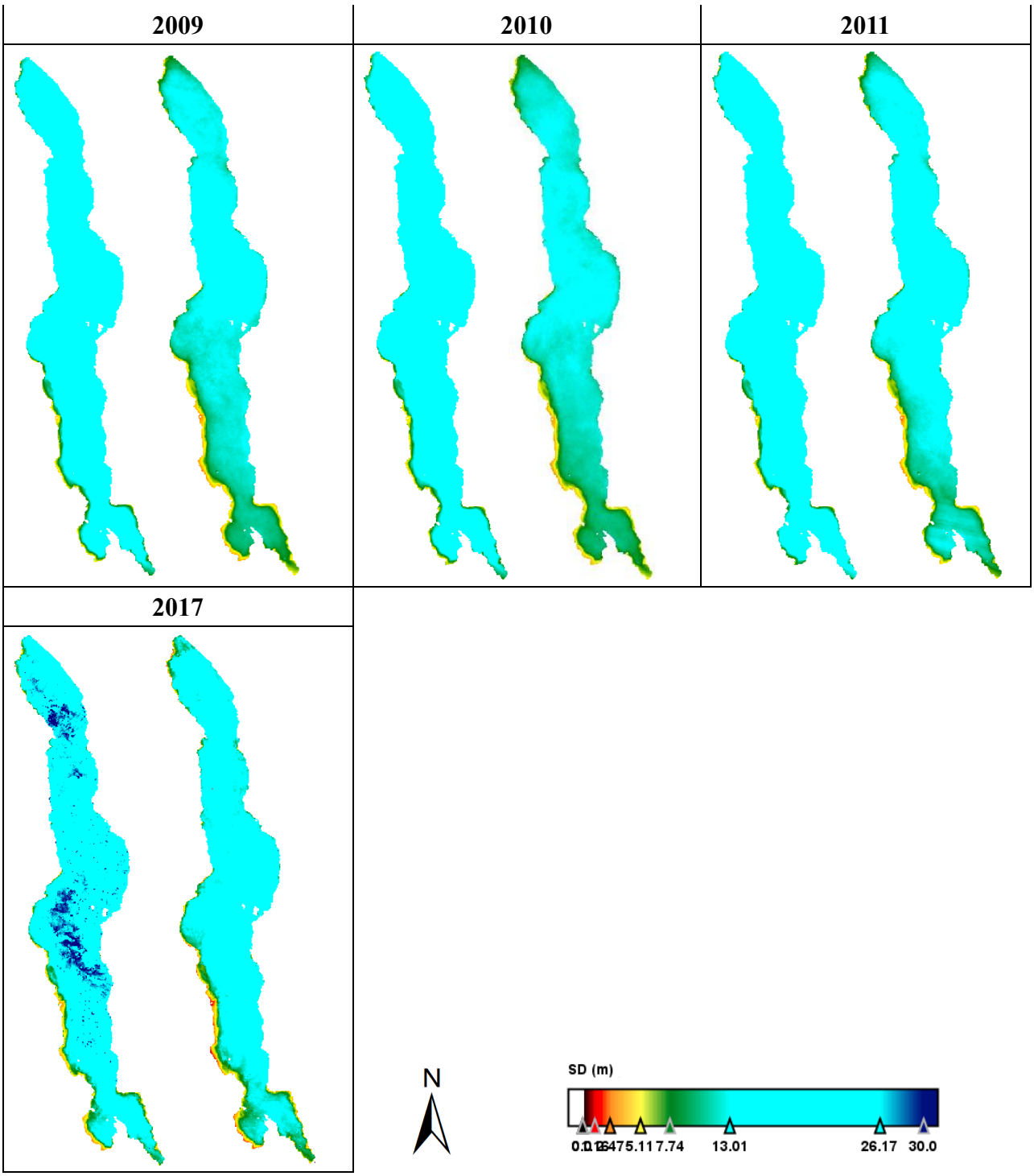

Figure 12. Distribution maps of the results from the two algorithms showing the yearly average data. Left: Doron11 and right: Lee15.

Because the two algorithms have shown similarities, further comparison were done including statistical evaluation on the pixel basis. In Figure 13 the yearly data from both algorithms are compared. From the scatter plot, the results from Doron11 are higher than Lee15. The results are more similar in the high SD values region than in the low SD values.

Table 8 shows more detailed information regarding the relationship between these two algorithms including the coefficient of determination, regression equations (polynomial fourth order), the absolute mean difference (AMD) and the relative mean difference (RMD). From 2003-2011 all the scatter plots have the same characteristic, where the relation between the two datasets is very close and narrow. The scatter plot from OLCI shows a different pattern as it is shown in figure referent to the year 2017. One possibility for this difference might be on the atmospheric correction procedure which might not have worked properly for this data since both SD retrieval algorithms have produced higher values than MERIS results.

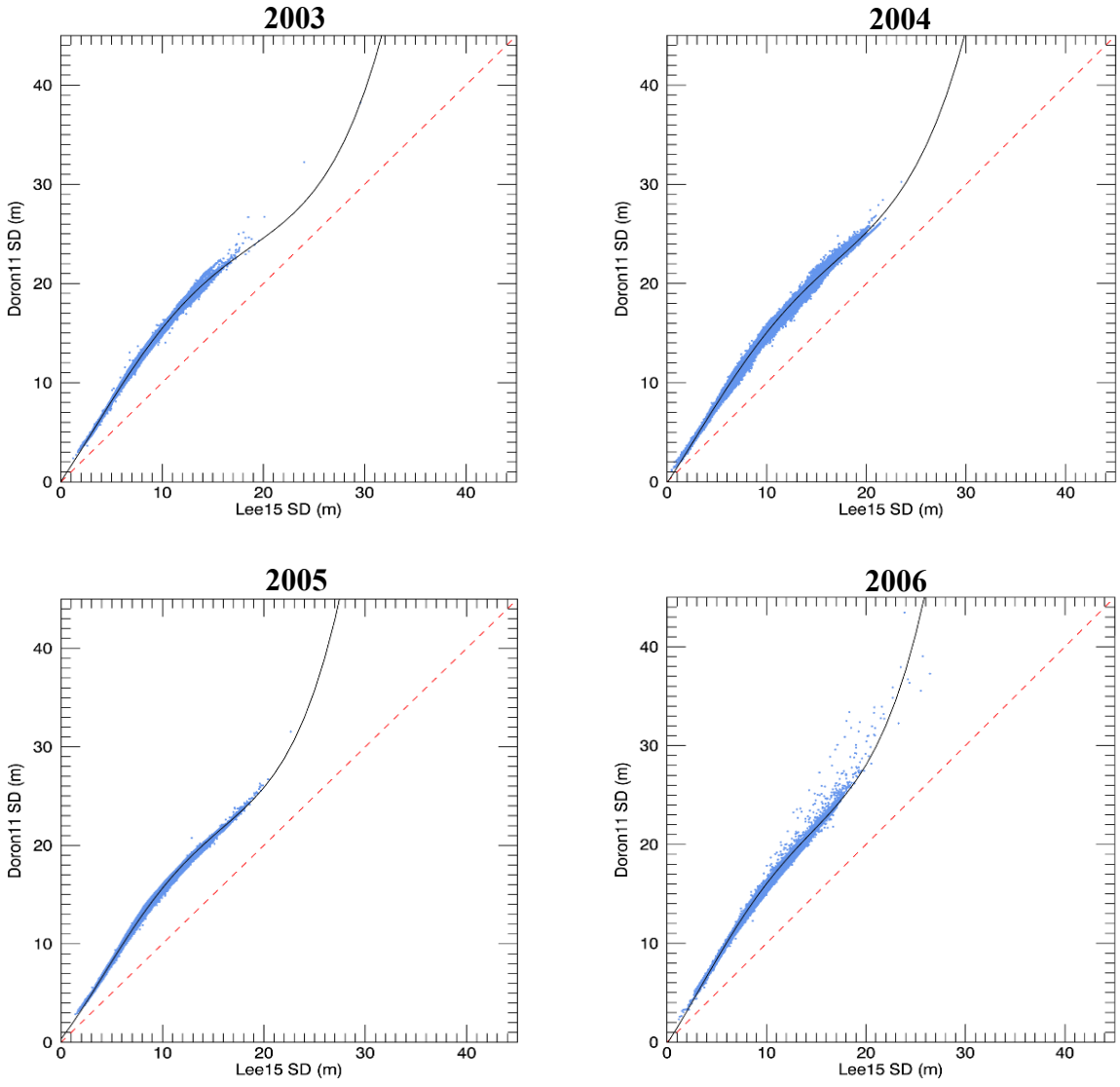

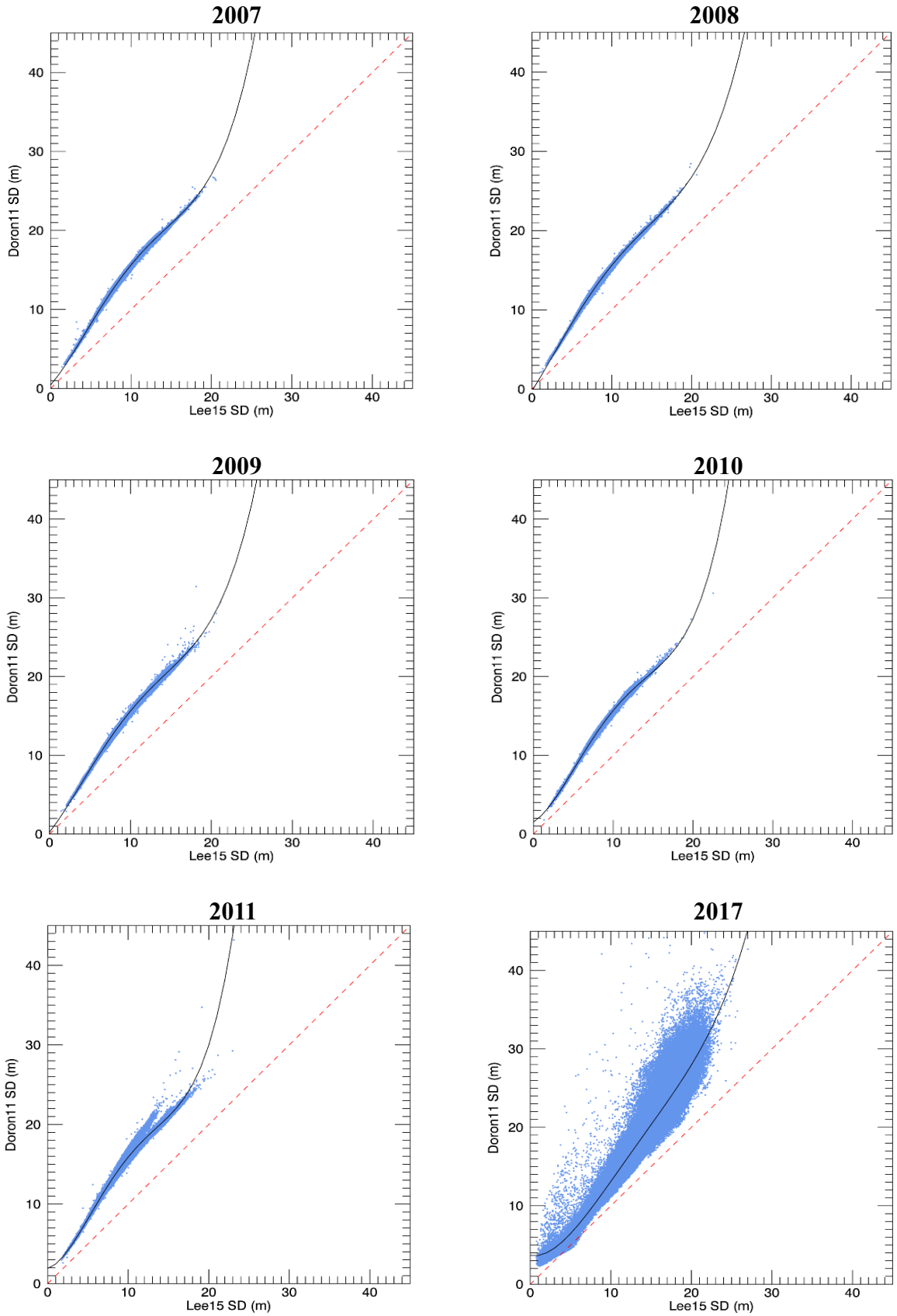

Figure 13. Pixel-based comparison of yearly estimated SD values using Doron11 algorithm and those using Lee15 algorithm in Lake Malawi.

The SD values derived from the Doron11 algorithm are strongly correlated with those derived from the Lee15 algorithm (Fig. 13), nonlinear but always with higher SD values. Similar relationships can be found in all years with high coefficients of determination larger than 0.96 for MERIS and 0.89 for OLCI, AMD ranging from 4.9 m to 6.5 m, and RMD ranging from 36.2% to 58.7% (Tables 8 and 9).

The summary of pixel-based comparison of yearly MERIS/OLCI - derived SD values using the Doron11 and Lee15 algorithms in Lake Malawi during the study period is found in Table 9. The absolute mean difference (AMD) is calculated as averaged |Doron11_SD – Lee15_SD|, and the relative mean difference (RMD) is calculated as averaged |Doron11_SD – Lee15_ SD|/ Lee15_ SD × 100.

Table 8. Summary of pixel-based comparison of yearly estimated SD values using Doron11 algorithm and those using Lee15 algorithm in Lake Malawi during the study period.

Year	R^2	Regression Equation	AMD (m)	RMD (%)
2003	0.99	$y = (0.00012)x^4+(-0.0054)x^3+(0.04)x^2+(1.51)x+(0.06)$	5.6	48.1
2004	0.98	$y = (0.00013)x^4+(-0.0050)x^3+(0.04)x^2+(1.53)x+(-0.10)$	5.2	42.5
2005	0.98	$y = (0.00024)x^4+(-0.0094)x^3+(0.09)x^2+(1.32)x+(0.34)$	5.8	45.0
2006	0.99	$y = (0.00025)x^4+(-0.0088)x^3+(0.07)x^2+(1.54)x+(-0.17)$	6.5	48.9
2007	0.98	$y = (0.00035)x^4+(-0.0131)x^3+(0.13)x^2+(1.18)x+(0.45)$	5.7	46.8
2008	0.99	$y = (0.00021)x^4+(-0.0074)x^3+(0.05)x^2+(1.61)x+(-0.23)$	5.7	46.6
2009	0.98	$y = (0.00030)x^4+(-0.0111)x^3+(0.10)x^2+(1.32)x+(0.25)$	5.8	48.7
2010	0.98	$y = (0.00053)x^4+(-0.0205)x^3+(0.23)x^2+(0.60)x+(1.54)$	5.7	50.0
2011	0.96	$y = (0.00072)x^4+(-0.0271)x^3+(0.31)x^2+(0.28)x+(1.91)$	5.9	47.1
2017	0.89	$y = (0.00020)x^4+(-0.0105)x^3+(0.20)x^2+(-0.20)x+(3.69)$	5.5	36.2
Average	0.97		5.7	46.0

Although their coefficient of determination shows a high correlation as shown in (Fig. 13) the error analysis indexes show that there is a considerable difference between Lee15 and Doron11 results. While the two algorithms originate from different theories, they still produce estimations that are highly correlated.

In terms of SD spatial distribution, both yearly and monthly results show similar pattern characterized by low SD along the West shore and the southern part of the lake. In Lake Malawi, there is an influence from the inflow rivers, and they can highly determine the change in SD depending on the amount of rain and suspended matters and other substances drained into the lake from the watershed. The results from, January, February, and April show the lowest SD values in the northern region from both algorithms. The West and South regions are lower in February, July, and August; this feature can only be detected from Lee15 results. This is due to the low SD values estimated by Lee15. The difference within the water body is more visible from Lee15 results than Doron11, especially in the low SD regions. Since Doron11 estimated higher values than Lee15, the highest SD value was also found in January from Doron11. See Figure 14 for more detailed monthly spatial distribution of SD.

January	February	March
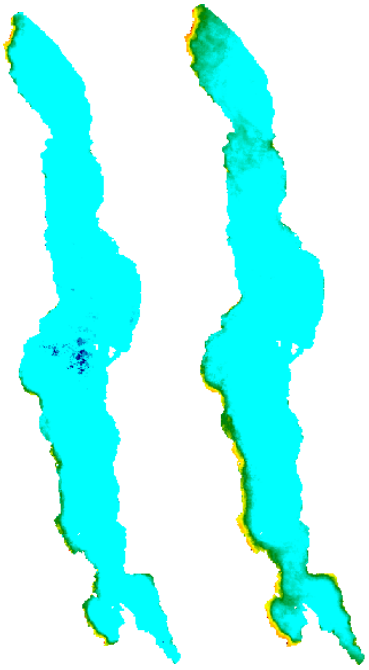	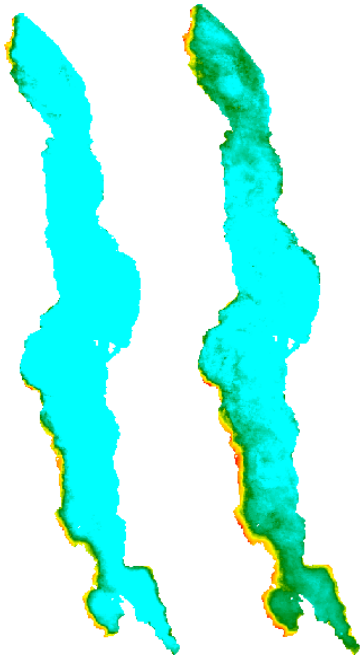	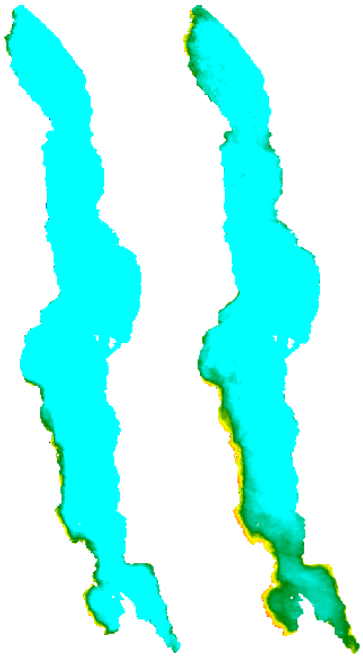

April	May	June
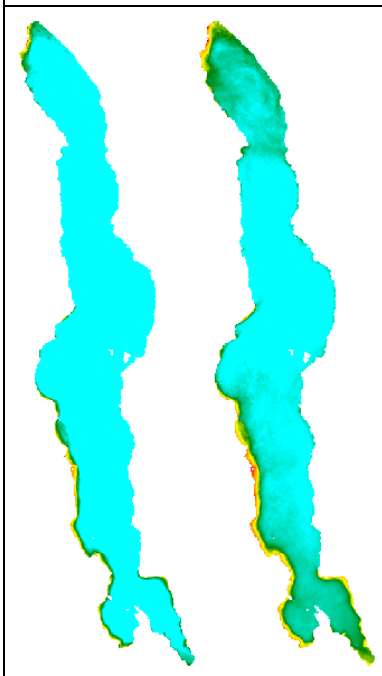	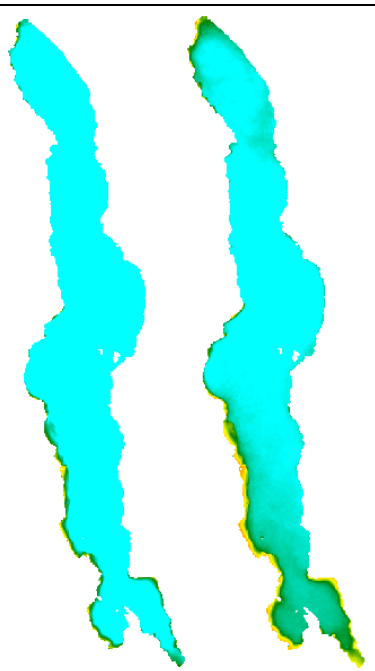	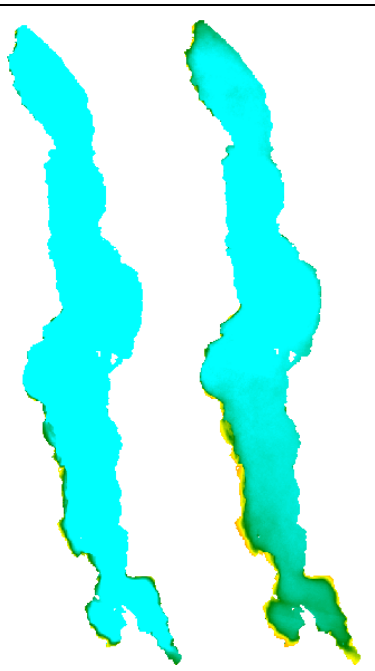
July	**August**	**September**
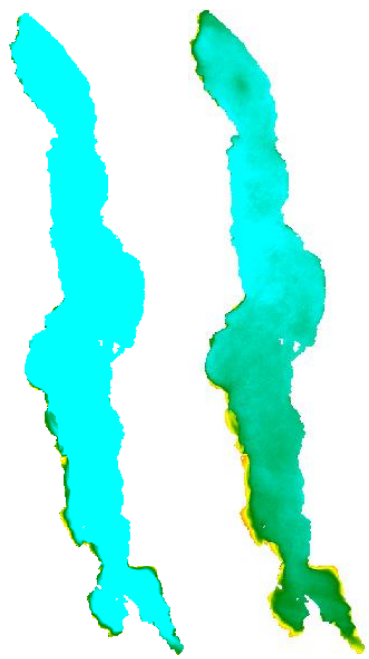	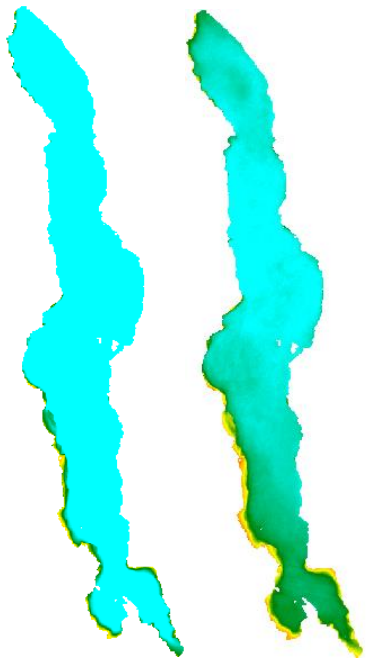	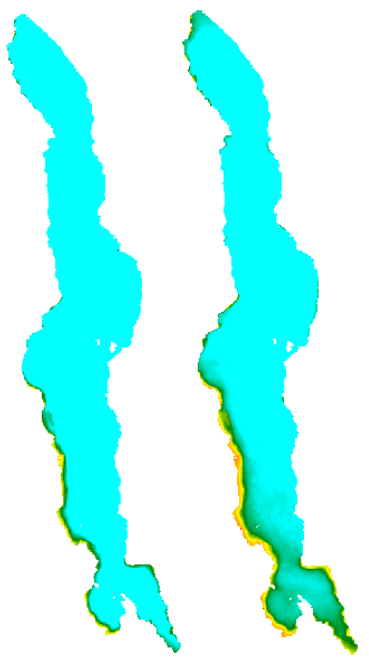

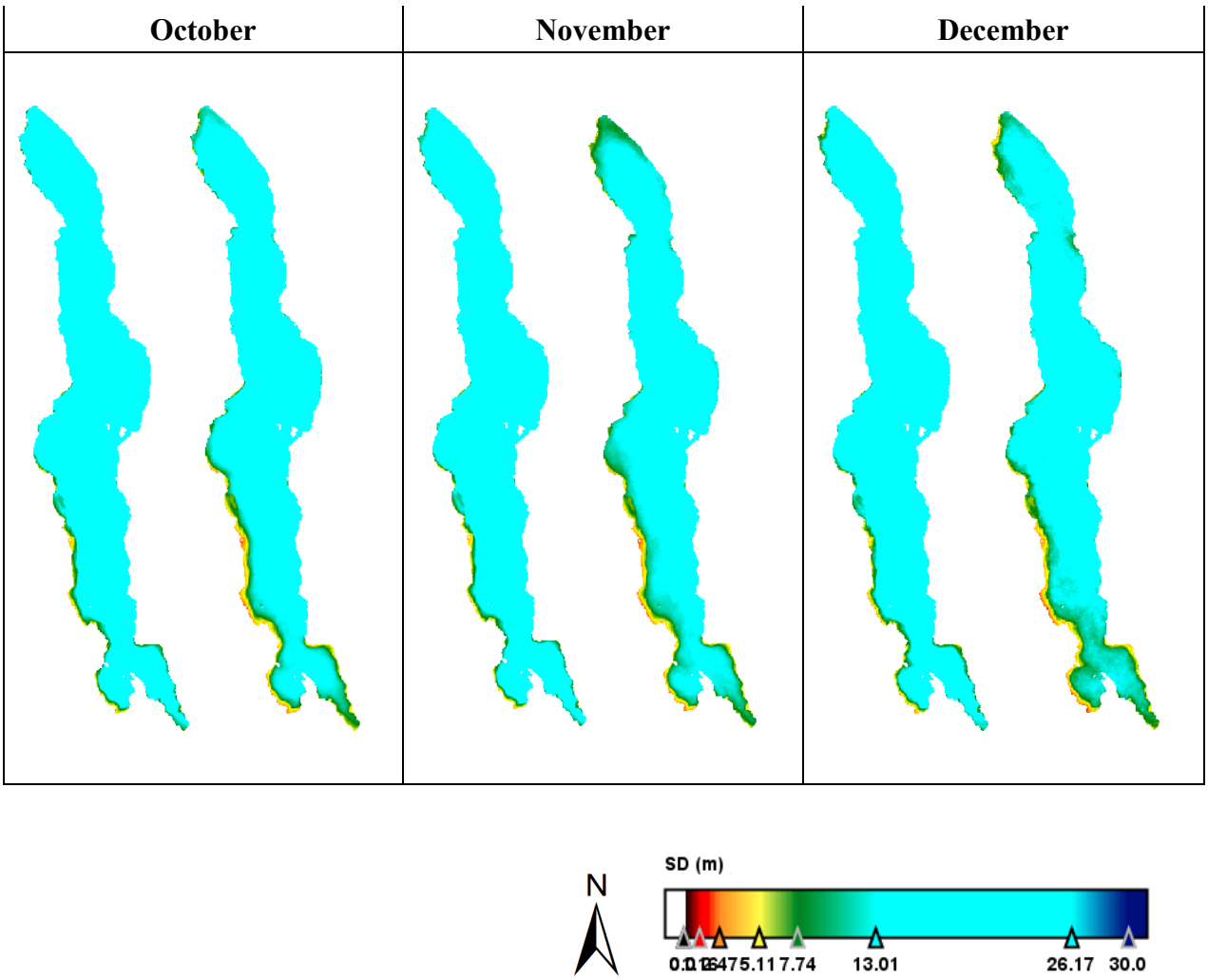

Figure 14. Distribution maps of the results from the two algorithms for the monthly average data during the 2003-2011 study period. Left: Doron11 and right: Lee15.

The scatter plot regarding the monthly comparison of the two algorithms results also illustrates a similar trend as the yearly data, where most of the pixels are concentrated in the higher SD levels.

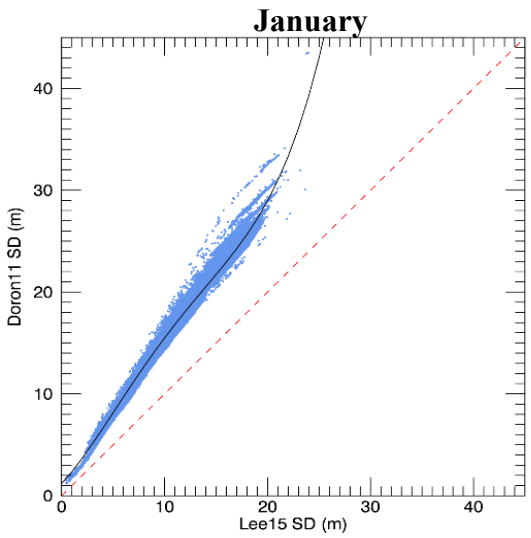
January
Doron11 SD (m)
Lee15 SD (m)
0
10
20
30
40

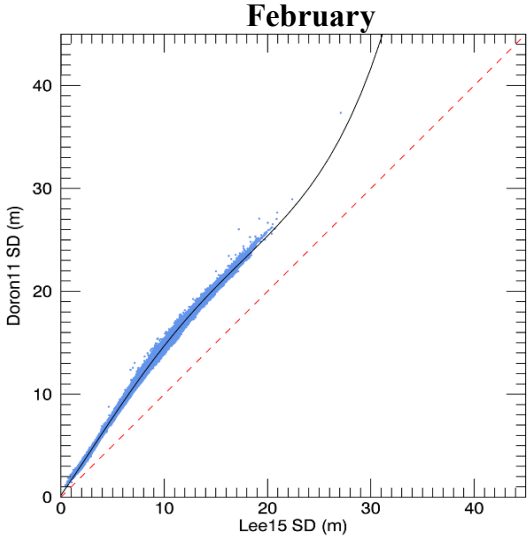
February
Doron11 SD (m)
Lee15 SD (m)
0
10
20
30
40

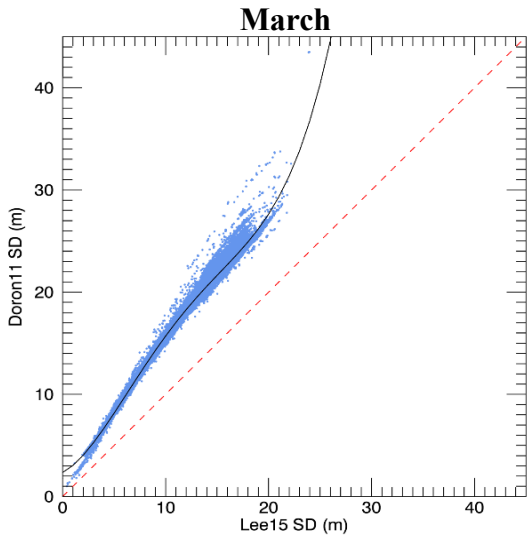
March
Doron11 SD (m)
Lee15 SD (m)
0
10
20
30
40

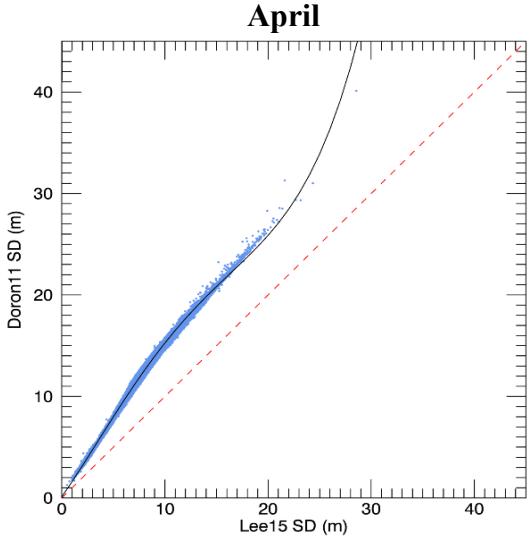
April
Doron11 SD (m)
Lee15 SD (m)
0
10
20
30
40

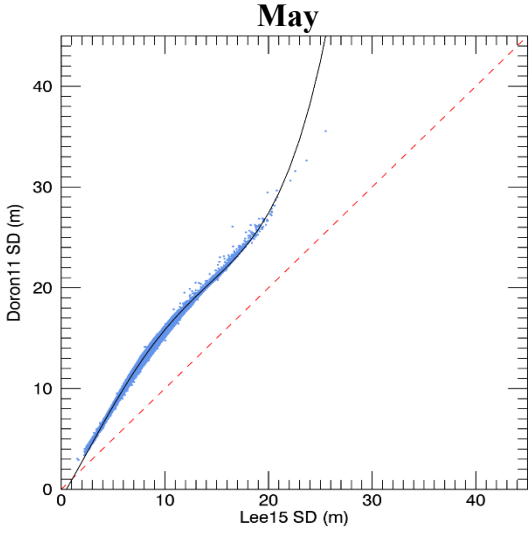
May
Doron11 SD (m)
Lee15 SD (m)
0
10
20
30
40

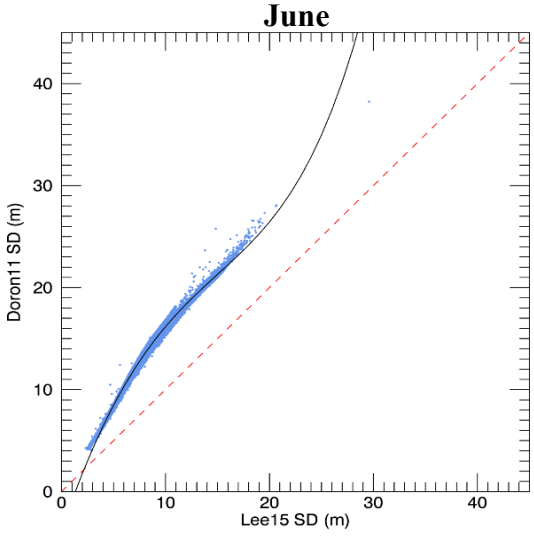
June
Doron11 SD (m)
Lee15 SD (m)
0
10
20
30
40

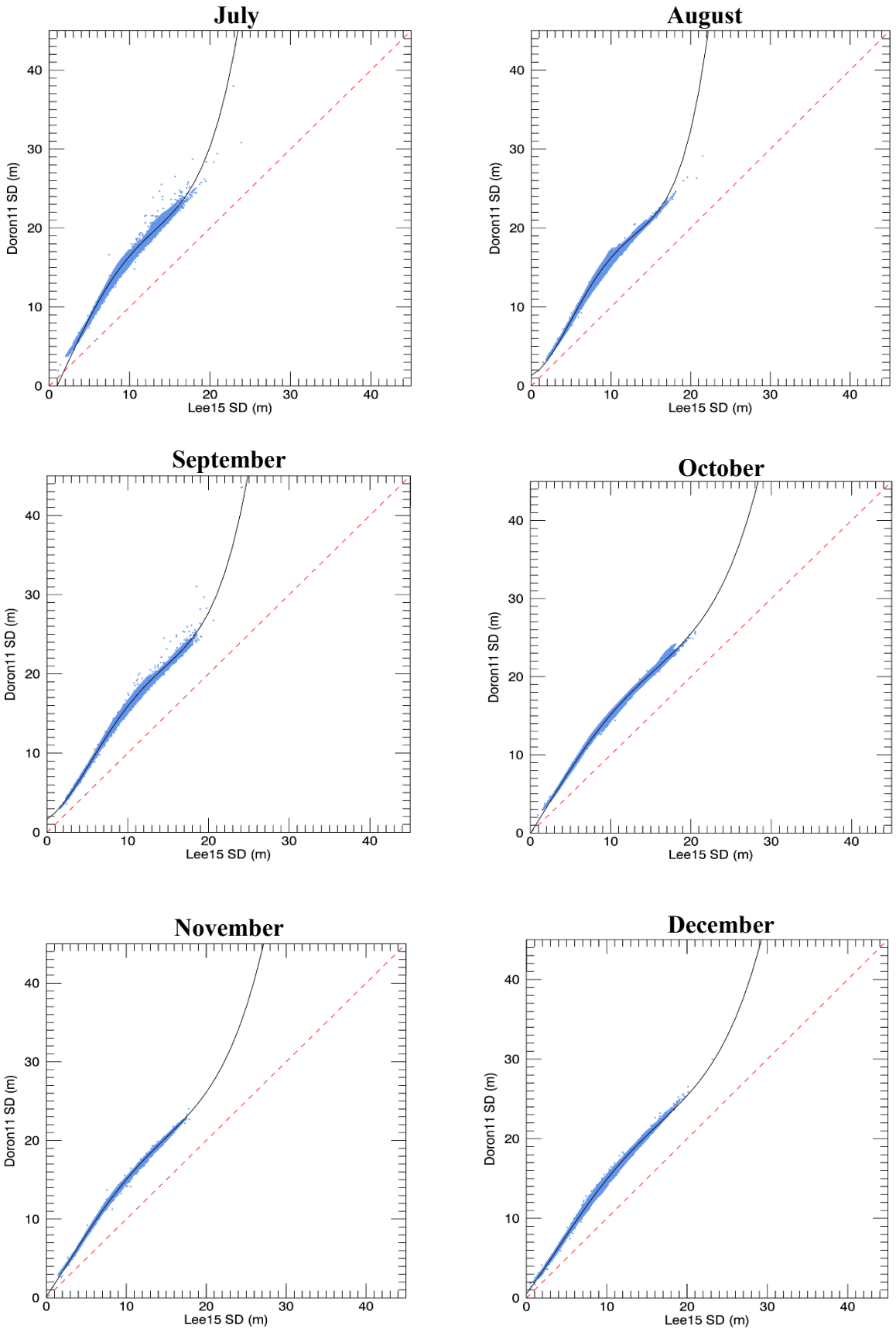

Figure 15. Pixel-based comparison of monthly estimated SD values using Doron11 algorithm

and those using Lee15 algorithm in Lake Malawi.

The summary of pixel-based comparison of monthly MERIS-derived SD values using the Doron11 algorithm and those using Lee15 algorithms in Lake Malawi during the study period is found in Table 9. The absolute mean difference (AMD) is calculated as averaged |Doron11_SD – Lee15_SD|, and the relative mean difference (RMD) is calculated as averaged |Doron11_SD – Lee15_SD|/ Lee15_SD × 100.

Table 9. Summary of pixel-based comparison of monthly estimated SD values using Doron11 algorithm and those using Lee15 algorithm in Lake Malawi during the study period.

Month	R^2	Regression Equation	AMD (m)	RMD (%)
Jan	0.98	$y = (0.00024)x^4+(-0.0093)x^3+(0.10)x^2+(1.07)x+(1.20)$	6.5	47.3
Feb	0.99	$y = (0.00008)x^4+(-0.0035)x^3+(0.03)x^2+(1.45)x+(0.18)$	4.9	42.7
Mar	0.98	$y = (0.00033)x^4+(-0.0145)x^3+(0.19)x^2+(0.52)x+(2.35)$	6.3	48.1
Apr	0.99	$y = (0.00015)x^4+(-0.0061)x^3+(0.05)x^2+(1.45)x+(0.12)$	5.5	46.4
May	0.98	$y = (0.00028)x^4+(-0.0094)x^3+(0.06)x^2+(1.72)x+(-0.87)$	5.9	48.9
Jun	0.98	$y = (0.00005)x^4+(0.0011)x^3+(-0.11)x^2+(2.98)x+(-3.73)$	6.2	51.8
Jul	0.97	$y = (0.00042)x^4+(-0.0124)x^3+(0.06)x^2+(2.12)x+(-2.13)$	6.4	58.7
Aug	0.97	$y = (0.00090)x^4+(-0.0323)x^3+(0.35)x^2+(0.37)x+(1.34)$	6.0	54.2
Sept	0.98	$y = (0.00046)x^4+(-0.0184)x^3+(0.22)x^2+(0.63)x+(1.66)$	6.1	45.9
Oct	0.99	$y = (0.00014)x^4+(-0.0049)x^3+(0.02)x^2+(1.63)x+(-0.08)$	5.2	37.0
Nov	0.99	$y = (0.00018)x^4+(-0.0064)x^3+(0.05)x^2+(1.49)x+(0.19)$	5.2	40.0
Dec	0.99	$y = (0.00014)x^4+(-0.0057)x^3+(0.05)x^2+(1.33)x+(0.55)$	5.2	40.3
Average	0.98		5.8	46.8

The combination of the two algorithms gave $R^2 \geq 0.89$. The annual results show a minimum $R^2 = 0.89$ and a maximum of $R^2 = 0.99$, which is like the monthly results, but the minimum is 0.97. On average the AMD and RMD are 5.8 m and 46.8 % for monthly data and 5.8 m and 47.1% for yearly respectively.

Figure 16 shows comparisons of in situ measured SD in 2007 and corresponding estimated SD values from MERIS data using Doron11 and Lee15 algorithms. First, all available in situ measured SD were compared to the estimated SD values from the closest MERIS data without consideration of the time difference between satellite acquisition day and in situ sampling day (Fig. 16a, b, N = 173). In this comparison, the maximum time difference was 31 days. The results show that the Lee15 algorithm generally performed better than the Doron11 algorithm with smaller RMSE value of 2.1 m (4.87 m for Doron11) and MAPE value of 30.76% (83.94% for Doron11). The SD values derived from the Doron11 algorithm showed obvious overestimations. In contrast, the SD values derived from the Lee15 algorithm almost distribute around the 1:1 line. However, the correlations between the estimated and in situ measured SD values are weak for both algorithms, although they were significant ($R = 0.24$ and $p < 0.001$ for both).

Second, it was compared the in situ measured and MERIS data estimated SD values only for the same day data to reduce effects due to dynamic variation of water quality (Fig. 16c, d, N = 23). Results revealed that the RMSE and MAPE values were reduced to 1.86 m and 21.01% using the Lee15 algorithm, and 3.68 m and 66.87% with the Doron11 algorithm. In addition, the correlation coefficients were increased to 0.63 for the Lee15 algorithm and 0.65 for the Doron11 algorithm (p <0.001). In this comparison, the Lee15 algorithm outperformed the Doron11 algorithm.

Third, it was further compared in situ measured and MERIS-derived SD values for matchups with a time gap smaller than 3h by considering NASA's recommendation (Bailey and Werdell, 2006) and the high dynamic variation of water quality in the southeast arm of Lake

Malawi (Fig. 16e, f, N = 12). Results showed that the RMSE and MAPE values were further reduced to 1.17 m and 18.7% for Lee15 algorithm, with a correlation coefficient of 0.66 (p < 0.05) and slope of 0.74. However, the RMSE and MAPE values using Doron11 algorithm were slightly increased with an insignificant correlation between the measured and estimated SD values (R = 0.52, but p > 0.05). This comparison also demonstrated that the Lee15 algorithm performed better than the Doron11 algorithm.

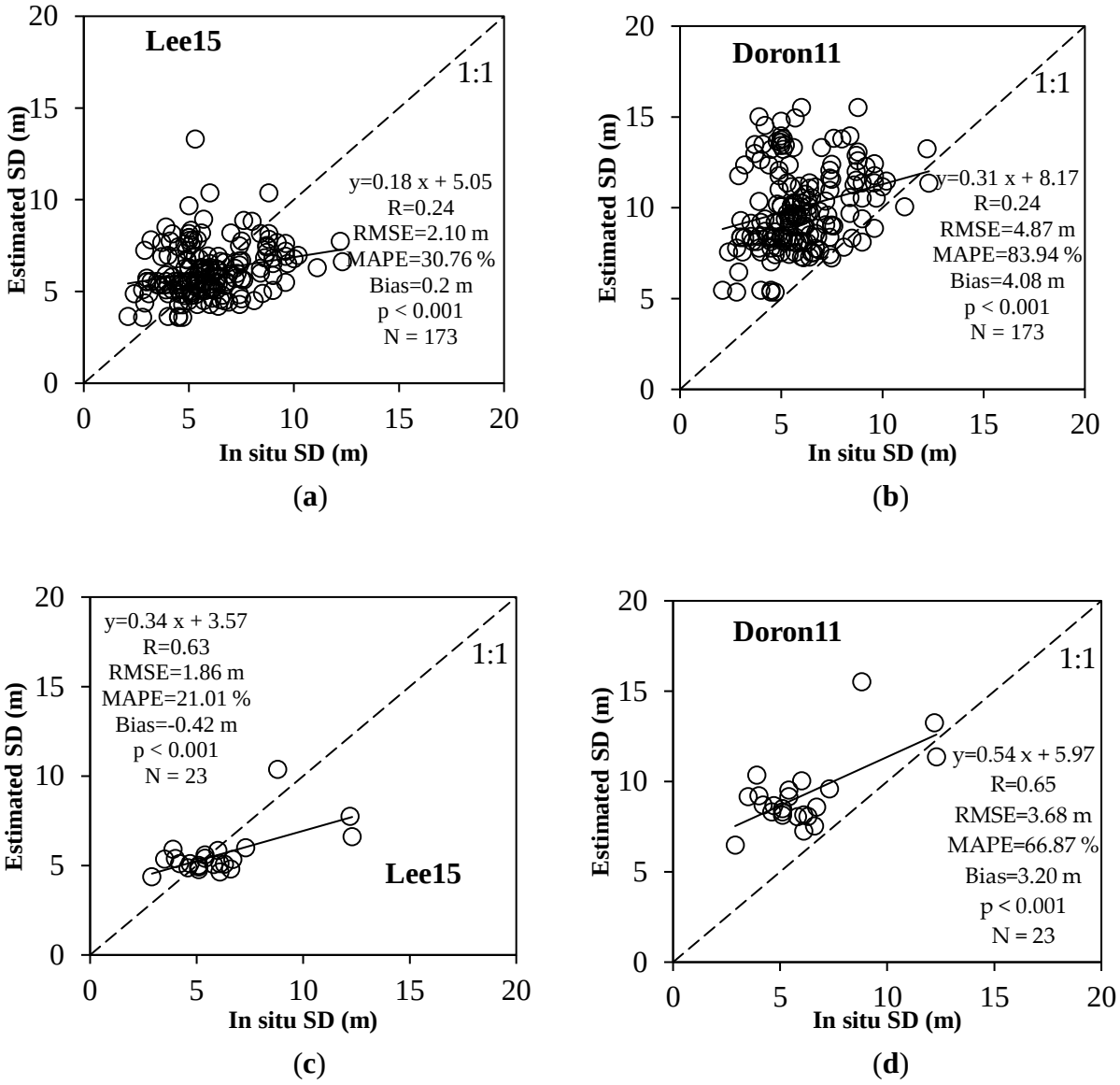

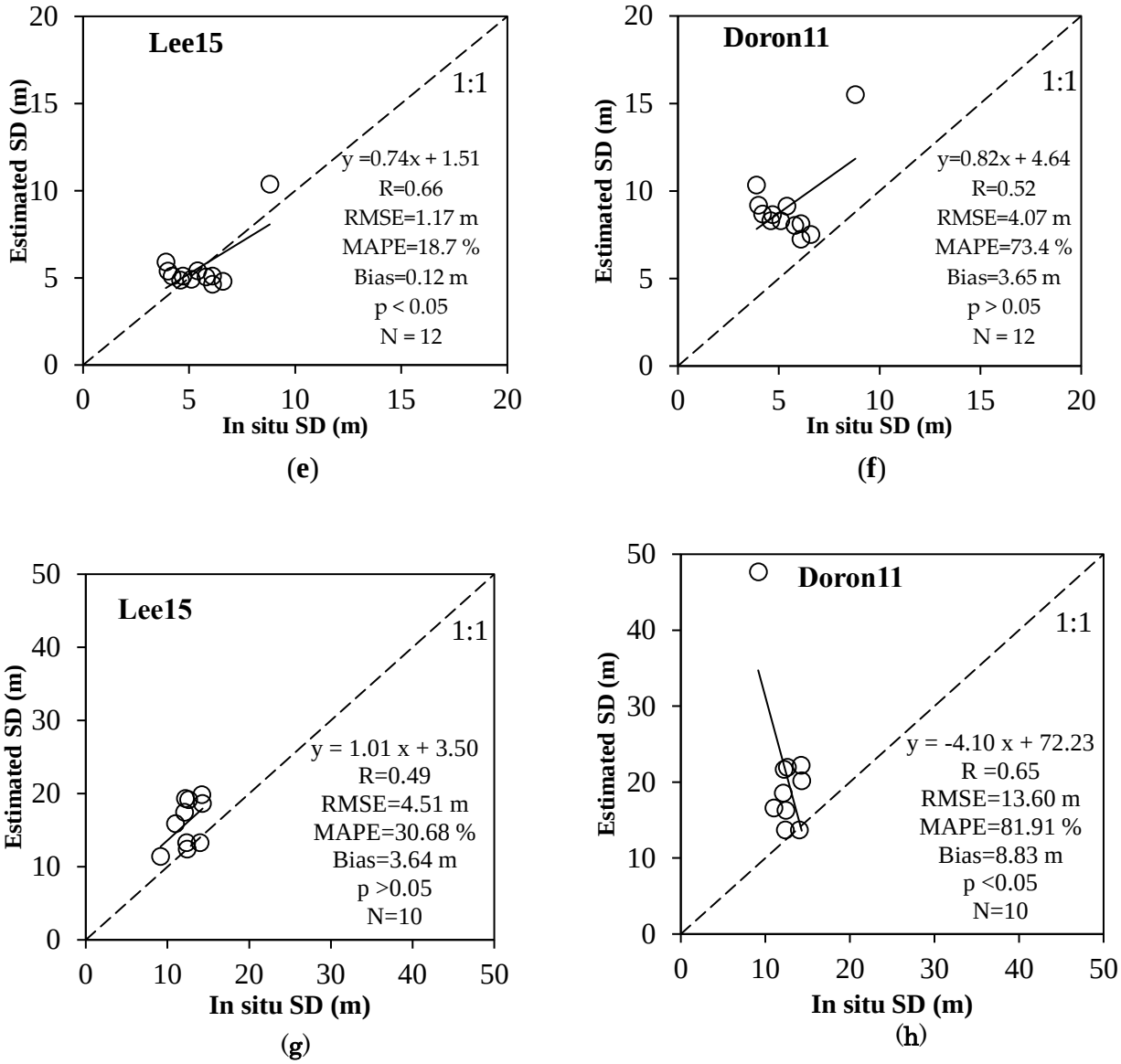

Figure 16. Comparison of in situ measured SD and estimated SD values from MERIS data. (a) using Lee15 algorithm for all available in situ SD measurements; (b) using Doron11 algorithm for all available in situ SD measurements; (c) using Lee15 algorithm for pairs at the same day; (d) using Doron11 algorithm for pairs at the same day; (e) using Lee15 algorithm for matchups within 3 h; (f) using Doron11 algorithm for matchups within 3 h, and (g) using OLCI for Lee15 on the same day as the sampling data; (h) using OLCI for Doron11.

The validation process of the 2017 data (Fig. 16g, h) was done under some limitations. The time gap between the measured and estimated data period had a difference of more than 3 h, thus restraining the possibility of having several combinations with a shorter time difference.

The closest dataset between the measured and estimated was on the same day as the satellite sensing day. In this pair of data, Lee15 had R = 0.49 and Doron11, R = 0.65. However, the other error evaluation indexs showed that Lee15 had better performance than Doron11 (RMSE = 4.51 m vs 13.60 m; MAPE = 30.68% vs 81.91%; Bias = 3.64 m vs 8.83 m). As it was shown from the 2017 SD map, the SD values from Doron11 were higher than Lee15's thus resulting in overestimation (Fig.16).

These validation results give useful information on the consistency of the performance of both algorithms yet applied to 'different' satellite sensors. The results from Lee15 suggest that this algorithm is suitable for estimating SD from Lake Malawi as it was earlier tested by Lee et al. (2015, 2016) in water bodies with the SD range of Lake Malawi in terms of clarity. With the recent progress in the field of remote sensing and its application, and the free access to a 'good' set of data, using these two-sensor data would be a good opportunity to start a long-term change study over African lakes in general and Lake Malawi in particular. However, the accuracy of OLCI results is yet to be confirmed.

2.5.2. Evaluation of Water Transparency in Lake Malawi

After the better performance of Lee15 over Doron11 was confirmed through the validation process, Lee15's results were then used as input for the water transparency evaluation. Figure 17 shows yearly water transparency level maps in Lake Malawi, which were generated from the yearly SD distribution maps (obtained from MERIS/OLCI data using the Lee15 algorithm) based on the OECD classification system (i.e.Table 7). The yearly percentages for each water transparency level are summarized in Table 10. From Figure 17 and Table 10, it is seen that: (1) Lake Malawi maintained four transparency levels throughout the period from 2003-2011 and 2017; (2) waters with transparency level 1 accounting for the largest area in the lake (58.7% -

84.6%), followed by waters with transparency level 2 (12.1% - 37.5%), level 3 (2.2% - 3.6%), and transparency level 4 (0.1% - 0.8%); (3) waters with transparency levels 3 and 4 always distributed along the southwestern and southern lakeshores, and sometimes found in the northern part (e.g., in 2004); (4) the largest change of transparency levels was found between level 1 and level 2; (5) waters with transparency levels 1 and 2 accounted for more than 95% of the lake.

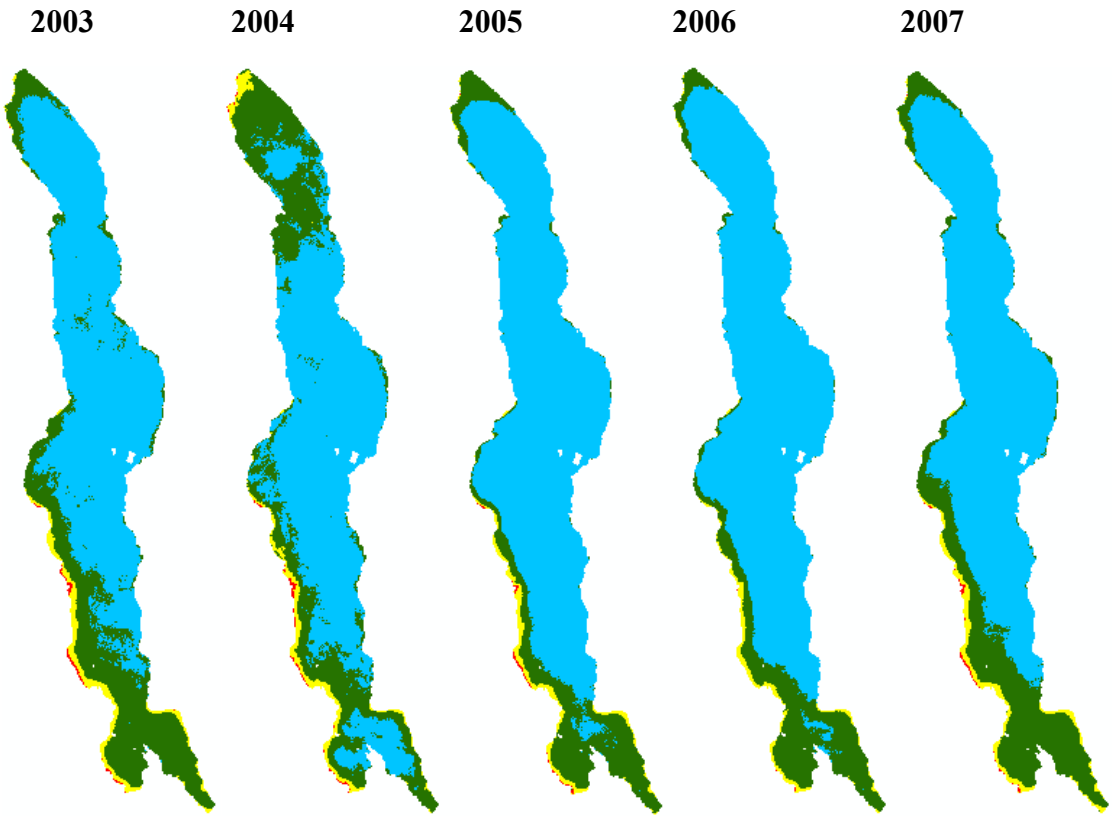

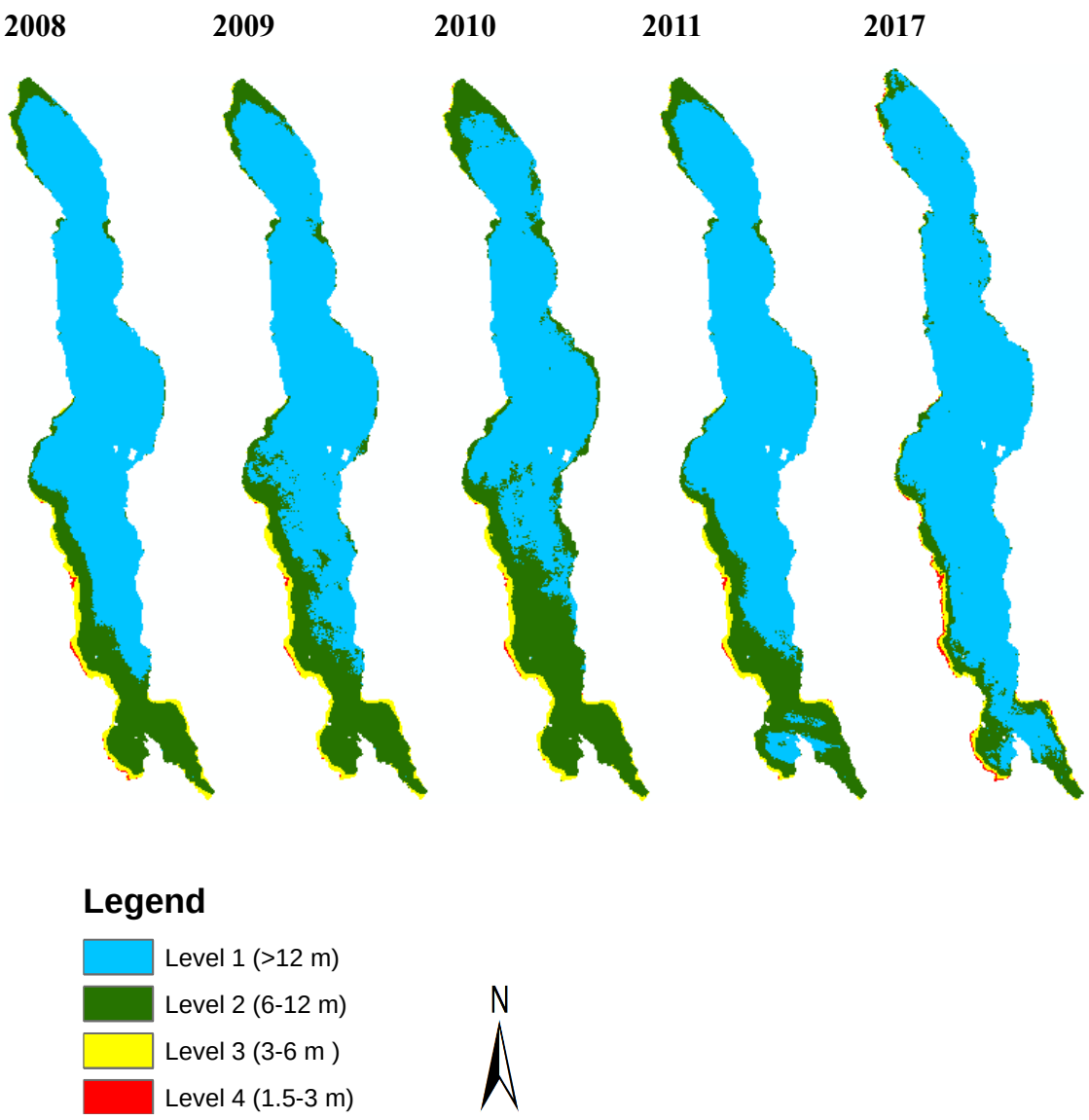

Figure 17. Yearly water transparency level maps in Lake Malawi. These maps were generated from yearly SD distribution maps (obtained from MERIS/OLCI data using Lee15 algorithm) based on OECD (1982) classification system.

Figure 18 shows monthly water transparency level maps in Lake Malawi, which were generated from monthly SD distribution maps (obtained from MERIS data using the Lee15 algorithm) based on OECD classification system (OECD, 1982). From Figure 18 and Table 11, there were several noticeable seasonal variations of SD in Lake Malawi. First, the SD values

during October - January were generally higher than in other months, and more than 78.5% water area was classified as transparency level 1 during this period. Second, the lake water was more turbid in February, April, July, and August than in other months due to water areas with transparency level 2 constituting more than 31.3% in these months, especially in July the lake was dominated by water transparency level 2 (59.4%). Third, Lake Malawi was dominated by transparency levels 1 and 2 throughout the year (more than 95%), but other two water transparency levels (i.e., levels 3 and 4) were also found in the lake for each month.

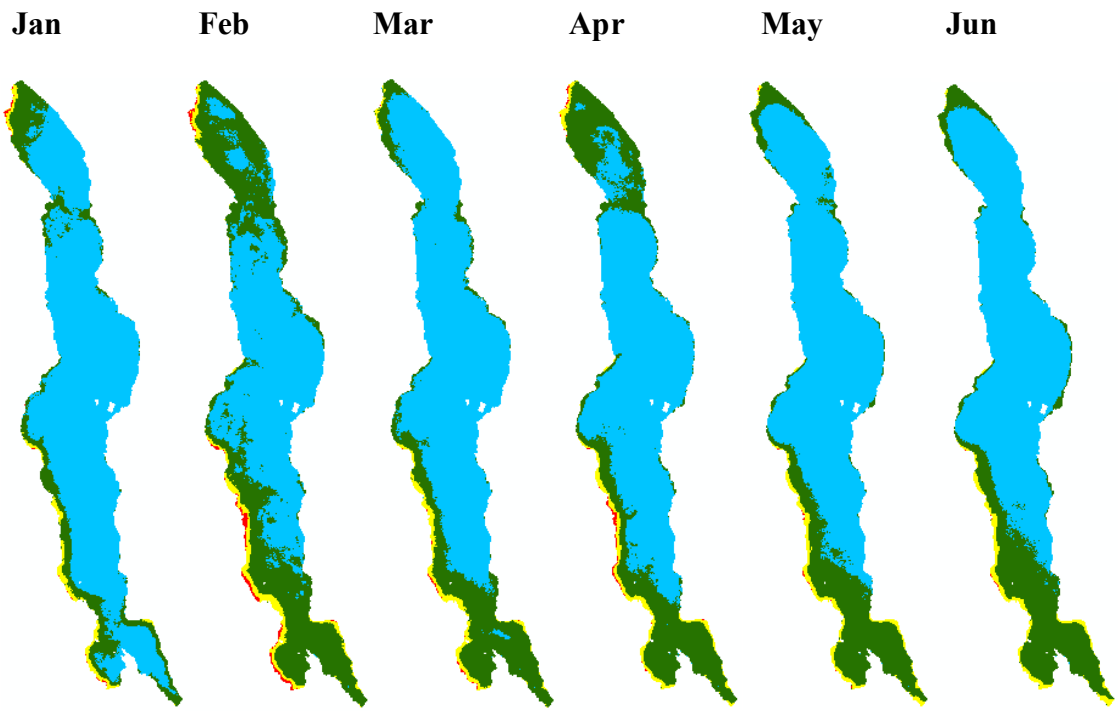

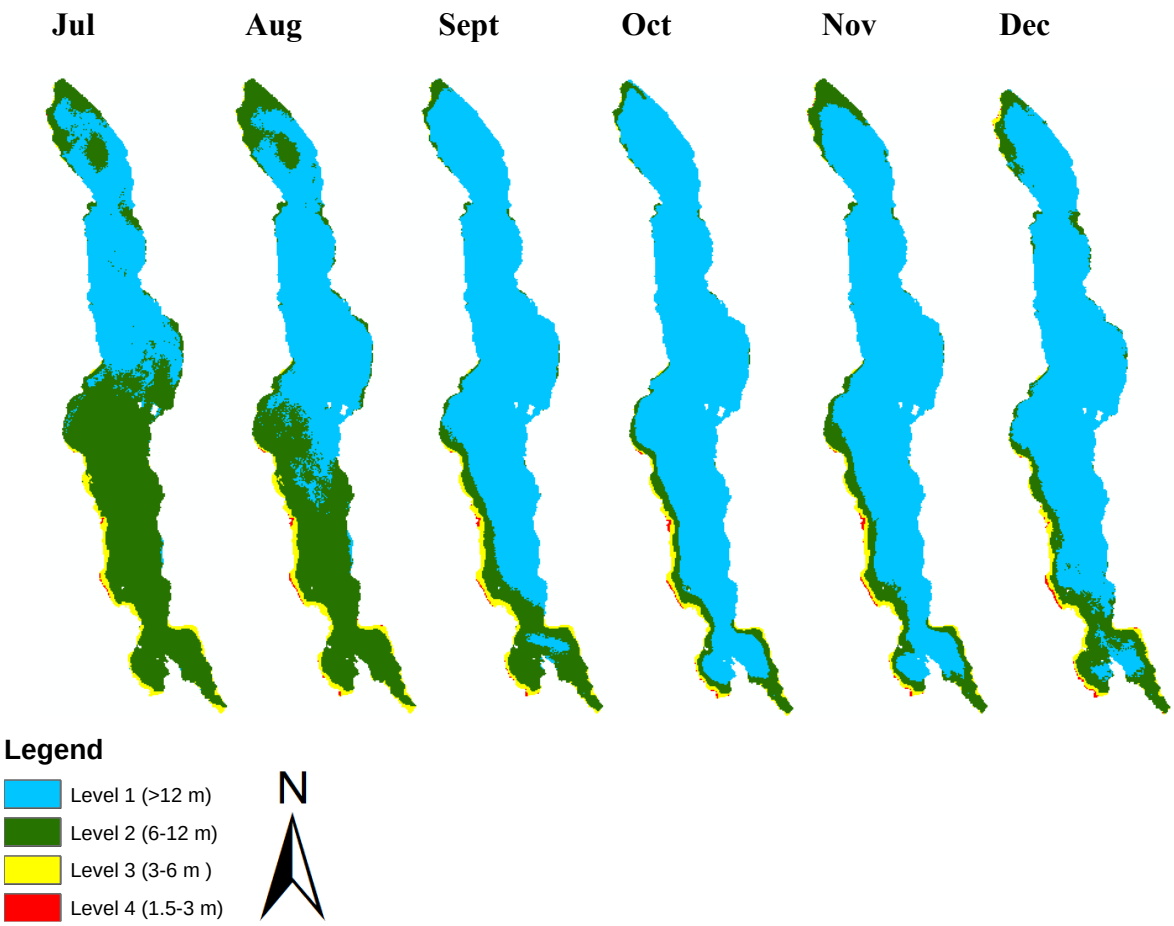

Figure 18. Monthly water transparency level maps in Lake Malawi. These maps were generated from monthly SD distribution maps (obtained from MERIS data using Lee15 algorithm) based on (OECD, 1982) classification system.

Table 10. The yearly percentage for each water transparency level shown in (Fig. 17).

Year	Level 1(%)	Level 2(%)	Level 3(%)	Level 4(%)
2003	67.6	28.4	3.6	0.4
2004	65.5	30.5	3.6	0.4
2005	79.7	17.3	2.8	0.2
2006	80.0	17.7	2.2	0.1
2007	72.5	23.9	3.3	0.3
2008	73.6	22.5	3.6	0.3
2009	68.6	27.6	3.6	0.2
2010	58.7	37.5	3.6	0.2
2011	74.5	22.8	2.5	0.2
2017	84.6	12.1	2.5	0.8
Average	72.5	24.0	3.1	0.3

Table 11. The monthly percentage for each water transparency level shown in (Fig. 18).

Month	Level 1(%)	Level 2(%)	Level 3(%)	Level 4(%)
Jan	81.4	16.0	2.4	0.2
Feb	53.8	40.8	4.2	1.2
Mar	73.7	23.0	3.1	0.2
Apr	64.7	31.3	3.5	0.5
May	72.2	24.5	3.2	0.1
Jun	70.0	26.7	3.2	0.1
Jul	37.1	59.4	3.4	0.1
Aug	50.9	45.1	3.8	0.2
Sept	78.5	17.9	3.4	0.2
Oct	87.5	9.5	2.7	0.3
Nov	82.4	14.7	2.6	0.3
Dec	79.2	17.4	3.0	0.4
Average	69.3	27.2	3.2	0.3

The yearly average results show that from 2003 there is a low SD value which then increased straight to 2006. From 2006 it dropped constantly until 2010 and from there increased all the way to 2017. Between 2005 and 2007, there was a peak in 2006. The lowest values of SD were found in 2010 and the highest in 2017. The trend line shows that SD in Lake Malawi increased from 2003 to 2017 (Fig. 19a). However, if the 2017 results are removed from the long term-analysis, then 2003-2011 results indicate that SD reduced during this period (Fig.19b). Additionally, if the overestimation is deducted from the 2017 results, (Fig. 19c) similar trend is found as in Figure 19b. Whether 2017 is included or not in the long-term analysis, the results indicate no significant change along the time as $p > 0.05$ in all three cases.

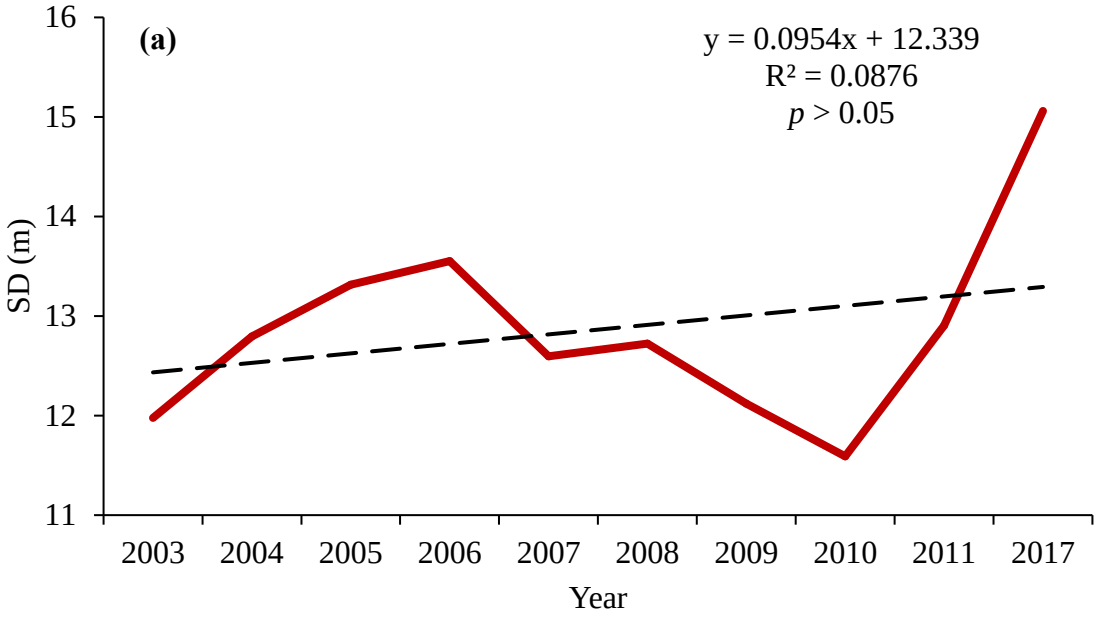
(a)
y = 0.0954x + 12.339
R² = 0.0876
p > 0.05
SD (m)
16
15
14
13
12
11
2003
2004
2005
2006
2007
2008
2009
2010
2011
2017
Year

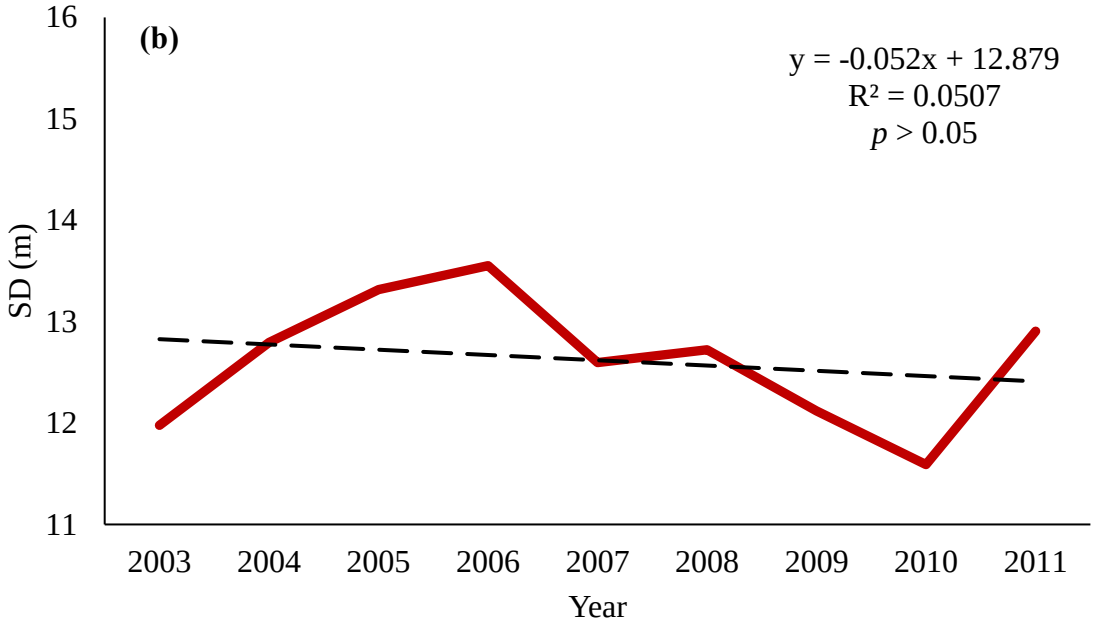
(b)
y = -0.052x + 12.879
R² = 0.0507
p > 0.05
SD (m)
16
15
14
13
12
11
2003
2004
2005
2006
2007
2008
2009
2010
2011
Year

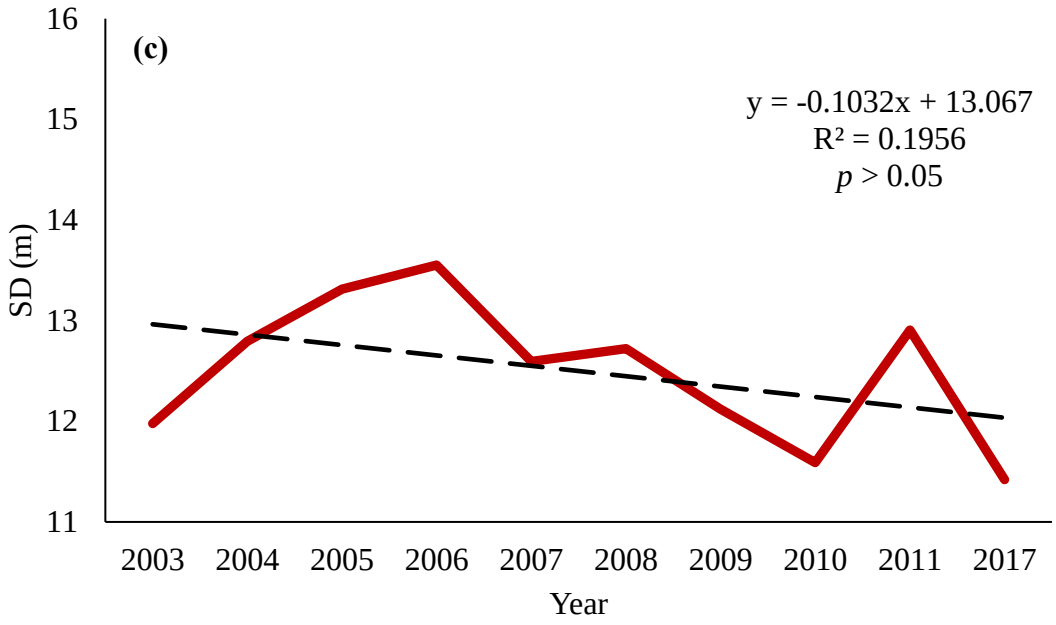

Figure 19. Yearly averaged SD from (2003-2017) (a), (b) (2003-2011), (c) (2003-2017 subtracted overestimation) in Lake Malawi (red solid line); the black dashed (---) line represents the trend line.

The seasonal change was also analyzed, and the results show that there is one cycle in terms of SD variation. The first phase of the cycle goes from August to March with a sudden drop in February, and this first phase has higher SD values than the other phase which starts from April down to July constantly descending. Figure 20 shows the temporal change of average SD during the study period for the monthly data.

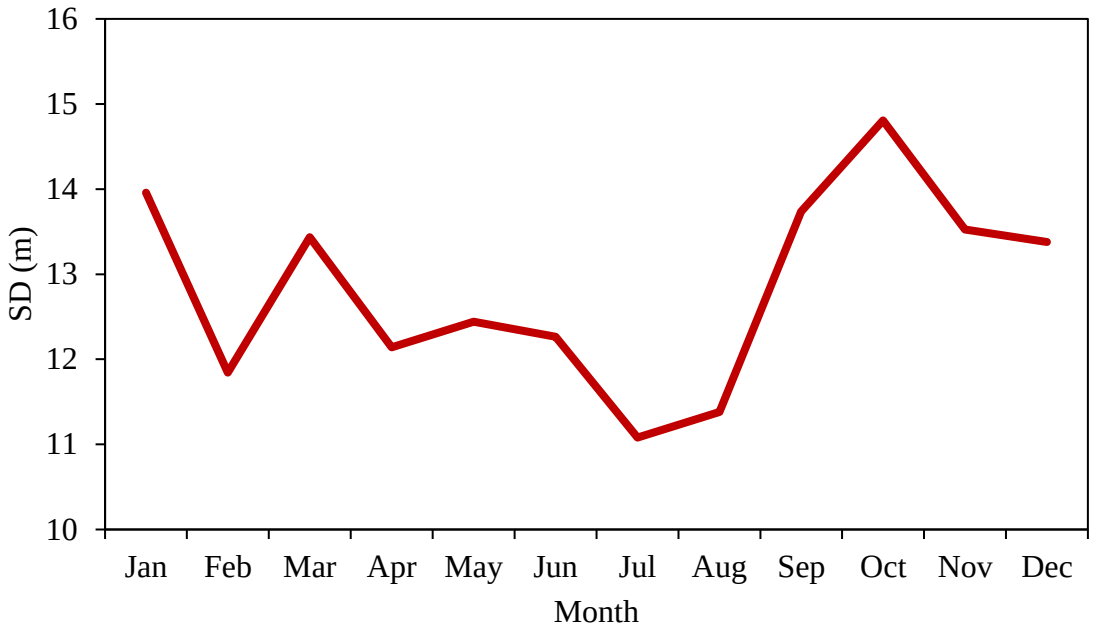

Figure 20. Temporal variability of SD during the study period, showing the lowest SD value in July and two negative peaks, in February and April.

2.6. Discussion

In this study, two semi-analytical algorithms were compared (i.e., Doron11 and Lee15) by applying them to Lake Malawi to estimate SD values from MERIS data (2003-2011) and OLCI data (2017). The results showed that although the two algorithms were developed based on different underwater visibility theories (i.e., classic and new), SD estimations using the two algorithms are highly correlated with R^2 larger than 0.96 for MERIS and OLCI, $R^2 = 0.89$ (Tables 8 and 9). Lee et al. (2018) also reported a high $R^2 = 0.89$ when comparing the relationship between the two algorithms with simulation data. These results indicate that there is no substantial difference between the two algorithms, especially if only one algorithm is used to evaluate water transparency change in a waterbody.

However, it was found that the Doron11 algorithm always gave higher SD estimations than the Lee15 algorithm, with an averaged AMD value of 5.8 m in Lake Malawi. A similar trend was

also found by Lee et al. (2018). In addition, by comparing the SD estimations from the two algorithms to in situ SD measurements, it was found that Lee15 algorithm outperformed Doron11 algorithm with a MAPE value of 18.7% (Fig. 16e). In contrast, the Doron11 algorithm overestimated SD values with the MAPE value of 73.4% (Fig. 16f). These findings indicate that water quality would probably be overestimated if one used SD values from Doron11 algorithm. For example, if used the SD distribution maps generated using the Doron11 to classify water transparency levels, it was found that on average more than 94% of Lake Malawi were classified as level 1 and the sum of levels 3 and 4 were less than 1%, and thus probably resulted in an over evaluation for Lake Malawi.

Preisendorfer (1968) reported that the value of the numerator of Equation (15) (i.e., Γ) could vary from 5 to 10. In the present study, the values of Γ were calculated in a range of 7.5–8.3, with an average of 7.9, within the range of initially published values. Therefore, it is considered that the overestimations of SD values by Doron11 mainly derived from the denominator of Equation (15) (i.e., $K_d(v) + c\ (v)$). Previous studies have pointed out that it is difficult to directly estimate $c\ (v)$ from R_{rs} because of the ratio's requirement of the backscattering and scattering coefficients, which cannot be obtained from R_{rs} (Doron et al., 2007). In addition, it is well known that the ratio of the backscattering and scattering coefficients can vary temporally and spatially (Doron et al., 2007; Twardowski et al., 2001; Loisel et al., 2007; Stramska et al., 2000). The Lee15 algorithm overcomes this difficulty because the algorithm requires only K_d. Therefore, Lee15 algorithm can be considered more robust than the Doron11 algorithm. However, it was still found some overestimations in lower SD values and underestimations in higher SD values with the Lee15 algorithm (Fig. 16), indicating that further improvements of the algorithm are necessary.

As mentioned in the introduction, there is no routine monitoring of water transparency in Lake Malawi due to the financial and institutional constraints in the surrounding countries (Ballatore et al., 2014). In addition, even though there have been several studies measuring SD

values by field surveys, it is difficult to use these measurements to evaluate water transparency or its changes for the entire lake, because all these studies focused on only a small part of the lake for a short period of time. For example, Gondwe (2009) investigated seasonal variation of SD in the southeast Arm of Lake Malawi (see Fig. 8) and reported that SD values ranged from 2.1 to 12.3 m; however, 79% of the SD values were between 4 and 8 m. Later, Macuiane et al. (2016) reported that SD values were between 2 and 6 m in the southeast part of the lake in 2012. In addition, Weyl et al. (2010) reported that SD values were between 12 and 20 m in Lake Malawi.

None of the previous studies could show water transparency status for the entire surface of Lake Malawi, which, based on the results presented here, always has four transparency levels (SD values ranging from 1.5 m to > 12 m). The SD distribution maps generated from MERIS/OLCI data can show not only the different water transparency levels, and the percentage and spatial distribution of each level, but also their seasonal and annual variations (Fig. 17 and 18). Such information is useful for lake water management. Therefore, it is considered that the combination of satellite data and the semi-analytical algorithm (Lee15) to be a useful tool for routinely monitoring water quality in Lake Malawi.

These results also showed that turbid waters (transparency levels 3 and 4) in Lake Malawi are mainly distributed along the southwestern lakeshore. This is probably because most of the inflowing rivers, population, and rainfall are concentrated in the southwestern watershed of the lake (Nicholson et al., 2014). Although no significant water transparency changes were found in Lake Malawi during the study period (2003-2011, 2017), continuous monitoring of the lake's water transparency remains necessary.

As pointed out by a previous study, loss of biodiversity due to fishing and nearshore water quality impacts has been a threat to Lake Malawi (Bootsma and Jorgensen, 2004). The information on the water quality of Lake Malawi provided in this study can be used to help in the management of the lake and its basin.

Chapter 3 Evaluation of trophic states in Lake Malawi during 2003-2017

Wang et al. (2018) focused on the assessment of the trophic states of the global inland waters using MODIS-derived Forel-Ule index (FUI) with results showing that within the water bodies considered in their study the eutrophic large lakes were in central Africa, eastern Asia, and mid-northern and southeast North America. Among the considered lakes only 3 were from Africa, of which 2 were considered eutrophic and 1 oligotrophic. When the lakes were analyzed based on their regional location, Lake Malawi was not considered as part of the African Great Lakes.

According to Weyl et al. (2010) Lake Malawi receives drained material from the watershed in the form of inflow from rivers during the long and heavy rainy season carrying nitrogen, phosphorus, and other nutrients and the atmospheric deposition due to burning, thus increasing productivity in the lake.

A long and intense practice of agriculture and other activities in the watershed can lead to an increase of nutrients in the lake resulting in eutrophication which is a process characterized by excess of nutrients in a water body (Bennett et al., 2001) but generally, this process is natural and takes time to occur if no human influence is detected. However, due to the water demands from the population living within the lake's basin, an increase in population and urbanization, the possibilities of increase in nitrogen and phosphorus to the lake are higher. The possibility of an increase of nutrients could put the fish diversity and the population in jeopardize due to increasing in phytoplankton in the lake.

Lake Malawi is generally qualified as oligotrophic (Macuiane et al., 2016, Chavula et al., 2009) with an average chlorophyll concentration of 1 mg/m^3. Bootsma and Jorgensen (2004) stated that Lake Malawi could be classified between oligotrophic to mesotrophic, considering its

Chl-a productivity. Weyl et al. (2010) considered the lake but with attention to the southern region and areas around major rivers which are mostly on the West shore as becoming increasingly eutrophic.

Most of these studies were based on empirical observations which are time and space specific, and thus the difficulty in determining the precise trophic state of Lake Malawi, its spatial and temporal variation, and evaluate qualitatively and quantitatively.

In Lake Malawi, an objective and descriptive evaluation of its trophic state are necessary. The focus of this chapter is on the qualitative and spatiotemporal evaluation of the trophic state of Lake Malawi based on Carlson's TSI (Carlson, 1977).

Several studies have been carried out based on Carlson's TSI (Saluja and Garg, 2017; Cunha et al., 2013; Sheela et al., 2011; Watanabe et al., 2015; Cheng and Lei, 2001; Lillesand et al., 1983; Jarosiewicz et al., 2011; Adamovich et al., 2016; Bekteshi and Cupi, 2014). Saluja and Garg (2017) performed the spatial and temporal evaluation of the Bhindawas Lake in India and found that the lake's trophic state varied between eutrophic and hypereutrophic. Membrillo-Abad et al. (2016) estimated the TSI of Lake Chapala in Mexico by combining the in situ measured water quality parameters (Chl-a and SD) and remotely sensed data. According to Cheng and Lei (2001) Carlson's TSI is based on empirical relationships of the water quality parameters of a water body, thus its modification is desirable to meet the specific characteristics of each water body. Based on this assumption, studies such as Membrillo-Abad et al. (2016), Cunha et al. (2013), Sheela et al. (2011), and Sługocki and Czerniawski (2018) were carried out and the original equations from Carlson's TSI were tuned into the target water bodies. Duan et al. (2007) performed a digital evaluation of Landsat TM data and field spectra measurements to estimate and map Chl-a and later converted into TSI. They concluded that Landsat TM data and in situ spectra could be used effectively to determine Chl-a concentration and evaluate the trophic state of their study area. Pomari et al. (2018) applied Carlson's TSI equations and other three derived equations to 8 tropical/subtropical reservoirs in Brazil. Their results indicated that

the original model overestimated the trophic levels whereas the modified ones had a better performance.

Considering the adjustable capability of the model to individual water bodies and independent evaluation of TSI, in this chapter, it is proposed the use of the TSI by Carlson (1977) combined with the water quality parameters derived from MERIS and OLCI sensor data, to help respond to the missing classification of Lake Malawi. For the calculation of TSI, Chl-a and SD from Lee15 algorithm were used as input in the individual regression analysis.

3.1. Estimation of chlorophyll-a concentration from MERIS and OLCI data using OC4E algorithm

NASA's standard MERIS algorithm OC4E was used to retrieve Chl-a from Lake Malawi using the R_{rs} from the earlier pre-processing steps. The algorithm is expressed as follows based on O'Reilly et al. (1998):

$$\text{Chla\_OC4E} = 10^{(0.3255-2.7677x+2.4409x^2-1.1288x^3-0.4990x^4)} \quad (23)$$

where x is the log_{10} of the maximum band ratio of the three bands at the Rrs_{443}, Rrs_{490}, Rrs_{510} to Rrs_{560} and the coefficients were derived using version 2 of the NASA bio-Optical Marine Algorithm Dataset (NOMAD).

The results of Chl-a distribution maps in Figure 21 and 22 show that the lake is clearer in the center (open waters) but the West shore and the southern region show high Chl-a concentration. The average Chl-a concentration for the entire dataset is about 0.69 mg/m^3, which is within the reported range (Chavula et al., 2009) but different from Macuiane et al. (2016) based on locally measured Chl-a in April 2012 (3.95 ± 0.19 µg/l in site 1, 4.79 ± 0.65 µg/l in site 2, and 5.54 ± 0.29 µg/l in site 3). In the present study, the average minimum is 0.55 mg/m^3 in 2017 and an average maximum of 0.92 mg/m^3 in 2003.

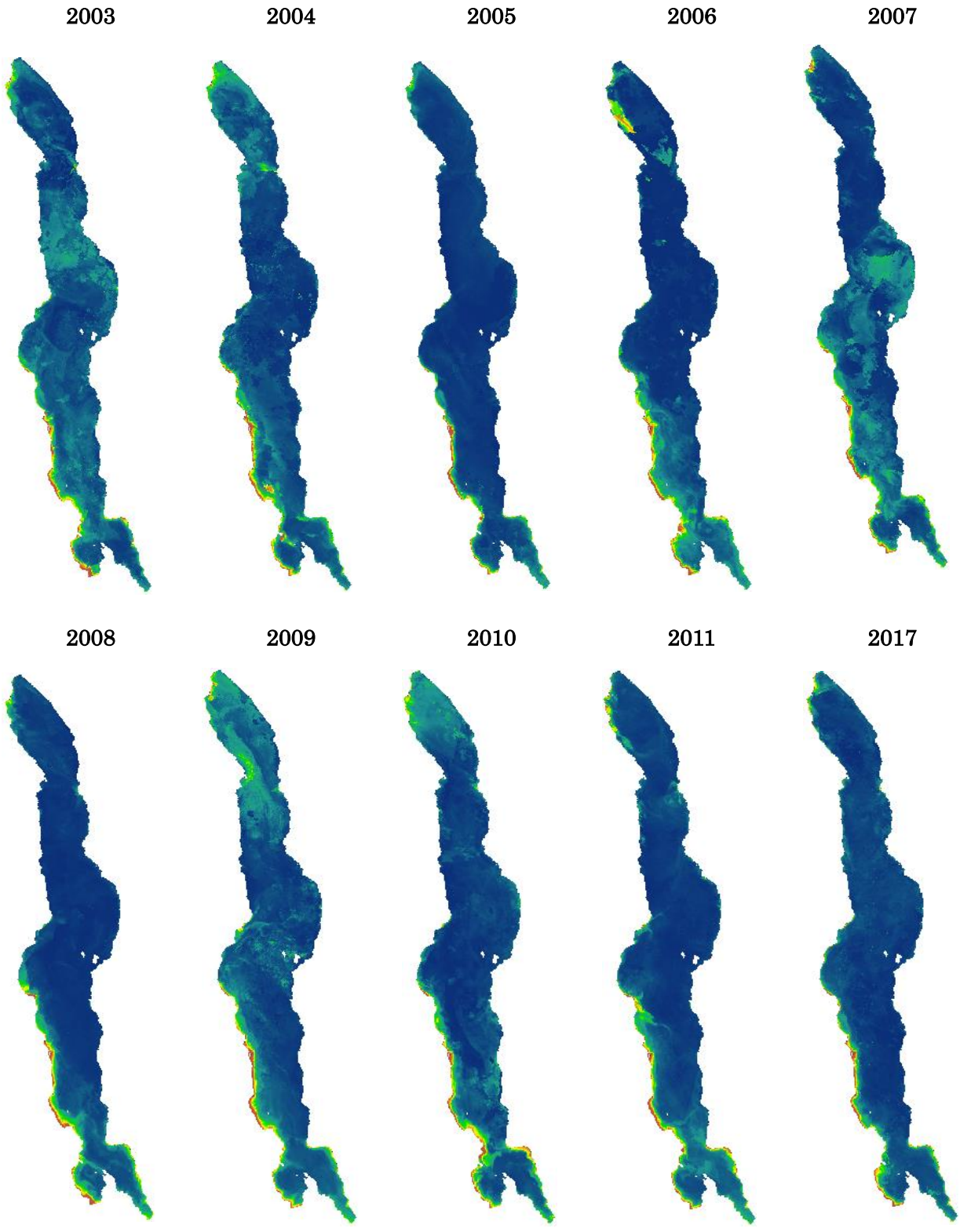

Figure 21. Yearly Chl-a spatial distribution for the entire lake.

Although high values of Chl-a are distributed along the shore, the area covered, and the values are still low. In terms of spatial distribution, both annual and monthly maps show similar pattern except for July and October where the concentration and area are higher than other months. High Chl-a concentration waters are along the shore and river mouth thus, denoting the influence from the rivers, and anthropogenic activities from the basin.

Comparatively, the Chl-a monthly distribution maps show more variations than the yearly. Like the yearly spatial distribution, the monthly maps show high Chl-a from the shore to the center of the lake and regions with strong influence from the inflow rivers. The results from the monthly Chl-a concentration yield average value of 0.73 mg/m^3 and an average minimum of 0.59 mg/m^3 in December and an average maximum of 0.96 mg/m^3 in July.

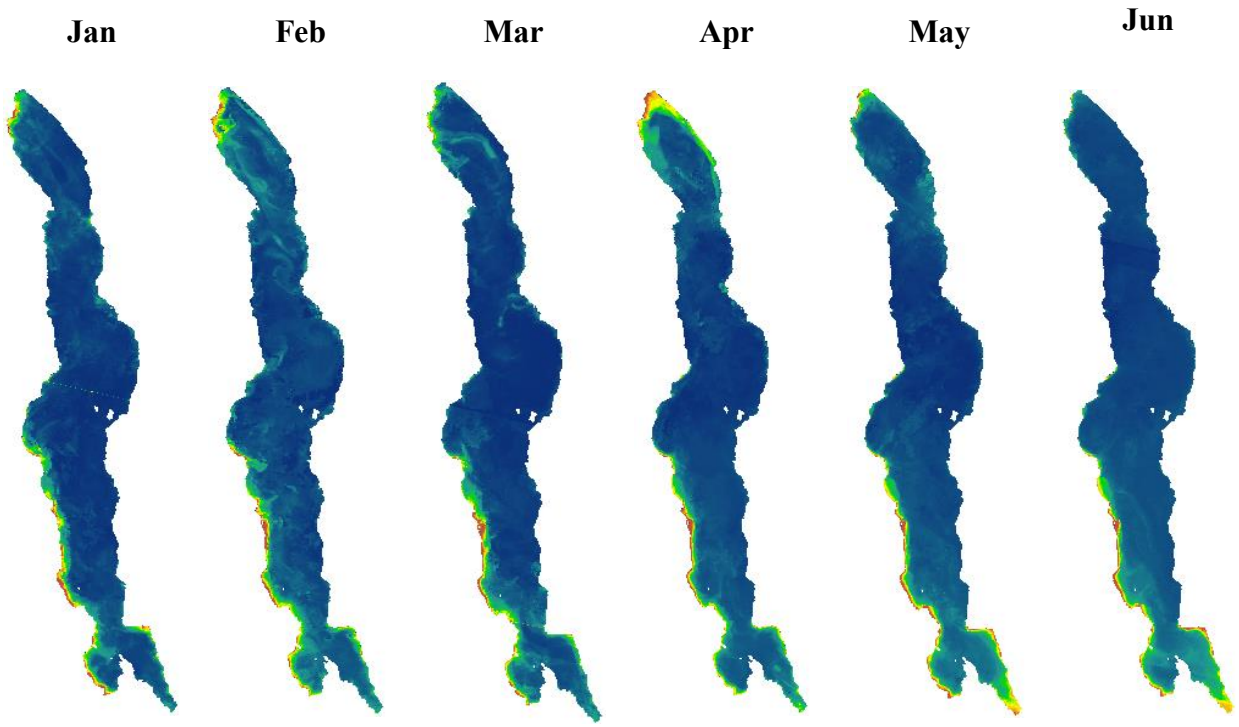

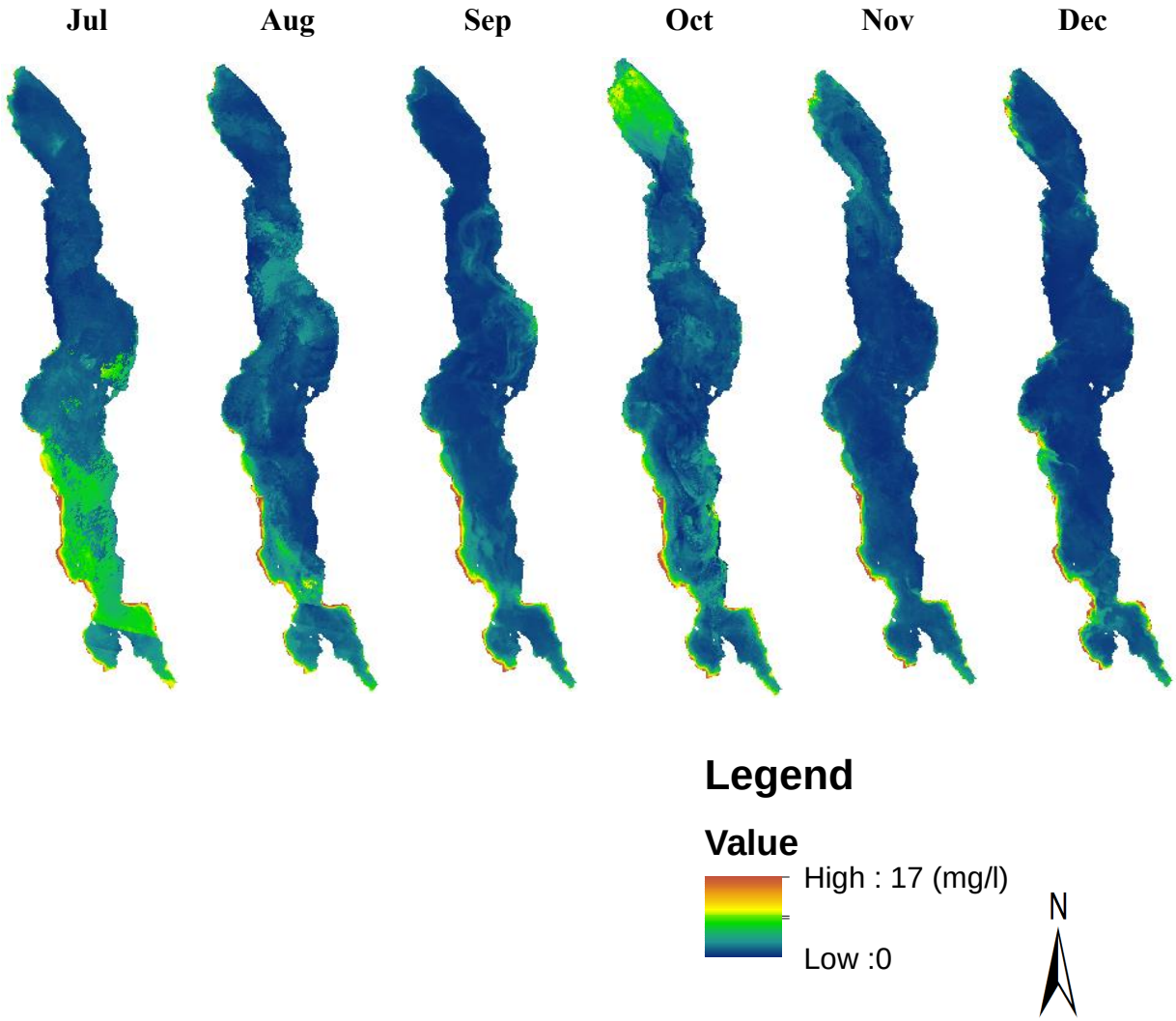

Figure 22. Monthly Chl-a spatial distribution for Lake Malawi from OC4E.

3.2. Adaptation of Carlson's Trophic State Index for Lake Malawi

From the traditional classification systems, three trophic states should be identified namely: oligotrophic: TSI < 40, mesotrophic: TSI 40-50 and eutrophic: TSI > 50 which could be found in any of the classification systems (Carlson, 1977; OECD, 1982). Carlson's TSI has been modified and applied to tropical lakes successfully (Cunha et al., 2013; Salas and Martino, 1991). This TSI

model converts the water quality parameters into a standard numerical scale ranging from 0 to 100. Cunha et al. (2013) developed and proposed a TSI model for tropical/subtropical reservoirs. In the results, they presented trophic state boundaries for TP and Chl-a and compared with other existing TSI boundaries.

In this study, regressions analysis was carried out between the satellite-derived SD data and the satellite-derived Chl-a data. These two parameters were transformed into natural logarithm, i.e. (ln (Chl-a) vs ln (SD)). This process was applied to both yearly and monthly SD and Chl-a data.

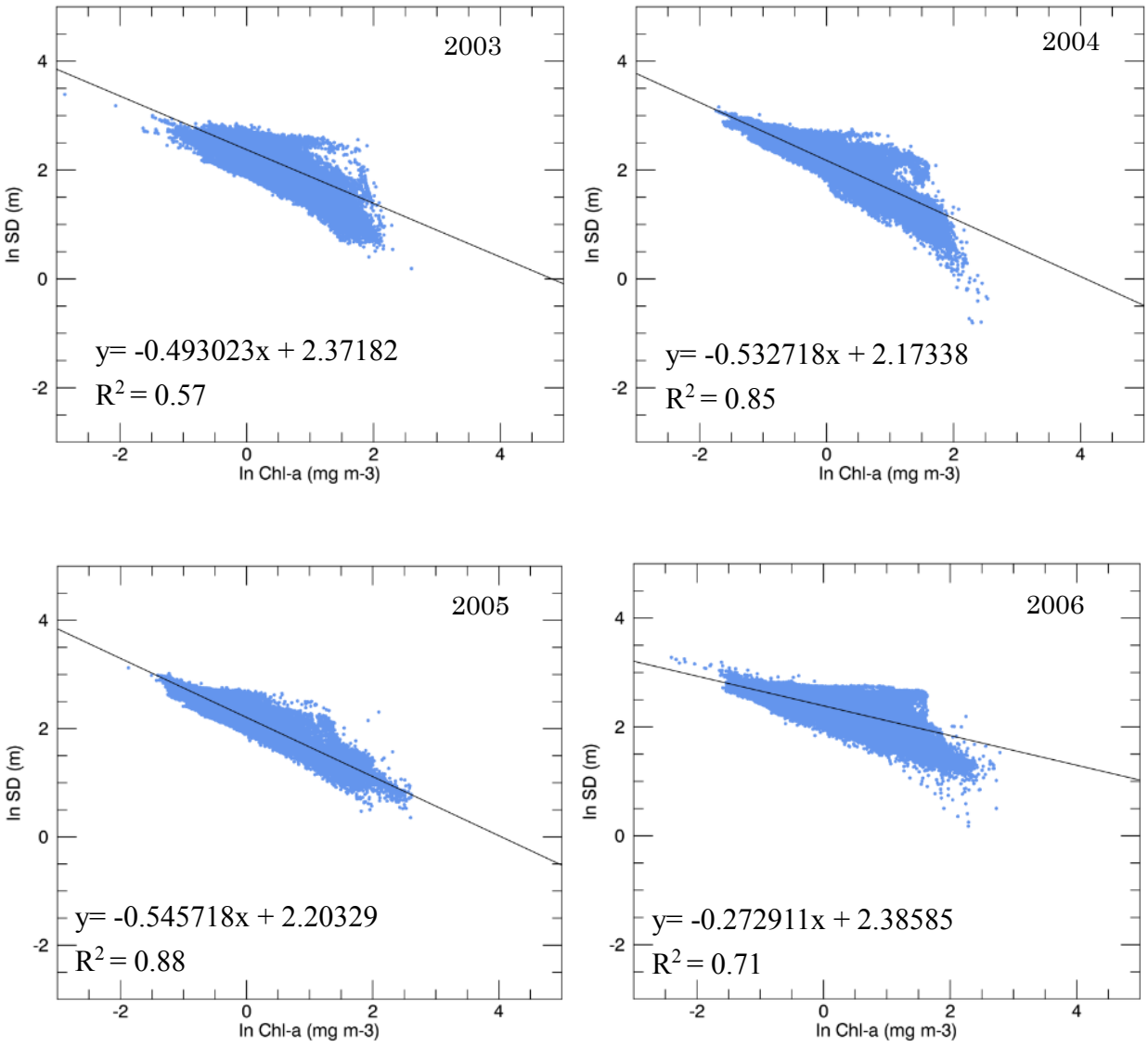

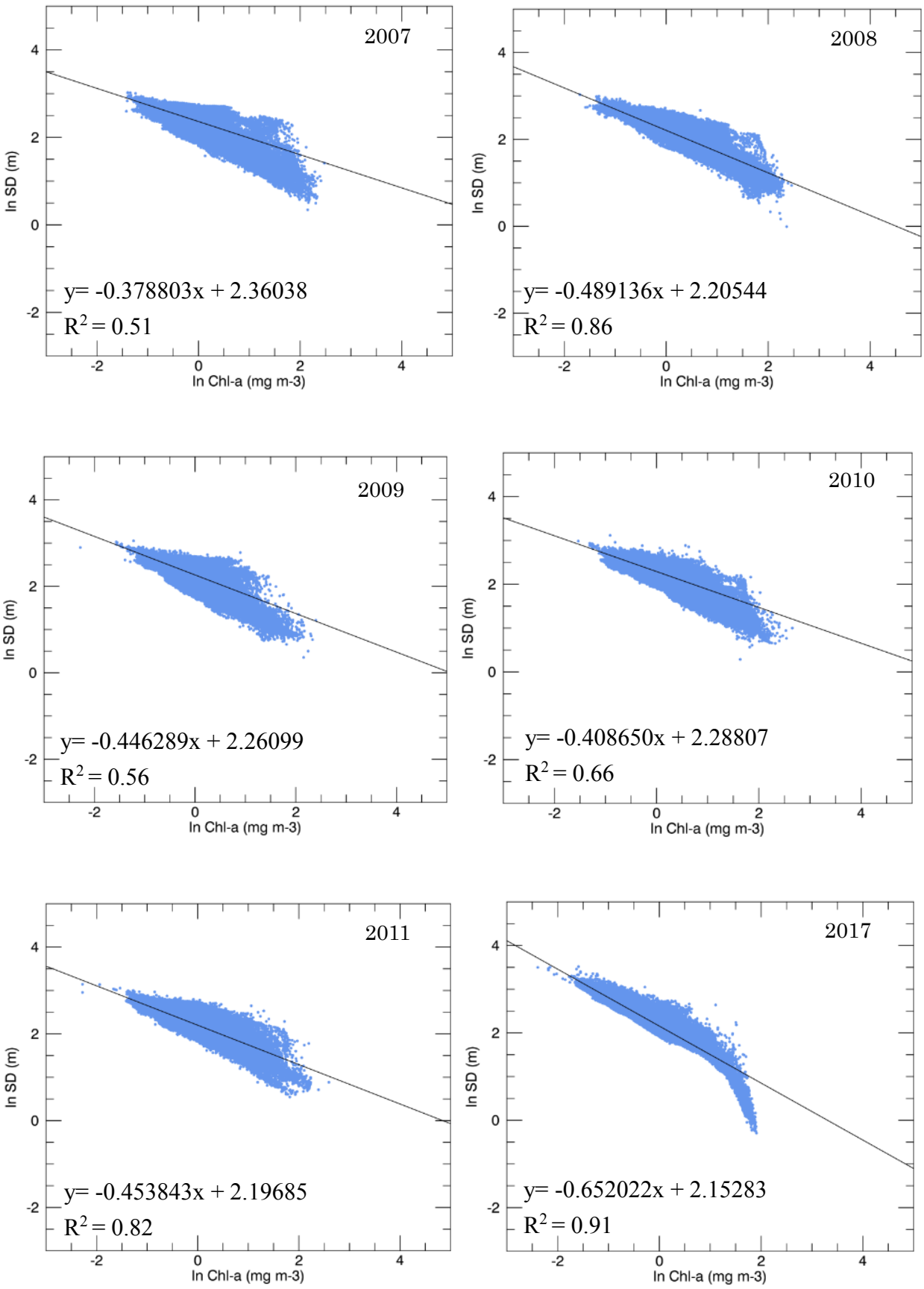

Figure 23. Regression analysis between ln Chl-a (mg/m^3) and ln SD (m) from 2003-2011 and 2017.

The relations of log-transformed parameters for the yearly data shows that the highest relationship is found in 2017, and as expected they all had a negative relation (Fig. 23). The least R^2 was found in 2007 (0.51). The relation of the log-transformed parameters was also built for the monthly datasets. These relationships from both yearly and monthly data were expected to produce linear relations. However, in some cases, the data are not as correlated as expected. Apart from October, all the other months have a high coefficient of determination (more than 0.62). The monthly relation shows a higher correlation than yearly.

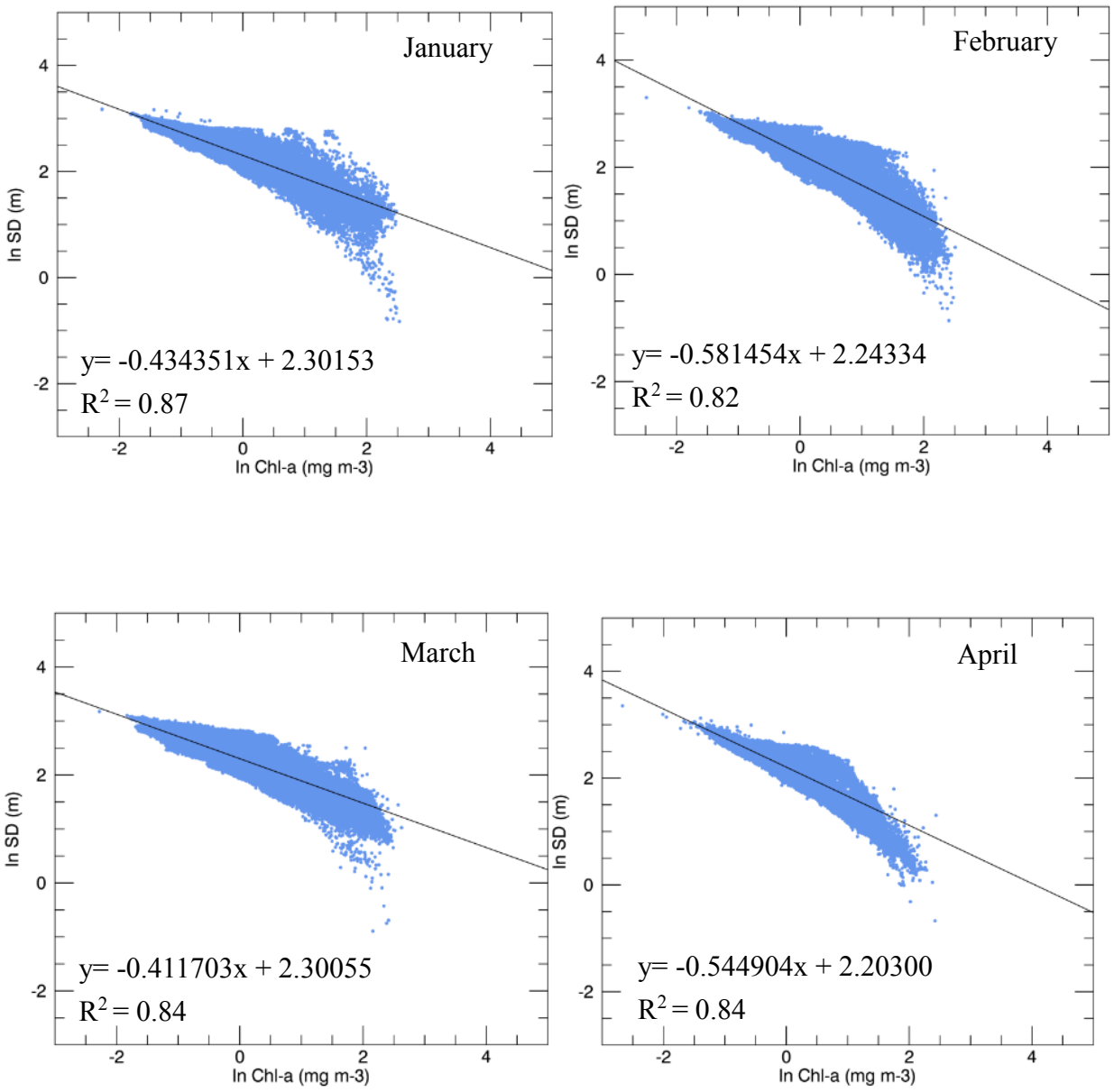

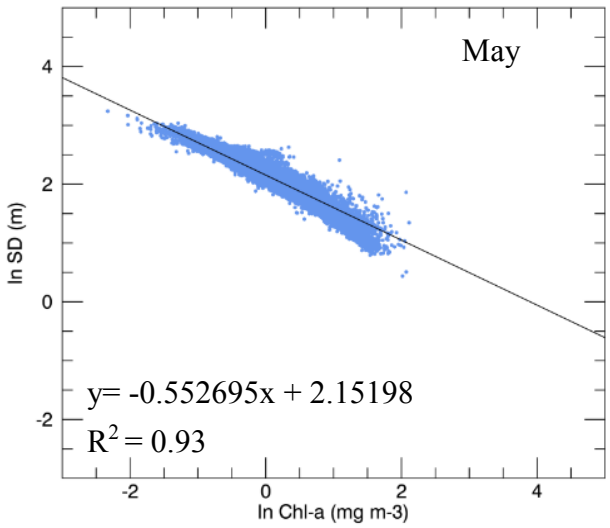
May
y= -0.552695x + 2.15198
R2 = 0.93
ln SD (m)
ln Chl-a (mg m-3)

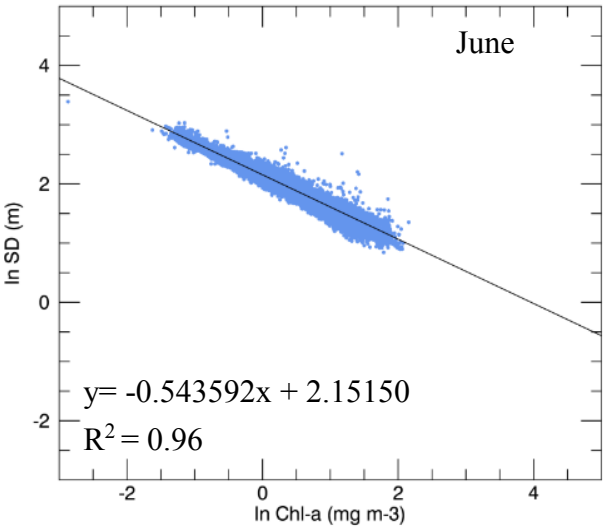
June
y= -0.543592x + 2.15150
R2 = 0.96
ln SD (m)
ln Chl-a (mg m-3)

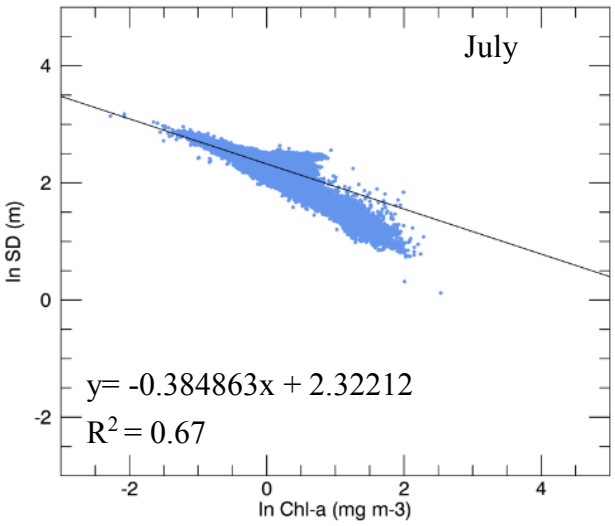
July
y= -0.384863x + 2.32212
R2 = 0.67
ln SD (m)
ln Chl-a (mg m-3)

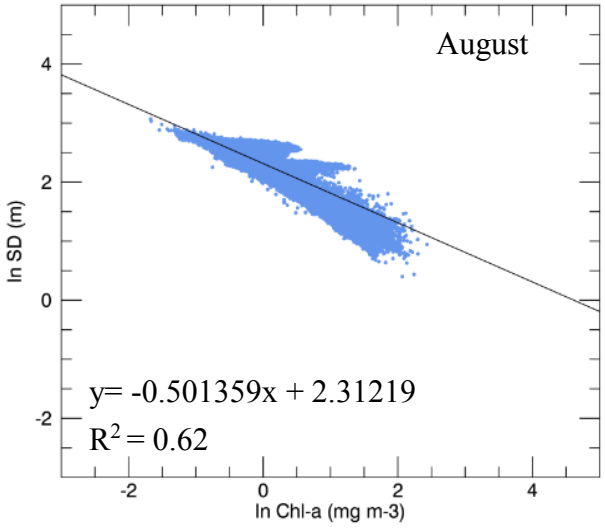
August
y= -0.501359x + 2.31219
R2 = 0.62
ln SD (m)
ln Chl-a (mg m-3)

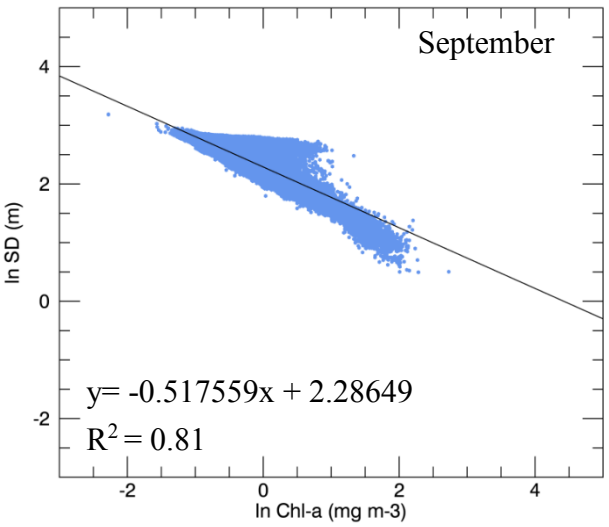
September
y= -0.517559x + 2.28649
R2 = 0.81
ln SD (m)
ln Chl-a (mg m-3)

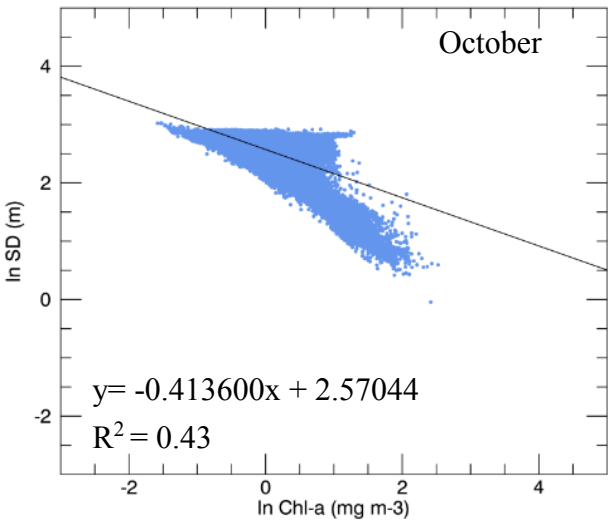
October
y= -0.413600x + 2.57044
R2 = 0.43
ln SD (m)
ln Chl-a (mg m-3)

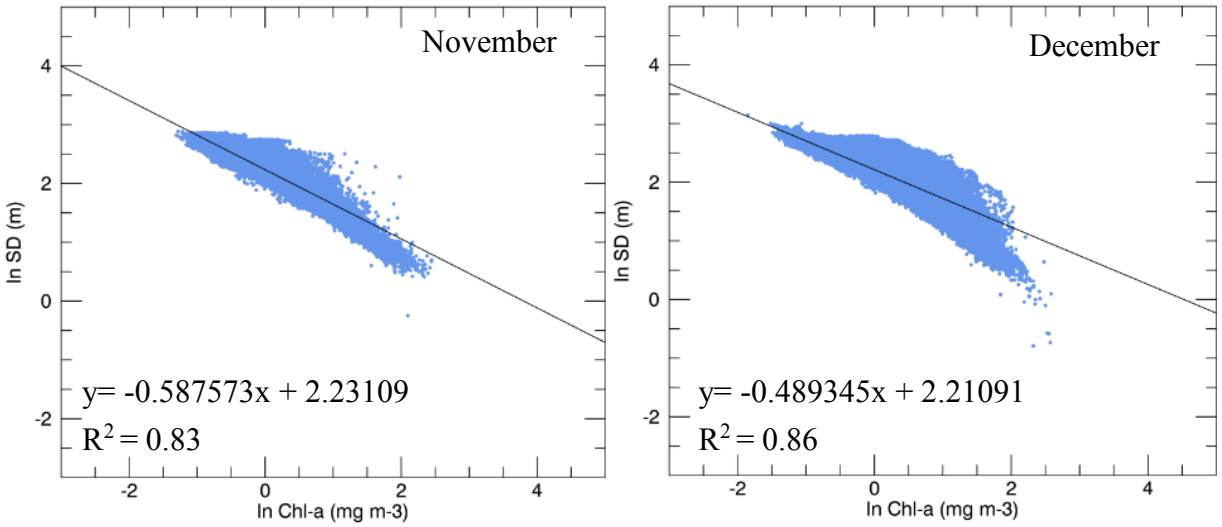

Figure 24. Regression analysis between ln Chl-a (mg/m^3) and ln SD (m) from January to December.

Carlson's model was developed for temperate lakes, thus its application to other types of water bodies requires some modifications. The original equations in Carlson (1977) are presented below. First, an empirical relationship between water quality parameters were built, i.e. ln (SD) vs ln (Chl-a) Equation 24. Based on this relationship, TSI (SD) and TSI (Chla) was calculated by using Equations 25 and 26.

$$ln\,SD = 2.04 - 0.68\,ln\,Chla \quad (24)$$

$$\text{TSI (SD)} = 10\left(6 - \frac{lnSD}{ln2}\right) \quad (25)$$

$$\text{TSI (Chl-a)} = 10\left(6 - \frac{2.04 - 0.68\,(ln\text{Chla})}{ln2}\right) \quad (26)$$

where 6 and 2 are the scale factor and Equation 24 is inserted into Equation 26.

Cheng and Lei (2001) suggested the replacement of the coefficients 6 and 2 in Eqs. (25 and 26) by the scale factor *a* and *b* to allow their adaptation to locally derived coefficients. Thus, the original equations from Carlson (1977) are rewritten as follows:

$$\text{TSI (SD)} = 10\left(a - \frac{lnSD}{lnb}\right) \tag{25a}$$

$$\text{TSI (Chl-a)} = 10\left(a - \frac{\text{intercept}-\text{slope}\ (ln\text{Chla})}{lnb}\right) \tag{26a}$$

The initial relationships between the two parameters ln (SD) vs ln (Chl-a) can be found in Figure 23, 24, and replaced in Equation 26a. Further, the scale factors *a* and *b* are generated from the range factor b^a using Eqs. (27 - 31).

$$b^a = SD_{\max} \tag{27}$$

$$TSI_{Chl-a} \approx Chl - a_{\max} = 100 \tag{28}$$

where $SD_{\max}$ is the maximum *SD* value and $Chl - a_{\max}$ is the maximum *Chl-a* value.
From Eq. (27) the following equations are derived:

$$a = log_b(SD_{\max}) \tag{29}$$

$$a = \frac{ln(SD_{\max})}{lnb} \tag{30}$$

In Eqs. (27 and 28) the $SD_{\max}$ and $Chl - a_{\max}$ can be obtained from the satellite-derived estimates. Here the year 2005 is used as an example. Therefore, the intercept and slope from Figure 23 in the year 2005 are replaced in Eq. (26a), simultaneously Eq. (28 and 30) are also

combined in Eq. (26a) and the $SD_{\max}$ and $Chl-a_{\max}$ are found in Table 12. Then, Equation 31 is used to calculate *b* and later replaced in Eq. (30) for the obtention of *a* for the year 2005.

$$
\begin{cases}
100 = 10\left(\frac{ln(SD_{\max})}{lnb} - \frac{\text{intercept} - \text{slope}(ln(Chl-a_{\max}))}{lnb}\right) \\
100 = 10\left(\frac{ln(22.64)}{lnb} - \frac{2.20 + 0.55(ln(13.59))}{lnb}\right) \\
100 = 10\left(\frac{3.12}{lnb} - \frac{2.20 + 0.55 \text{ x } 2.61}{lnb}\right) \\
10 = \frac{3.12 - 2.20 + 0.55 \text{ x } 2.61}{lnb} \\
lnb = \frac{3.12 - 2.20 + 0.55 \text{ x } 2.61}{10} \\
lnb = 0.23 \\
b = e^{0.23} \\
b = 1.26
\end{cases}
\tag{31}
$$

Finally, a = 13.33 and the modified Carlson's TSI for Lake Malawi is expressed as follows for the year 2005:

$$\text{TSI (SD)} = 10\left(13.33 - \frac{lnSD}{ln1.26}\right) \tag{32}$$

$$\text{TSI (Chl-a)} = 10\left(13.33 - \frac{2.20 - 0.55\ (ln\text{Chla})}{ln1.26}\right) \tag{33}$$

The same steps were used to generate *a* and *b* for the remaining years and months.

Table 12. Yearly coefficients for the modified TSI in Lake Malawi.

Year	$SD_{\max}$	$Chl-a_{\max}$	a	b
2003	29.58	13.44	14.75	1.26
2004	23.49	12.62	13.53	1.26
2005	22.64	13.59	13.33	1.26
2006	26.44	16.22	19.86	1.18
2007	20.55	11.93	18.88	1.17
2008	20.67	11.69	14.95	1.22
2009	21.14	11.00	16.40	1.20
2010	22.52	14.21	16.30	1.21
2011	23.12	13.35	14.81	1.24
2017	33.63	6.74	13.49	1.30

Table 13. Monthly coefficients for the modified TSI in Lake Malawi

Month	$SD_{\max}$	$Chl-a_{\max}$	a	b
Jan	23.97	12.54	16.10	1.22
Feb	27.08	12.31	13.12	1.29
Mar	23.95	13.79	16.24	1.22
Apr	28.56	11.42	13.54	1.28
May	25.52	8.26	14.37	1.25
Jun	29.58	8.64	14.07	1.27
Jul	23.89	12.62	17.37	1.20
Aug	21.51	11.38	15.53	1.22
Sep	24.17	15.32	13.78	1.26
Oct	20.53	12.47	20.21	1.16
Nov	17.86	11.55	13.80	1.23
Dec	23.15	13.22	14.32	1.25

If the trophic state is generated for more than one parameter for a given lake it can serve as an internal evaluation of both the methodology and the assumption based on the relationships between parameters (Carlson, 1977).

Table 14. Carlson's TSI and corresponding water quality parameters boundaries (Carlson, 1977).

Characteristics	TSI	SD (m)	Chl-a (mg/m^3)
Oligotrophic	0	64	0.04
	10	32	0.12
	20	16	0.34
	30	8	0.94
Mesotrophic	40	4	2.6
	50	2	6.4
Eutrophic	60	1	20
	70	0.5	56
Hypereutrophic	80	0.25	154
	90	0.12	427
	100	0.062	1.183

The TSI classification boundary was based on Carlson's model scheme from Table 14. From these boundaries, the coverage of the trophic state in percentage was calculated to scrutinize how much water belonged to the existing TSI in Lake Malawi. Primarily, the four TSI ranges were found in the lake and then evaluated for their annual and monthly TSI (SD) and TSI (Chl-a) (see Table 15-18).

Table 15. The yearly percentage for each TSI (SD) level**.**

Percentage (%)										
	Year									
TSI (SD)	2003	2004	2005	2006	2007	2008	2009	2010	2011	2017
Oligo	70.68	89.19	93.05	66.90	82.17	89.63	86.68	78.51	90.69	85.23
Meso	22.81	7.11	4.35	24.94	11.28	6.23	8.04	15.65	5.92	10.09
Eutro	4.30	2.88	2.13	4.50	3.37	2.87	3.31	3.60	2.58	3.05
Hyper	2.21	0.82	0.48	3.65	3.17	1.27	1.97	0.81	0.81	1.63

Oligotrophic: < 40
Mesotrophic: 40 - 50
Eutrophic: 50 -70
Hypereutrophic: > 70

The TSI (SD) shows that major portion of the lake belongs to the oligotrophic category followed by mesotrophic, eutrophic and hypereutrophic. On average, 83.27% of the lake was oligotrophic during the study period, 11.64% mesotrophic, 3.26% eutrophic and 1.68 % hypereutrophic. There is stabilization in terms of the distribution of the TSI (SD) since no extreme changes were found in the interannual variation of the portion covering each trophic level. This indicates that the lake is stable with most of its waters being oligotrophic to mesotrophic (Table 15).

Table 16. The yearly percentage for each TSI (Chl-a) level**.**

Percentage (%)										
	Year									
TSI (Chl-a)	2003	2004	2005	2006	2007	2008	2009	2010	2011	2017
Oligo	54.86	87.85	93.14	59.47	77.94	88.86	84.24	75.19	89.24	85.51
Meso	41.47	9.42	4.77	31.61	19.15	7.44	13.40	20.58	8.04	9.52
Eutro	3.33	2.50	1.74	8.09	2.52	3.18	2.22	3.91	2.57	3.43
Hyper	0.34	0.22	0.35	0.83	0.39	0.52	0.14	0.15	0.15	1.53

Oligotrophic: < 40
Mesotrophic: 40 - 50
Eutrophic: 50 -70
Hypereutrophic: > 70

As to the TSI (Chl-a), the lake is also mostly dominated by oligotrophic waters on average 79.63%, 16.54% for mesotrophic, 3.35% for eutrophic and 0.46% for hypereutrophic (Table 16). The results from Table 16 show that the lowest percentage of the oligotrophic index was found in 2003, which is different from the TSI (SD). The TSI (Chl-a) percentage for the mesotrophic is higher than TSI (SD) and this pattern can be observed from the individual trophic state levels. While there are dissimilarities in the yearly percentage distribution for each TSI, their temporal variation is similar in the oligotrophic and mesotrophic levels but different in the eutrophic and hypereutrophic levels.

Table 17. The monthly percentage for each TSI (SD) level.

Percentage (%)				
TSI (SD)	Oligo	Meso	Eutro	Hyper
Jan	87.61	7.90	3.00	1.49
Feb	78.76	15.92	3.39	1.94
Mar	81.19	13.01	3.93	1.86
Apr	83.67	11.63	3.36	1.34
May	87.81	8.04	3.40	0.74
Jun	77.72	17.50	3.94	0.83
Jul	48.15	44.42	4.62	2.81
Aug	80.80	14.18	3.37	1.65
Sep	90.23	6.11	2.78	0.88
Oct	89.49	4.61	2.71	3.20
Nov	94.69	3.34	1.45	0.52
Dec	90.79	5.55	2.57	1.10
Average	82.58	12.68	3.21	1.53

Oligotrophic: < 40
Mesotrophic: 40 - 50
Eutrophic: 50 -70
Hypereutrophic: > 70

The results from the monthly TSI (SD) show similar percentage distribution like the annual considering the coverage of oligotrophic, mesotrophic, eutrophic and hypereutrophic waters. However, in July there is an abnormal deviation from the remaining months showing that the oligotrophic state covers only 48.15%, mesotrophic 44.42% and eutrophic 4.62% and hypereutrophic 2.81%. Except for the data from July, the oligotrophic and eutrophic levels are stable when compared to the other two levels (mesotrophic and hypereutrophic) showing huge variations. The presence of the hypereutrophic level is obvious although with variations in terms of coverage between a minimum of 0.52% and maximum 3.20% and 1.53% on average. The percentage values of the eutrophic categories are higher and more stable on average 3.21% and a minimum of 1.45% and a maximum of 4.62%.

Table 18. The monthly percentage for each TSI (Chl-a) level.

Percentage (%)				
TSI (Chl-a)	Oligo	Meso	Eutro	Hyper
Jan	86.54	8.96	3.80	0.71
Feb	78.26	16.26	4.69	0.79
Mar	79.91	15.02	4.20	0.87
Apr	81.36	13.67	4.63	0.34
May	86.95	9.09	3.70	0.25
Jun	77.49	18.03	3.96	0.52
Jul	50.60	44.60	4.66	0.14
Aug	81.18	16.08	2.49	0.26
Sep	89.90	7.55	2.47	0.08
Oct	86.70	12.03	1.21	0.06
Nov	95.56	3.22	1.08	0.14
Dec	88.92	7.89	2.97	0.23
Average	81.95	14.37	3.32	0.37

Oligotrophic: < 40
Mesotrophic: 40 - 50
Eutrophic: 50 -70
Hypereutrophic: > 70

From Table 18 it can be observed that the TSI (Chl-a) shows stability in terms of the percentage distribution between the months, where the oligotrophic and eutrophic are comparatively stable. The distribution is like the previous results TSI (SD). These two TSI (Chl-a and SD) are closer at the oligotrophic and eutrophic levels.

Attention should be given to the mesotrophic category as it can easily exchange positions with the oligotrophic and the eutrophic which in turn will influence the hypereutrophic. Based on the reports from Weyl et al. (2010) that some areas of Lake Malawi were becoming increasingly eutrophic, the results presented here show that not only eutrophic waters are present in the lake but also hypereutrophic. The results from both TSI (SD) and TSI (Chl-a) show that the percentage of eutrophic and hypereutrophic waters increase from December to April.

The SD average, minimum and maximum for the yearly data for the entire study period varied from 8.9 to 33.6 m corresponding to oligotrophic waters. In the mesotrophic waters, the SD ranges between 5.6 and 13.7 m. As for the eutrophic waters, the range varies from 3.5 to 9.8 m and 0.4 to 7.1 m for hypereutrophic. This range covers the entire dataset from 2003-2017.

Equally an analysis of the Chl-a average, minimum and maximum was made, and the following boundaries were found: 0.1 to 1.0 mg/m^3 corresponding to the oligotrophic TSI; 0.4 to 2.4 mg/m^3 mesotrophic TSI; 1.4 to 5.8 mg/m^3 eutrophic TSI; and 2.3 to 16.2 mg/m^3 TSI. When evaluated individually, the maximum of SD (m) corresponding to the oligotrophic boundary could be representing a small number of pixels. The same applies to the maximum of Chl-a (mg/m^3) boundary value corresponding to the hypereutrophic state.

3.3. Spatiotemporal variations of trophic states in Lake Malawi

The trophic state estimation using satellite data has the advantage of being able to assess its spatiotemporal variability. The spatiotemporal differences between the two TSI (Chl-a and SD) are visible from Figure 25 and Figure 26. Generally, oligotrophic waters are in the pelagic zone of the lake. Some years (e.g. 2003) have shown a huge difference in their TSI spatial distribution. However, the difference was caused by the water pixels found in the limit of the TSI boundaries. This can be observed from the mean values of the TSI from both Chl-a and SD (Fig. 27).

2003	2004	2005
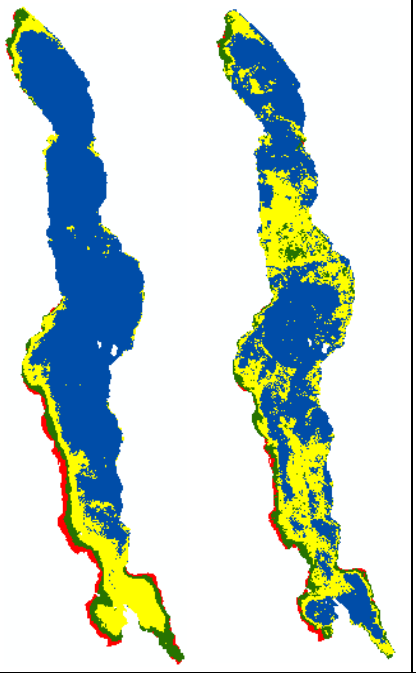	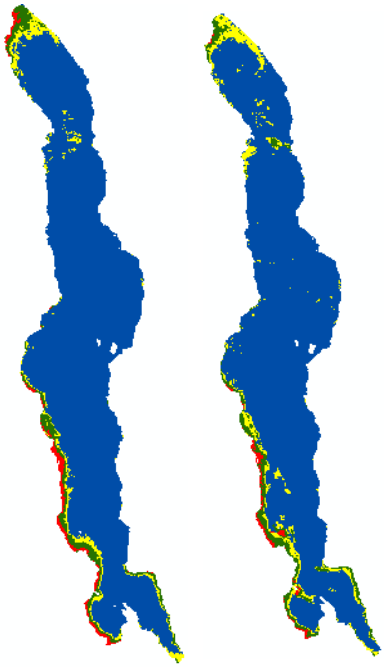	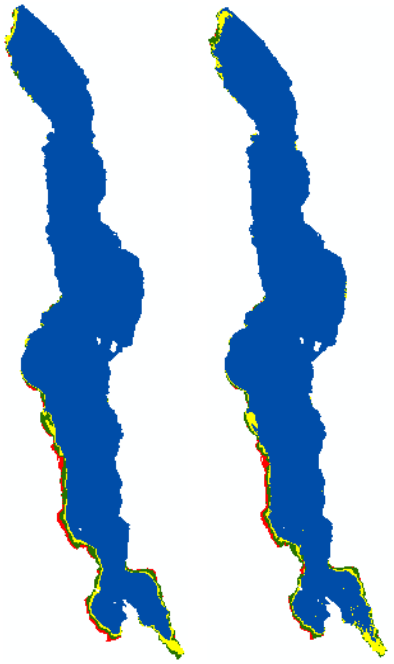
2006	**2007**	**2008**
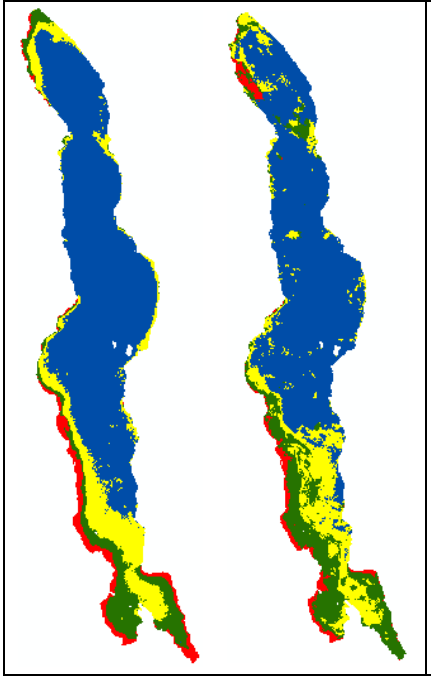	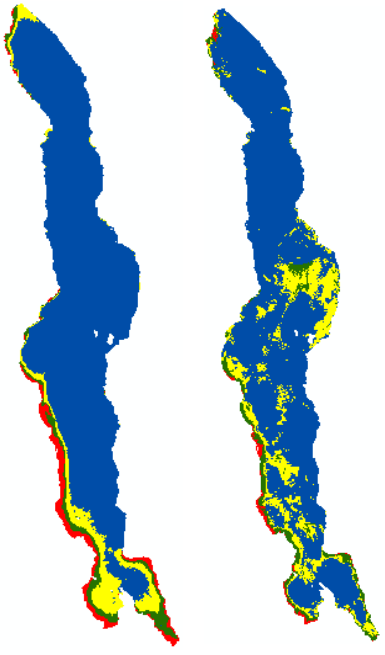	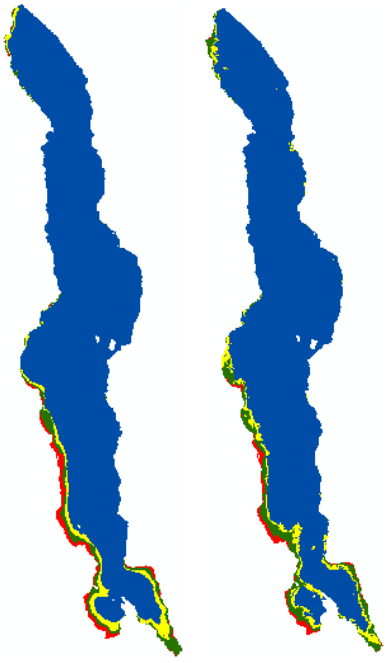

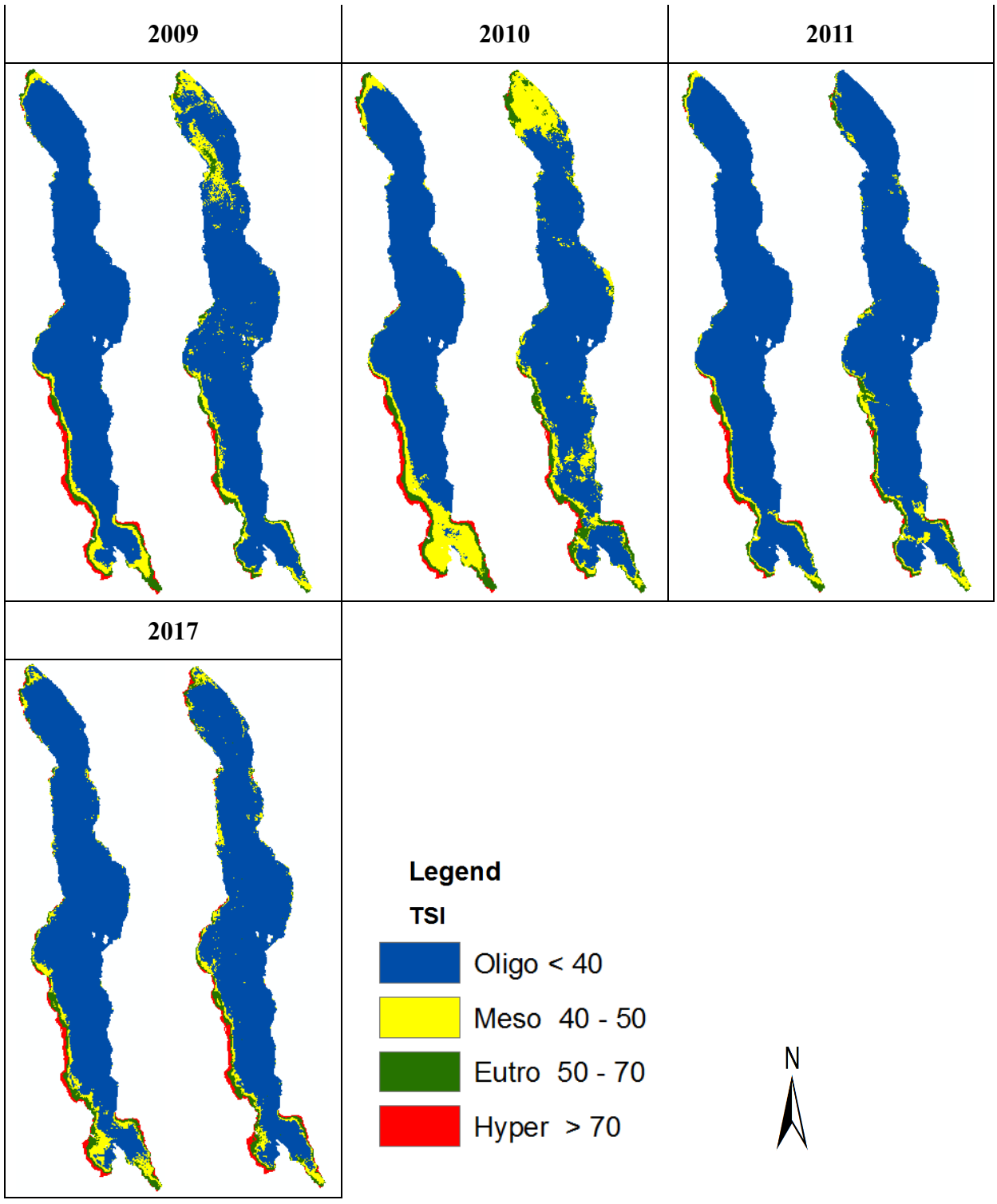

Figure 25. Comparison of the yearly spatiotemporal distribution of the TSI. Left: TSI (SD) and right: TSI (Chl-a).

The spatial distribution shows that 2003 has the biggest discrepancy between the TSI (Chl-a) and TSI (SD), and the Chl-a derived TSI seems to be more sensitive to changes. In 2003 for example, there was an enormous difference between TSI (Chl-a) and TSI (SD) in the

oligotrophic and mesotrophic levels. But in the eutrophic and hypereutrophic the distribution seemed to have matched. In 2004, 2005, 2008, 2011 and 2017 the TSI have similar spatial distribution. However, in the remaining years, they showed some differences (see Fig. 25). Despite these differences, the general pattern of the TSI spatial distribution is from the shore to the lake's open waters. The hypereutrophic and eutrophic waters are located along the western shore and close to the river mouth. The same distribution could be said about the mesotrophic which functions as a transitioning level but mostly located in the western shore as well as the southern part of the lake.

Figure 26 shows the monthly spatial distribution of the TSI. The northern region of the lake shows hypereutrophic waters during the warm wet season. In March TSI (Chl-a) shows an inflow from the Songwe River in the northern part of Lake Malawi.

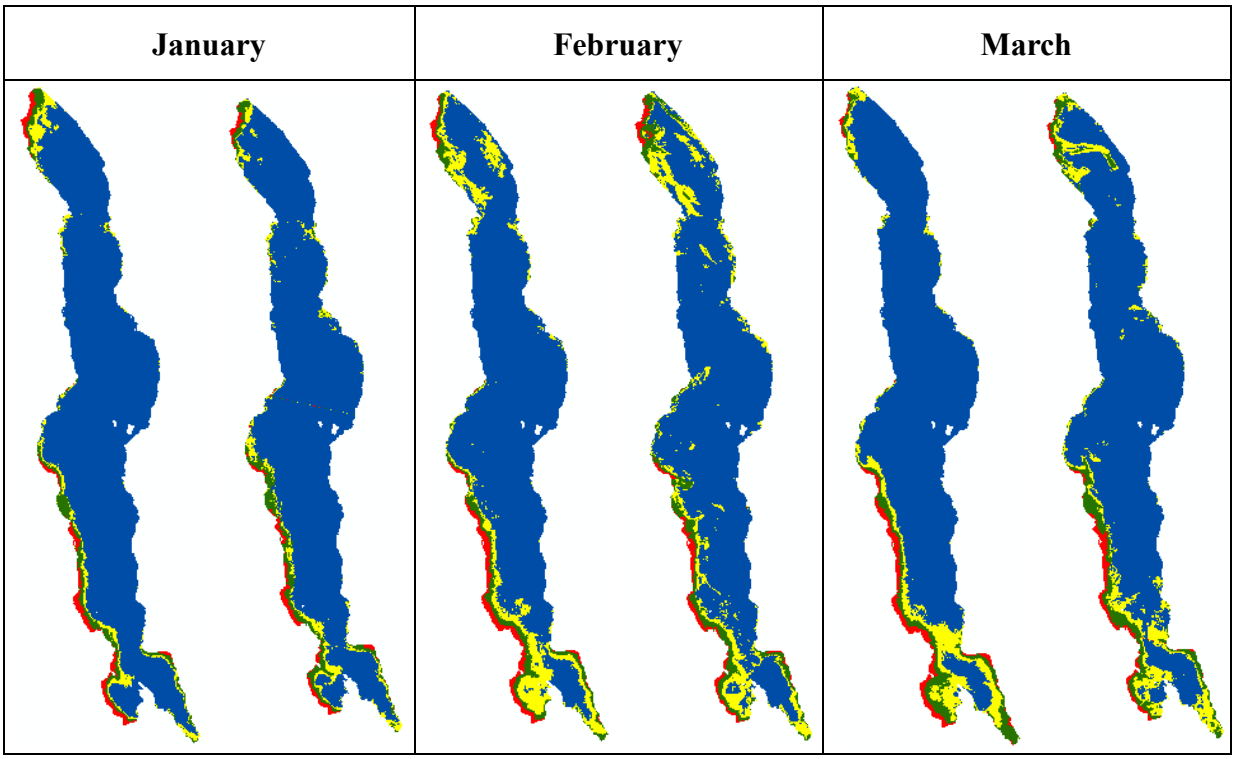

April	May	June
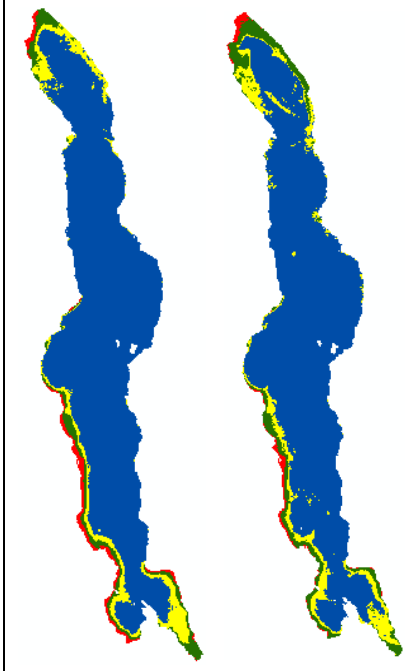	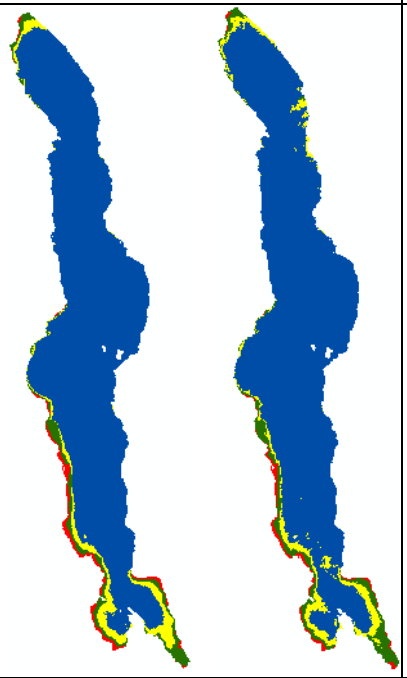	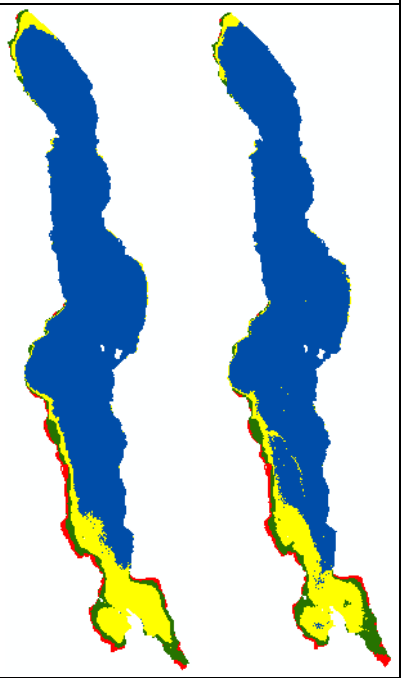
July	**August**	**September**
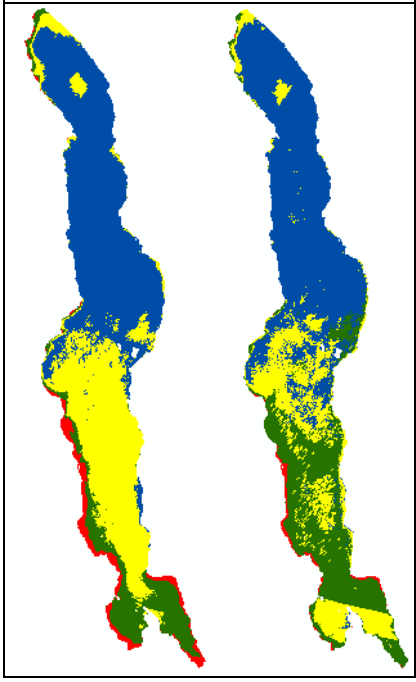	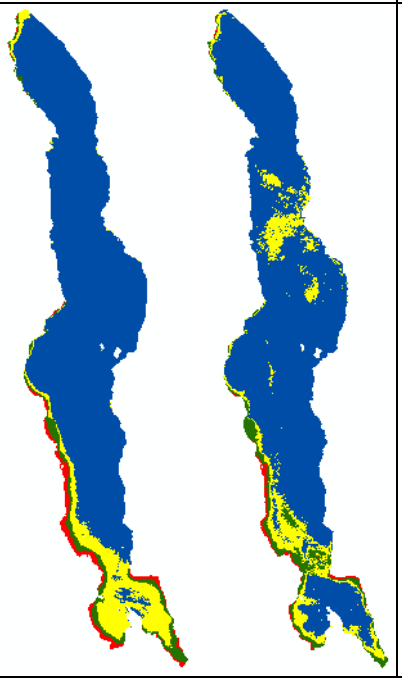	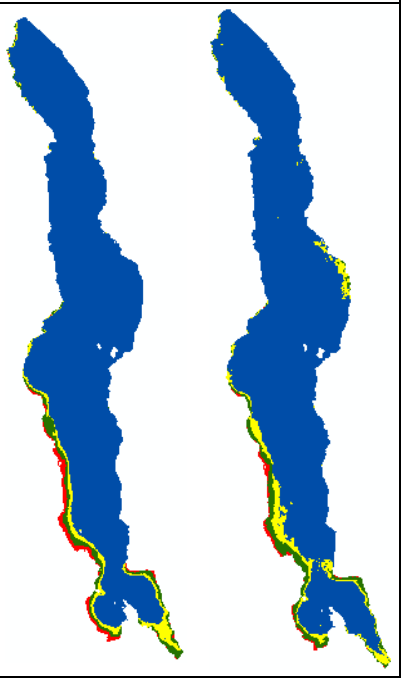

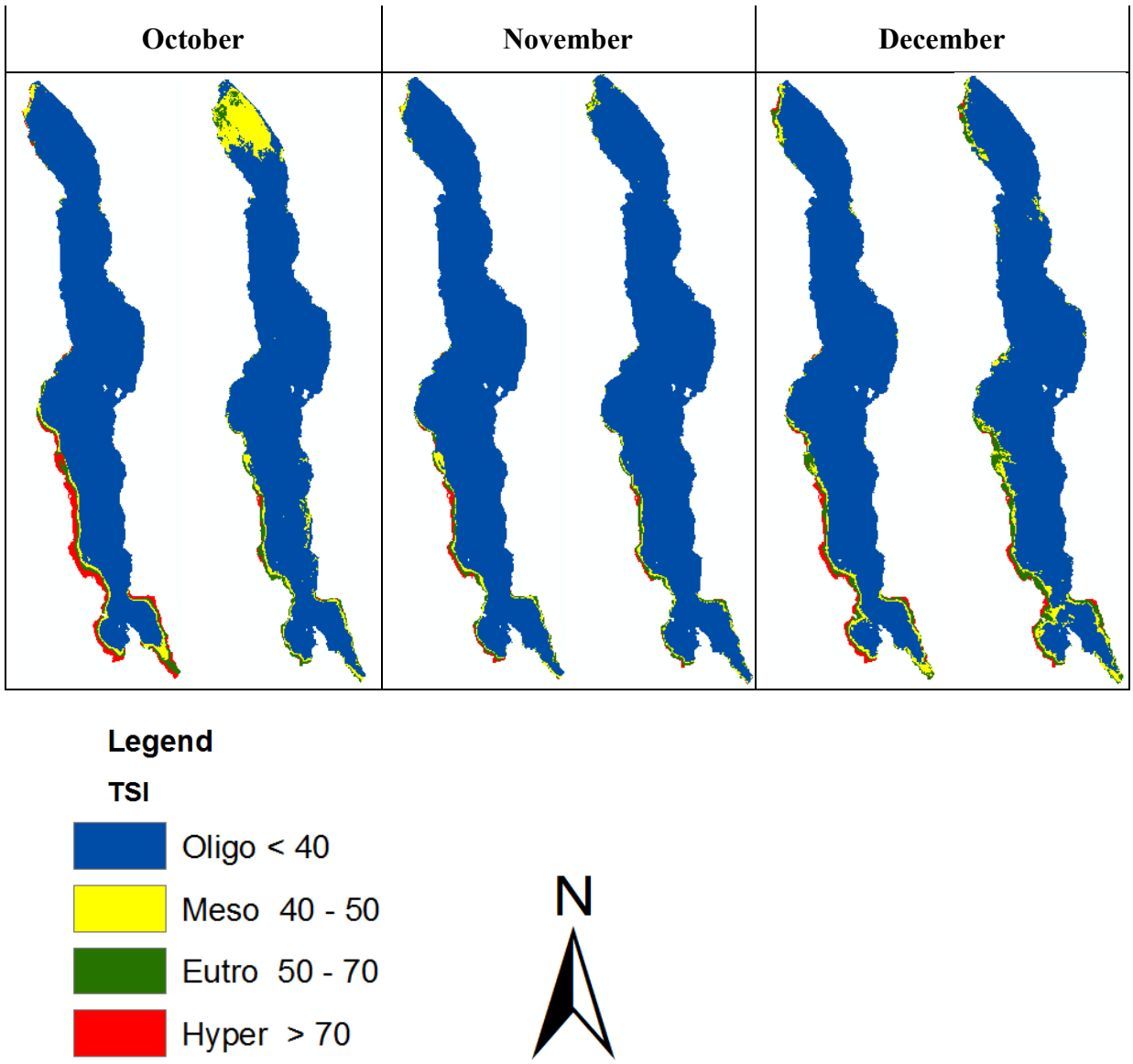

Figure 26. Comparison of the monthly spatiotemporal distribution of the TSI. Left: TSI (SD) and right: TSI (Chl-a).

The comparison shows that the average value of the TSI is very close as expected and referred by Carlson (1977), and Carlson and Havens (2005). The average monthly data were compared, and similar results were found. However, while the least coefficient of determination in the annual data was 0.50 in 2007, the monthly data showed the lowest coefficient of determination equal to 0.42 in October.

The results shown here from the annual and monthly average data indicate that Lake Malawi is still oligotrophic with an annual and monthly average TSI around 31 for both TSI

(SD) and TSI (Chl-a) derived. And the individual year and month also do not exceed the determined limit for the oligotrophic except for 2003 and 2006 with a slight increase. The two TSI (SD) and TSI (Chla) have the same temporal variability. Their change over time is not significant, ($p > 0.05$) and it tends to reduce over time.

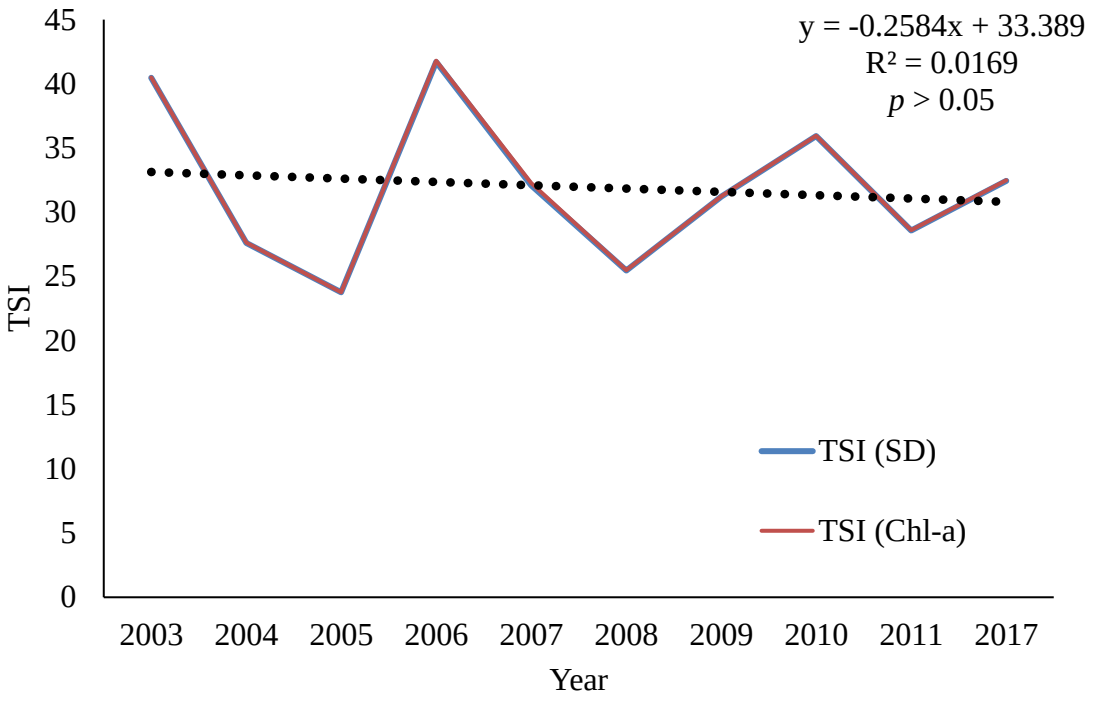

Figure 27. Average temporal variability of TSI in Lake Malawi showing almost no deviation.

A further evaluation was carried out based on each trophic levels and the results indicate that: (1) temporally the trend analysis for the oligotrophic levels does not have any significance, ($p > 0.05$ and $R^2 = 0.02$), (2) the temporal change for the mesotrophic level is also insignificant, ($p > 0.05$ and $R^2 = 0.08$). For the eutrophic level, (3) it is increasing but not significantly like the (4) hypereutrophic level (Fig. 28a-d).

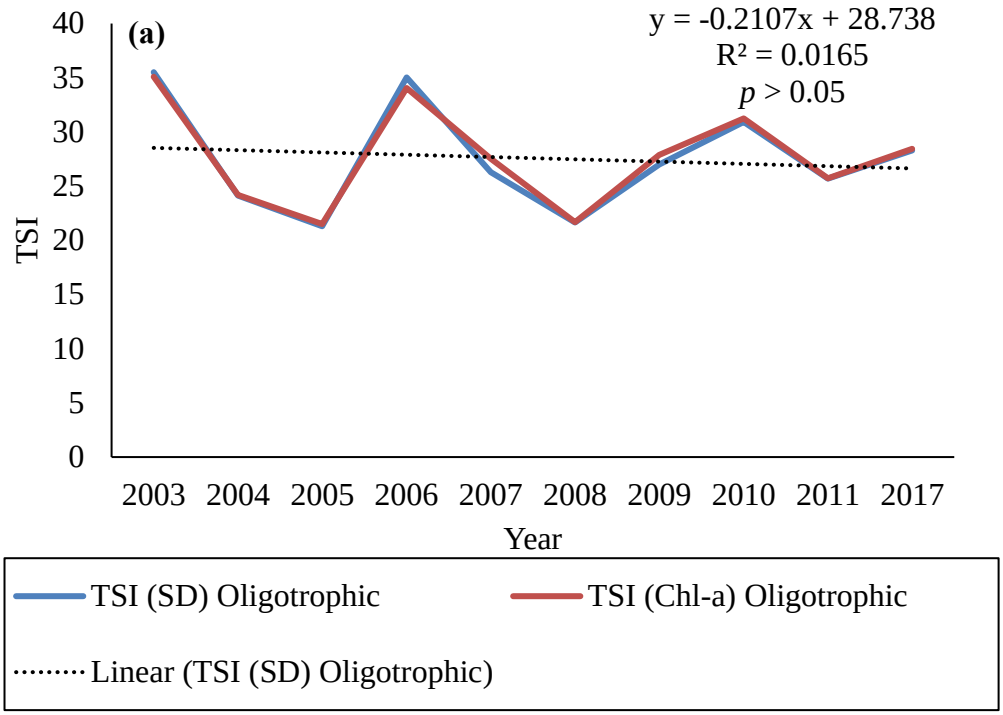
(a)
y = -0.2107x + 28.738
R² = 0.0165
p > 0.05
TSI
40
35
30
25
20
15
10
5
0
2003 2004 2005 2006 2007 2008 2009 2010 2011 2017
Year
TSI (SD) Oligotrophic
TSI (Chl-a) Oligotrophic
Linear (TSI (SD) Oligotrophic)

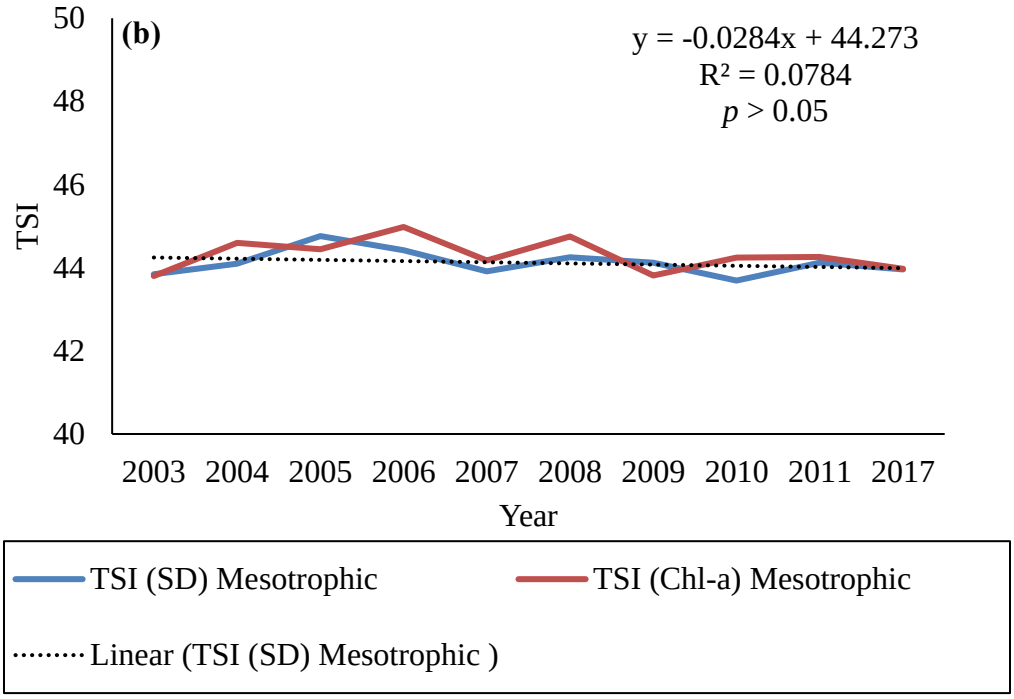
(b)
y = -0.0284x + 44.273
R² = 0.0784
p > 0.05
TSI
50
48
46
44
42
40
2003 2004 2005 2006 2007 2008 2009 2010 2011 2017
Year
TSI (SD) Mesotrophic
TSI (Chl-a) Mesotrophic
Linear (TSI (SD) Mesotrophic)

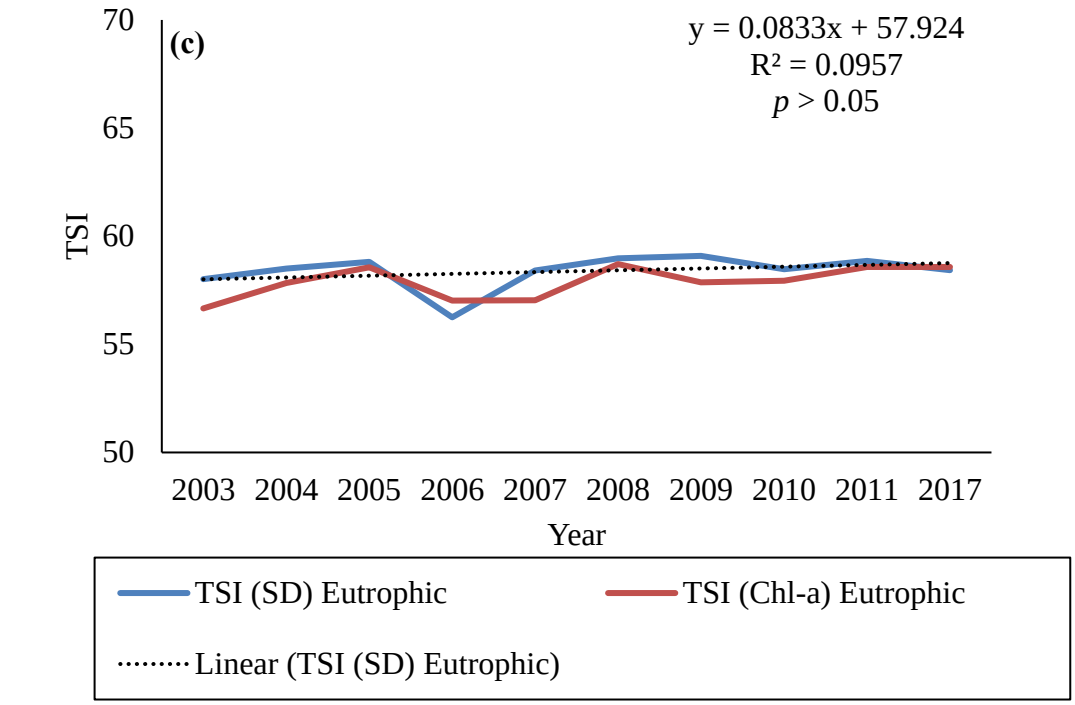

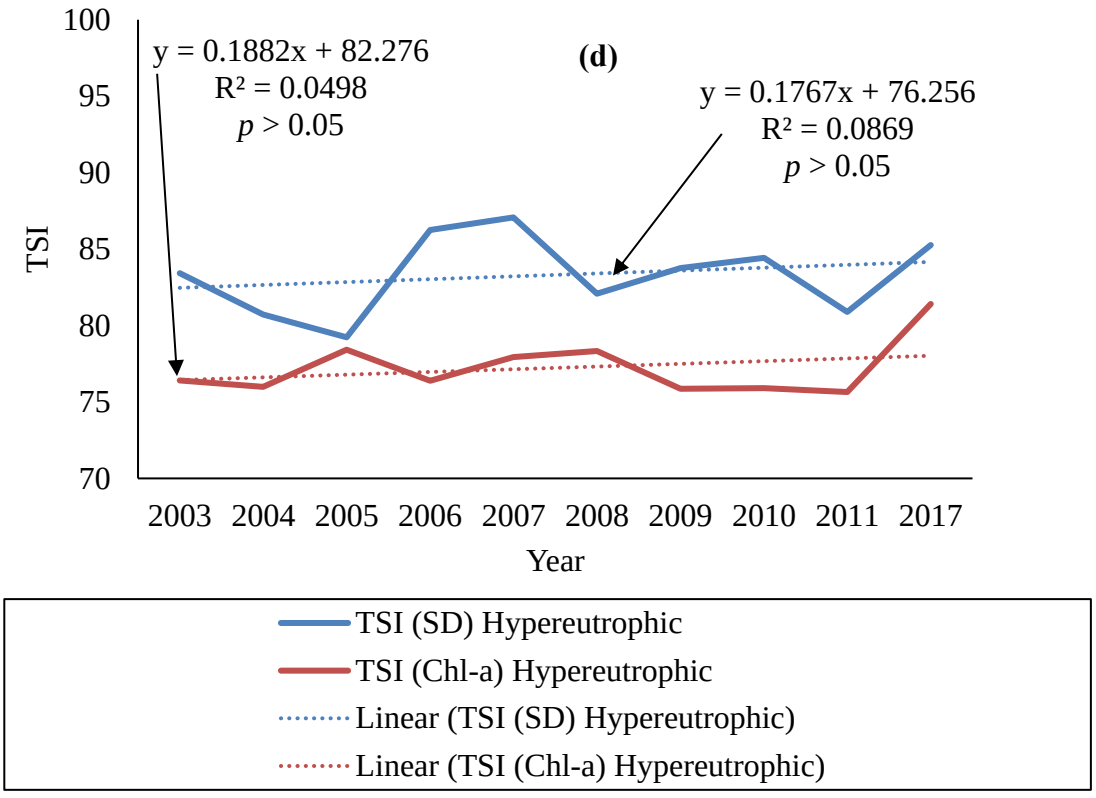

Figure 28. Temporal variability of the individual TSI level (a) oligotrophic, (b) mesotrophic, (c) eutrophic and (d) hypereutrophic.

The monthly variation of the TSI from the two (Chl-a and SD) parameters show that from July to November the TSI in Lake Malawi drops substantially. From November to July it increases up to the boundary between oligotrophic and mesotrophic (Fig. 29a). This trend seems to agree with the rainy season and some additional months. A similar trend of variability was found in the oligotrophic level due to its huge percentage in the lake (Fig. 29b). In the mesotrophic level, it increases from August to March with a slight drop in February (Fig. 29c). This pattern combines with the rainfall variation described by Nicholson et al. (2014). The eutrophic level shows stability throughout the year except for a drop in July for TSI (SD) and another in October for TSI (Chl-a), and it increased for the TSI (SD) in the same period (Fig. 29d). Finally, the hypereutrophic level also shows stability throughout the year with two peaks in July and October for TSI (SD) whereas the TSI (Chl-a) shows to be more stable (Fig. 29e).

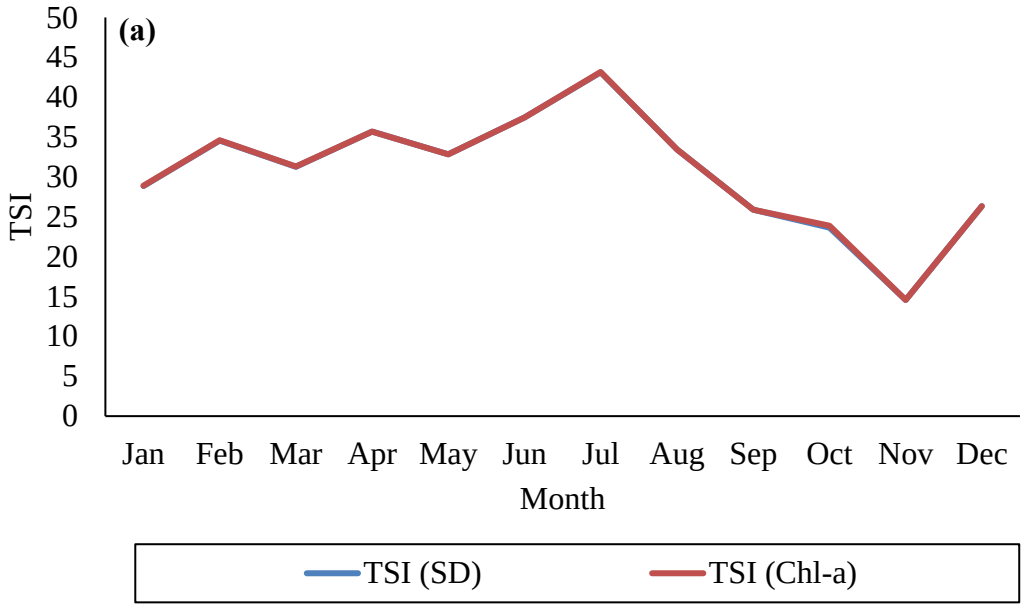

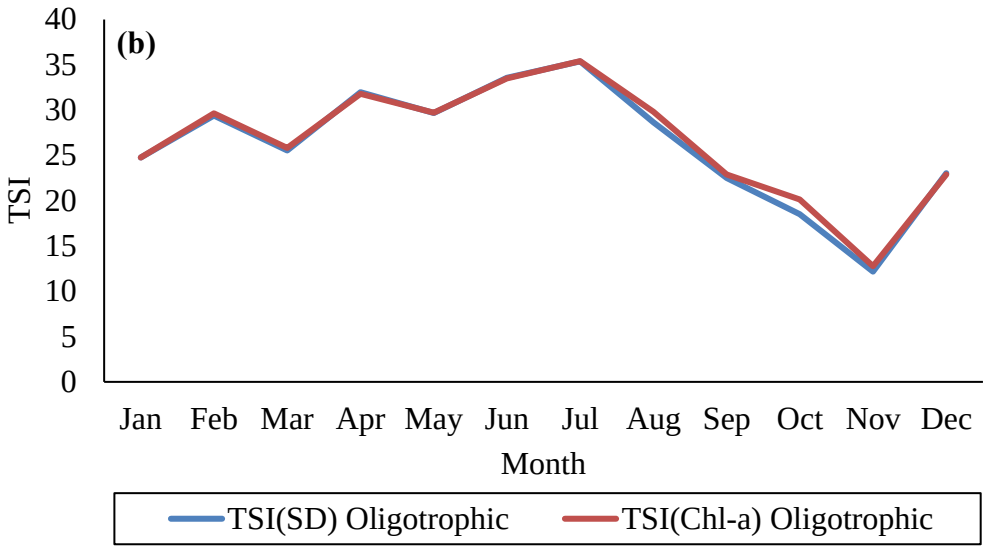
(b)
TSI
40
35
30
25
20
15
10
5
0
Jan Feb Mar Apr May Jun Jul Aug Sep Oct Nov Dec
Month
TSI(SD) Oligotrophic
TSI(Chl-a) Oligotrophic

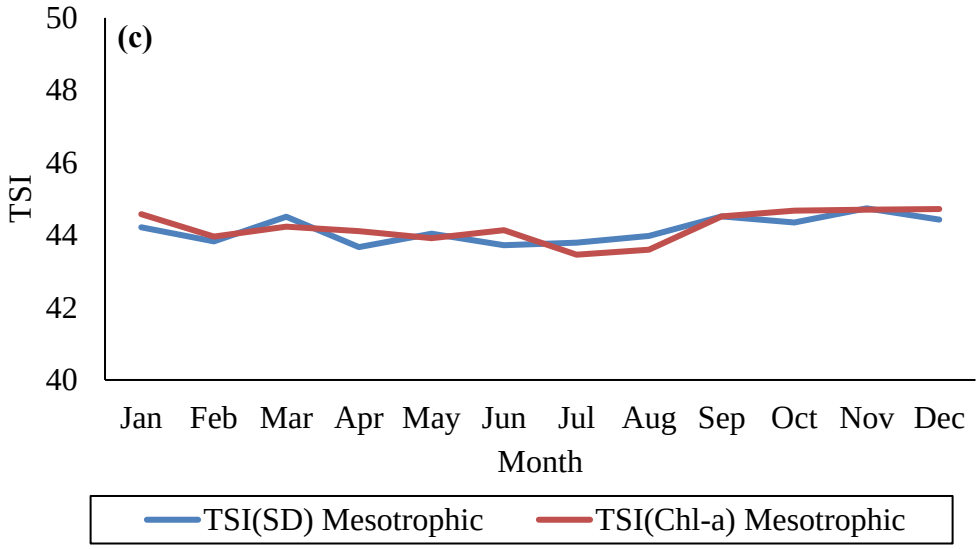
(c)
TSI
50
48
46
44
42
40
Jan Feb Mar Apr May Jun Jul Aug Sep Oct Nov Dec
Month
TSI(SD) Mesotrophic
TSI(Chl-a) Mesotrophic

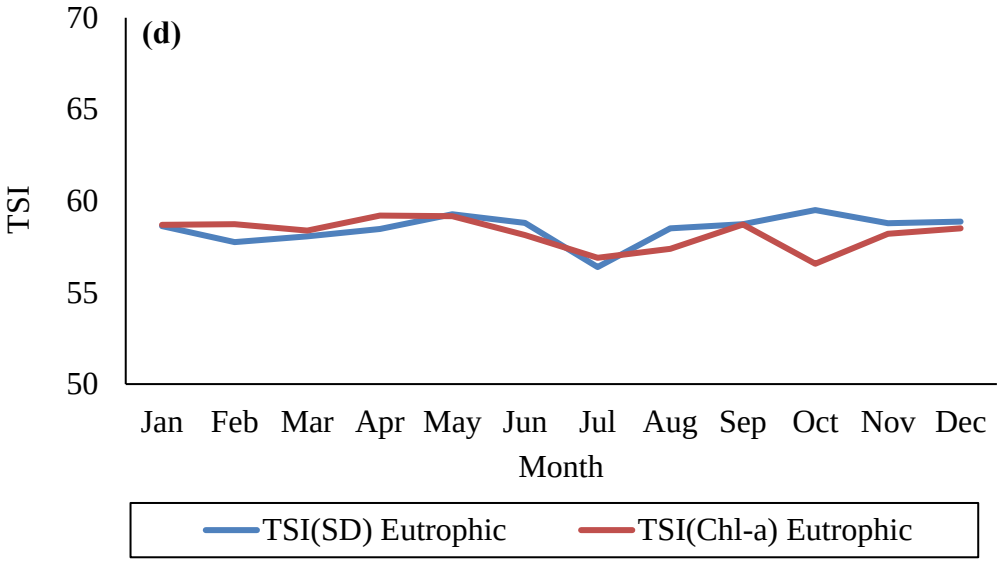
(d)
TSI
70
65
60
55
50
Jan Feb Mar Apr May Jun Jul Aug Sep Oct Nov Dec
Month
TSI(SD) Eutrophic
TSI(Chl-a) Eutrophic

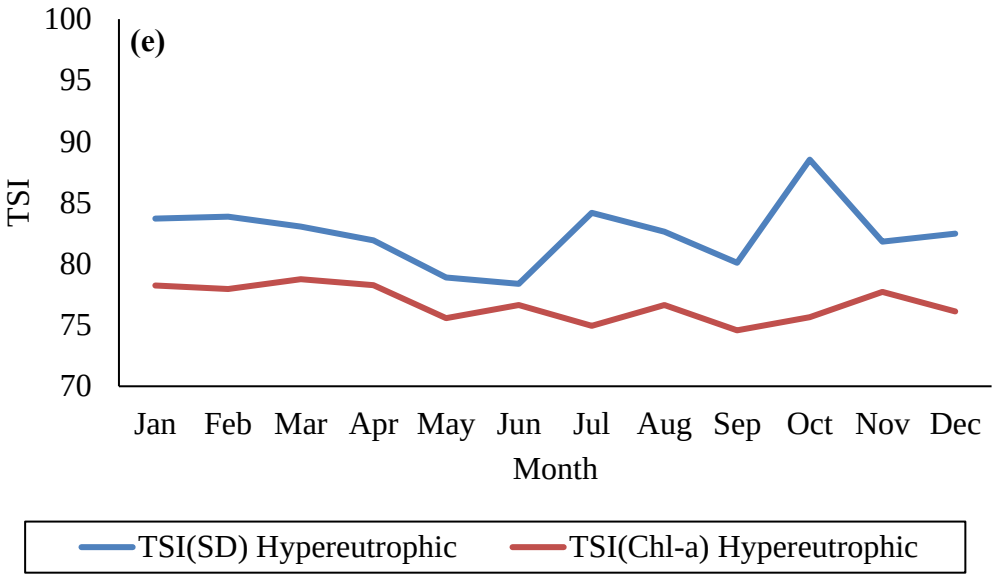

Figure 29. Monthly variability of TSI in Lake Malawi (a) monthly average TSI (Chl-a and SD), (b) monthly average TSI (Chl-a and SD) oligotrophic, (c) monthly average TSI (Chl-a and SD) mesotrophic, (d) monthly average TSI (Chl-a and SD) eutrophic and (e) monthly average TSI (Chl-a and SD) hypereutrophic.

3.4. Analysis of the Deviation between the Trophic State Index from Chlorophyll-a concentration and from Secchi Disk Depth

The TSI is a biomass classification using chlorophyll as the main trophic definition parameter in the presence of the other two parameters, TP and SD (Carlson, 1977). The three parameters (Chl-a, SD and TP) independently estimate algal biomass and should produce the same index value for a given combination of parameters. This assumption is only valid in the presence of an 'ideal' pair of datasets and if no misclassification is found or occurs during the classification process (Cheng and Lei, 2001). Following the work from Carlson (1977), Carlson

(1991) and Carlson and Havens (2005) stated that the interrelationships between the parameters can be used to identify trophic state misclassification and this can indicate either methodological problems or provide additional insights about the lake's dynamics. Using Carlson's TSI and their deviations, Ndungu et al. (2013) found that Lake Naivasha in Kenya had a TSI that varied between eutrophic and hypereutrophic and the graphical representation of the deviations showed that the lake was phosphorus limited TSI (Chl-a) > TSI (TP). Mamun and An (2017) analyzed the TSI deviation of 182 agricultural reservoirs in Korea and found that phosphorus was also the limiting factor regulating phytoplankton growth and supported their statement with the deviation relations TSI (Chl-a) – TSI (SD) < TSI (Chl-a) – TSI (TP). In both studies, the results indicated that the lakes and reservoirs were phytoplankton productive as Lake Naivasha was more eutrophic than previous reports and the agricultural reservoirs in Korea had influence from high amounts of fertilizers (Ndungu et al., 2013; Mamun and An, 2017).

Using the three (Chl-a, SD, and TP) parameters provides the opportunity for a more complete evaluation of the deviations, considering that the three can be cross-checked. Nevertheless, in this study, only the estimated parameters were used for the calculation of the TSI, and the deviation analysis.

The TSI (SD) and TSI (Chl-a) estimates correspond to a series of boundaries. For Lake Malawi, the following trophic state boundaries for SD (m) and Chl-a (mg/m^3) were found. The data are presented in pairs of two for each TSI and their equivalent parameter (Table 18). Each pair of data is made up of average minimum and average maximum for a specific TSI. From the values presented in Table 18 and the previous reports about the SD values and Chl-a concentration in Lake Malawi (Weyl et al., 2010; Chavula et al., 2009; Bootsma and Jorgensen, 2004) the boundaries are still within the threshold since Chl-a at the oligotrophic boundary is still below 1 mg/m^3. As for SD, there is a deviation of about 2.6 m between the reference value 12 m and 10.6 m. More detailed comparison could not be made based on the other TSI levels (i.e. mesotrophic, eutrophic and hypereutrophic) due to lack of reference study regarding the

boundary of the trophic state in Lake Malawi. Thus, in the absence of such type of information, the values from Table 19 and its approximations can be used as a base for further evaluation of these boundaries.

Table 19. Trophic state boundaries for SD (m) and Chl-a (mg/m^3) found in this study.

TSI Level	TSI Value	SD (m)	Chl-a (mg/m^3)
Oligotrophic	< 40	10.6 - 24.4	0.1 - 0.8
Mesotrophic	40 - 50	7.0 - 10.6	0.8 - 2.0
Eutrophic	50 - 70	4.7 - 7.0	2.0 - 5.0
Hypereutrophic	> 70	1.2 - 4.7	4.7 - 12.5

The existing deviations between the two TSI (Chl-a) and TSI (SD) were evaluated based on Carlson (1991). Table 20 shows the conditions associated with the deviations proposed by Carlson (1991). Due to the limitation on the number of parameters only three conditions and their corresponding description are given.

Table 20. Conditions associated with deviations between trophic state, modified from Carlson (1991).

Condition	Description
TSI (Chl-a) ≈ TSI(SD)	Algae dominate light attenuation
TSI (Chl-a) > TSI(SD)	Large particulate, such as *Aphanizomenon flakes, dominate
TSI (Chl-a) < TSI(SD)	Sediments or other organic matter dominate

* Aphanizomenon: is a brackish and freshwater species of cyanobacteria.

The yearly deviation analysis based on the average of the difference between the two TSI TSI (Chl-a) – TSI (SD) was performed and indicated that light attenuation in Lake Malawi was

dominated by algae because almost all the years from the comparison were equal to zero (0.0) except for 2006 (0.1), 2007 (0.2) and 2017 (0.1). Even though there were these exceptions, it can be considered that overall the light attenuation in the lake is dominated by algae.

The deviation results were then used to evaluate the lake's light attenuation based on each TSI level. This information can be useful for regional, spatial or local understanding of the different elements influencing the light attenuation at each trophic level. The results from the TSI deviations analysis per trophic level show that for the oligotrophic and mesotrophic levels, the light is either attenuated by algae or larger particles such as Alphanizomenon as the average values for all years in this trophic are positive except for 2003 difference of -0.42 and -0.97 for 2006. The difference in the mesotrophic level has the exception of 2003 with a difference of -0.04, -0.32 for 2005, and -0.31 for 2009. On average, the differences are positive (see Figure 28a and 28b).

The other two trophic states (eutrophic and hypereutrophic) show TSI (Chl-a) < TSI (SD) (see Figure 28c and 28d) and thus the light in these trophic levels is attenuated by non-algal particles most probably sediments from the watershed as they are distributed along the shore.

The monthly deviation results also show that TSI (Chl-a) ≈ TSI(SD) in oligotrophic level. Thus, it can be considered that the monthly light attenuation in Lake Malawi is also determined by algae biomass which can include Asterionella Formosa, Melosira Granulate and others. These algae species are said to belong to oligotrophic waters (Rawson, 1956).

When individually evaluated, the seasonal variation can be observed from the monthly average data. In the oligotrophic level, the deviations show that on average TSI (Chl-a) < TSI (SD) in January, April, June and December, TSI (Chl-a) > TSI (SD) in August and October and TSI (Chl-a) ≈ TSI (SD) in the rest of the months (see Figure 29b).

The mesotrophic deviations show that TSI (Chl-a) < TSI (SD) in March, May, July, August and November and the remaining months TSI (Chl-a) ≈ TSI (SD) (Figure 29c). The eutrophic deviations show that from May to December except for July, TSI (Chl-a) < TSI (SD) and the

remaining ones TSI (Chl-a) ≈ TSI (SD) (Figure 29d). The hypereutrophic level indicates that TSI (Chl-a) < TSI (SD) through the year (Figure 29e). The deviations between the two TSI show that it is less than 1 TSI for oligotrophic, mesotrophic and eutrophic and less than 10 TSI for hypereutrophic.

The growth and productivity of phytoplankton in Lake Malawi is very low, thus the absence of large amounts of nutrients or their dispersion in the lake makes the effects of nutrients to the lake neutral. According to Dardeau et al. (1992) there are five limiting factors for phytoplankton growth, they are light, temperature, circulation, grazing, and nutrients. Some studies have indicated that light and nutrient limitation could play an alternating role within different longitudinal zones (Cunha and Calijuri, 2011). The results from this study indicate that nutrient is not a limiting factor in Lake Malawi, but probably sun light.

Chapter 4 General Conclusions

In this study, first the performance of two semi-analytical algorithms (i.e., Doron11 and Lee15) in Lake Malawi was compared from MERIS and OLCI sensor data. The results showed that even though the SD estimations from the two algorithms were highly correlated, with R^2 larger than 0.96, Lee15 algorithm outperformed Doron11 algorithm in Lake Malawi with a high estimation accuracy (RMSE = 1.17 m, MAPE = 18.7%, R = 0.66, $p < 0.05$) for MERIS and (RMSE = 4.51 m, MAPE = 30.7%, R = 0.49, $p > 0.05$) for OLCI data. These values indicate that the estimated SD can fairly represent the actual value from the measured data as $p < 0.05$ for the data compared within 3 h interval between the matchup. Doron11 algorithm usually overestimated SD values. These results indicate that water transparency in Lake Malawi can be evaluated by combining MERIS/OLCI data and Lee15 algorithm without algorithm recalibration using in situ data. This finding is important for most African lakes due to lack of in situ data for evaluating water quality or recalibrating algorithm in these lakes.

It was then evaluated the water transparency in Lake Malawi using the SD values estimated from 9-year MERIS and 1-year OLCI data (2003-2011, 2017) a total of 14 years span, using Lee15 algorithm. The results showed that there always existed four water transparency levels in Lake Malawi throughout the study period. The levels 1 and 2 water areas tended to shift and trade places, depending on the year or season. In contrast, level 3 and 4 water areas were relatively stable and constantly distributed along the southwestern and southern lakeshores. Generally, Lake Malawi is dominated by waters with SD values larger than 6 m (> 95%). There was a change in terms of water area based on the transparency levels percentage. In 2003 level 1 had about (67.6 %), level 2 (28.4 %), level 3 (3.6 %), and level 4 (0.4 %), and in 2011 it changed to (74.5 %), (22.8 %), (2.5 %) and (0.2 %) respectively and finally in 2017 (84.6 %), (12.1 %), (2.5 %) and (0.8 %). Considering these statistical values, it can be said that level 1 has increased

from 2003 to 2017, while level 2 decreased by almost half, level 3 decreased from 2003 to 2011 but maintained in 2017. As for level 4, it decreased from 2003 to 2011 but then increased in 2017 as much as double the initial year.

This study provided an overall and comprehensive understanding of transparency levels and their spatiotemporal variation in Lake Malawi. The findings that were previously described in isolation from different field survey-based studies are now summarized into one.

Along the first 9 years study, no significant change was found (Fig.19a). The results from the additional data from OLCI were independently analyzed. These results confirmed the strength of Lee15 over Doron11 (Fig. 16g, h).

The SD distribution increases from the near shore to the center of the lake. Despite the existence of transparency level 4, the lake is still dominated by the first two levels. Yearly change in SD shows that 2006 and 2017 had the highest values, and they did not go over the reported values, 12-20 m but there was a small decrease to 11.5 m from Lee15. It can be concluded that the SD in Lake Malawi is still high but with a slight decrease in some regions, not significant.

On the other hand, the monthly results show that February and the interval between April and August have the lowest SD in Lake Malawi.

Second, Chl-a was estimated from the MERIS/OLCI data by using NASA's OC4E Chl-a algorithm. The Chl-a results indicated that the average value of Chl-a concentration in Lake Malawi was < 1 mg/m^3 corroborating with previous studies mainly in the pelagic zone. Nevertheless, the nearshore and river mouth regions have shown a higher concentration of Chl-a 1-12.5 mg/m^3.

Third, both the SD results from Lee15 and Chl-a from NASA's OC4E Chl-a algorithm were used as input for the modification of a TSI scheme by Carlson (1977). The yearly average TSI was about 31 for both SD and Chl-a derived TSI in the annual analysis and 30 for the monthly analysis demonstrating that Lake Malawi is oligotrophic. The spatial distribution of the trophic levels was progressive from the nearshore to the inner lake. Nearshore regions and close

to the river mouths showed eutrophic and hypereutrophic water areas. Based on studies from Carlson (1991) and Carlson and Havens (2005) the deviations of the TSI results from SD and Chl-a were analyzed. The deviation analysis indicated that algae was a key factor influencing the light attenuation in the pelagic zone and the nearshore was influenced by non-algae particles. The monthly deviation results also showed that TSI (Chl-a) ≈ TSI (SD) (see Fig. 29a). In the oligotrophic level, the deviations show that on average TSI (Chl-a) < TSI (SD) in January, April, June, and December, TSI (Chl-a) > TSI (SD) in August and October and TSI (Chl-a) ≈ TSI (SD) for the remaining months. In the mesotrophic deviations, results showed that TSI (Chl-a) < TSI (SD) in March, May, July, August and November and the remaining months TSI (Chl-a) ≈ TSI (SD). The eutrophic deviations showed that from May to December except for July, TSI (Chl-a) < TSI (SD) and the remaining months TSI (Chl-a) ≈ TSI (SD). The hypereutrophic level indicated that TSI (Chl-a) < TSI (SD) through the year.

The results presented here provide good foundation for further investigation on the limiting factors in the eutrophic and hypereutrophic waters of Lake Malawi. This is the first analysis to provide an overall and comprehensive assessment of water quality status and spatiotemporal variation in Lake Malawi by combining remote sensing data, and semi-analytical algorithms.

Nevertheless, some limitations were found throughout the study: (1) small size of the measured SD data for validation, and (2) lack of measured Chl-a for validation of estimated Chl-a. Based on the limitations, future studies should be carried out by increasing the sample size with SD data range covering a wider range, investigate the performance of C2R processor over OLCI data and find appropriate mechanisms to validate the results from the TSI.

Acknowledgement

I would like to express my gratitude to my academic advisor Professor Bunkei Matsushita for all his guidance, and support throughout my study period. His suggestions and comments enabled me to carry out this study.

Special thanks go to Professor Takehiko Fukushima, Professor Kenlo Nasahara, and Professor Hiroaki Kato for accepting to be my referee and part of my reading committee.

I thank all my friends and members of the Water Environment Laboratory – the University of Tsukuba for their support and assistance during my research. I thank Rossi Hamzah, Jiang Dalin, and Fajar Setiawan for our fruitful discussions.

My gratitude goes to my parents for everything they have done for me, their support and encouragement. I would also like to thank my brothers for their support, all my friends who have also supported me directly and indirectly especially, Narciso Lumbela, Shaka Francis, Alex Aguacheiro, and Placido Monteiro.

Thanks are due to my government through my employer the Pedagogical University of Mozambique - Nampula for allowing me to pursue my studies.

I thank Dr. Mangaliso Gondwe for providing me with part of the in situ data, Dr. António Pegado and his team in Mozambique for supporting me in the data collection, Mr. Titus Phiri and his team for their guidance and support during fieldwork in Malawi.

I would like to say thanks to my wife Estrela Muchiguere, and children Alden Vundo and Yasmin Vundo for being there whenever I needed and even when I did not need, the people who have abdicated their lives to live my life.

I would like to thank the Japanese Government through the Ministry of Education, Culture, Sports, Science, and Technology for the opportunity given to study in Japan.

Reference

Adamovich, B. V., Zhukova, T. V., Mikheeva, T. M., Kovalevskaya, R. Z., Luk'yanova, E. V. 2016. Long-term variations of the trophic state index in the Narochanskie Lakes and its relation with the major hydroecological variables. *Water Resources*. 43:5. 809-817.

Alikas, K., Kratzer, S. 2017. Improved retrieval of Secchi depth for optically-complex waters using remote sensing data. *Ecolog. Indicators*. 77. 218-227.

Bailey, S.W., Werdell, P. J. 2006. A multi-sensor approach for the on-orbit validation of ocean color satellite data products. *Remote Sens. Environ*. 102. 12-23.

Ballatore, T. J., Bradt, S. R., Olaka, L., Cózar, A., Loiselle, S.A. 2014. Remote Sensing of African Lakes: A Review. In Remote Sensing of the African Seas; Barale, V., Gade, M., Eds.; *Springer:* Dordrecht, The Netherlands, 2014; Chapter 20; 403-422.

Bekteshi, A., Cupi, A. 2014. Use of trophic state index (Carlson, 1977) for assessment of trophic status of the Shkodra lake. *J. Environ. Protec. Ecol.* 15:1. 359-365.

Bennett, E. M., Carpenter, S. R., Caraco, N. F. 2001. Human Impact on Erodable Phosphorus and Eutrophication: A Global Perspective. *BioScience.* 51: 227-232.

Bootsma, H. A., Hecky, R. E. 1993. Conservation of the African Great Lakes: A limnological Perspective. *Conserv. Biology*. 7. 3.

Bootsma, H. A., Hecky, R. E., Johnson, T. C., Kling, H. J., Mwita, J. 2003. Inputs, outputs, and internal cycling of silica in a large, tropical lake. J. *Great Lakes Res.* 29 (Supp. 2). 121-138.

Bootsma, H., Jorgensen, S.E. Lake Malawi/Nyasa. Experiences and Lessons Learned Brief. Available online: http://www.worldlakes.org/uploads/16_lake_malawi_nyasa_27february2006.pdf (accessed on 21 January 2019).

Carlson, R. E. 1977. A trophic state index for lakes. *Limnology and Oceanography*, 22:2. 361-369.

Carlson, R. E. 1991. Expanding the Trophic State Concept to Identify Non-Nutrient Limited Lakes and Reservoirs. In: Carpenter, L., Ed., Proceedings of a National Conference on Enhancing the States' Lake Management Programs, *North American Lake Management Society*, Chicago, 59-71.

Carlson, R. E., Havens, K. E. 2005. Simple Graphical Methods for the Interpretation of Relationships Between Trophic State Variables, *Lake and Reser. Manage*, 21:1, 107-118.

Cunha, D. G. F., Calijuri, M. do C. 2011. Limiting factors for phytoplankton growth in subtropical reservoirs: the effect of light and nutrient availability in different longitudinal compartments, *Lake and Reser. Manage*, 27:2, 162-172.

Cunha, D. G. F., Calijuri, M.L., Lamparelli, M.C. 2013. A trophic state index for tropical/subtropical reservoirs (TSItsr): *Ecological Engineering*, 60, 126-134.

Chavula, G., Brezonik, P., Thenkabail, P., Johnson, T., Bauer, M. 2009. Estimating chlorophyll concentration in Lake Malawi from MODIS satellite imagery. *Phys. Chem. Earth* 34,755-760.

Cheng, K. S., Lei, T. C. 2001. Reservoir Trophic State Evaluation using Landsat TM Images: *J. Ameri. Water Res. Assoc*, 37, 1321-1334.

Dardeau, M. R., R. F. Mode In, W. W. E. Schroeder, and J. J. Stout. 1992. Estuaries. In: C. T. Hackney, S. M. Adams, and W. H. Martin (eds.). Biodiversity of the southeastern United States: *Aquatic communities*. John Wiley and Sons Inc., New York, p.615-744.

Doerffer, R., H, Schiller. 2007. The MERIS Case 2 Water Algorithm. *Intern. J. Remote Sens*. 28, 3-4.

Doerffer, R., Schiller, H. Algorithm Theoretical Basis Document (ATBD). 2008. MERIS Regional Coastal and Lake Case 2 Water Project Atmospheric Correction ATBD. GKSS Research Center: Geesthacht, Germany,

Doerffer, R., Brockmann, C. 2014. Consensus Case 2 Regional Algorithm Protocols. Technical Report; Brockmann Consult: Geesthacht, Germany.

Doron, M., Babin, M., Mangin, A., Hembise, O. 2007. Estimation of light penetration, and horizontal and vertical visibility in oceanic and coastal waters from surface reflectance. *J. Geophys. Res.* 112, C06003.

Doron, M., Babin, M., Hembise, O., Mangin, A., Garnesson, P. 2011. Ocean transparency from space: validation of algorithms using MERIS, MODIS and SeaWiFS data. *Remote Sens. Environ.* 115, 2986-3001.

Duan, H., Zhang, Y., Zhang, B., Song, K., Wang, Z. 2007. Assessment of Chlorophyll-a Concentration and Trophic State for Lake Chagan Using Landsat TM and Field Spectral Data. *Environ. Monit. Assess.* 129, 295–308.

Dube, T., Mutanga, O., Seutloali, K., Adelabu. S., Shoko, C. 2015. Water quality monitoring in Sub-Saharan African lakes: a review of remote sensing applications. *Afr. J. Aquat. Scine.* 40, 1-7.

Duntley, S. Q. 1952. The visibility of submerged objects; Visibility Lab., Mass. Inst. Tech. San Diego, CA, USA.74.

Fukushima, T., Matsushita, B., Oyama, Y., Yoshimura, K., Yang, W., Terrel, M., Kawamura, S., Takegahara, A. 2016. Semi-analytical prediction of Secchi depth using remote sensing reflectance for lakes with a wide range of turbidity. *Hydrobiologia*. 780, 5-20.

Gilerson, A. A., Gitelson, A. A., Zhou, J., Gulrin, D., Moses, W., Ioannou, I., Ahmed, S. 2010. Algorithms for remote sensing of chlorophyll-a in coastal and inland waters using red and near infrared bands. *Opt. Express.* 18, 24109-24125.

Gitelson, A. A., Dall'Olmo, G., Moses, W., Rundquist, D. C., Barrow, T., Fisher, T. R., Gurlin, D., Holz, J. 2008. A simple semi-analytical model for remote estimation of chlorophyll-a in turbid waters: Validation. *Remote Sens. Environ. 112*, 3582-3593.

Gitelson, A. A., Gurlin, D., Moses, W. J., Yacobi, Y. Z. 2011. Remote estimation of chlorophyll-*a* concentration in inland, estuarine and coastal waters. In: Weng Q, editor. *Advances in Environ. Remote Sensing.* CRC Press.

Gondwe, M. J. G. S. 2009. Environmental impacts of cage aquaculture in the southeast arm of Lake Malawi: water and sediment quality and food web changes. Ph.D. Thesis, University of Waterloo, Waterloo, ON, Canada.

Gondwe, M. J. S., Guildford, S. J., Hecky, R. E. 2011. Physical-chemical measurements in the water column along a transect through a tilapia cage fish farm in Lake Malawi, Africa. *J. Great Lakes Res.* 37,102- 113.

Gordon, H. R., Menghua, W. 1994. Retrieval of Water-Leaving Radiance and Aerosol Optical Thickness over the Oceans with SeaWiFS: A Preliminary Algorithm. *Appl. Optics.* 33,443-52.

Guildford, S. J., Hecky, R. E. 2000. Total nitrogen, total phosphorus, and nutrient limitation in lakes and oceans: Is there a common relationship? *Limnol. Oceanography*. 45, 1213-1223.

Haddeland et al. 2014. Global water resources affected by human interventions and climate change. *PNAS*. 111, 3251-3256.

Hamblin, P. F., Bootsma, H. A., Hecky, R. E. 2003. Modeling Nutrient Upwelling in Lake Malawi/Nyasa. *J. Great Lakes Res.* 29 (Suppl 2): 34-47.

Hecky, R. E., Bootsma, H. A., Kingdon, M. L. 2003. Impact of Land Use on Sediment and Nutrient Yields to Lake Malawi/Nyasa (Africa). *J. Great Lakes Res*. 29 (Suppl. 2), 139-158.

Hu, C., Lee, Z., Franz, B. 2012.Chlorophyll-a algorithm for oligotrophic oceans: A novel approach based on three-band reflectance difference, *J. Geophys. Res*.

IOCCG. 2006. "Remote Sensing of Inherent Optical Properties: Fundamentals, Tests of Algorithms, and Applications. Lee, Z. P. (ed.), Reports of the International Ocean-Colour Coordinating Group, No. 5". Dartmouth, Canada.

International Ocean-Colour Coordinating Group (IOCCG) Available online:http://ioccg.org/resources/missions-instruments/historical-ocean-colour-sensors/ (accessed 3 October 2018).

Jaelani, L. M., Matsushita, B., Yang, W., Fukushima, T. 2013. Evaluation of four MERIS atmospheric correction algorithms in Lake Kasumigaura, Japan. *Intern. J. Remote Sens*. 34, 8967-8985.

Jarosiewicz, A., Ficek, D., Zapadka, T. 2011. Eutrophication variables and Carlson-type trophic state indices in selected Pomeranian lakes, *Limnol. Rev.* 11: 1, 15-23.

Kiefer, I., Odermatt, D., Anneville, O., Wüest, A., Bouffard, D. 2015. Application of remote sensing for the optimization of in-situ sampling for monitoring of phytoplankton abundance in a large lake, *Scien. Total Environ*, 493-506.

Koponen, S., Ruiz-Verdu, A., Heege, T., Heblinski, J., Sorensen, K., Kallio, K., Pyhälahti, T., Doerffer, R., Brockmann, C., Peters, M. 2008. Development of MERIS Lake Water Algorithms Validation Report. ESRIN: Frascati, Italy.

Kratzer, S., Brockmann, C., Moore, G. 2008. Using MERIS full resolution data (300 m spatial resolution) to monitor coastal waters-a case study from Himmerfjärden, a fjord like bay in the North-western Baltic Sea. *Remote Sens. Environ*. 112, 2284-2300.

Lamparelli, M. C. 2004. Trophic Status in Sao Paulo State Water Bodies Evaluation of Monitoring Methodologies. Thesis (Doctoral). Universidade de Sao Paulo (USP). São Paulo (BR).

Lee, Z., Carder, K. L., Arnone, R. A. 2002. Deriving inherent optical properties from water color: a multiband quasi-analytical algorithm for optically deep waters. *Appl. Opt*, 41, 5755-5772.

Lee, Z. P., Carder, K., Arnone, R. 2009. Quasi-Analytical Algorithm (Chapter 10: updated in March 2009 and November 2014 http://www.ioccg.org/groups/software.html.

Lee, Z. P., Hu, C., Shang, S., Du, K., Lewis, M., Arnone, R., Brewin, R. 2013. Penetration of UV-visible solar light in the global oceans: Insights from ocean color remote sensing. *J. Geophys. Res.* 118, 4241-4255.

Lee, Z. P., Shang, S., Hu, C., Du, K. P., Weidemann, A., Hou, W., Lin, J., Lin, G. 2015. Secchi disk depth: a new

theory and mechanistic model for underwater visibility. *Remote Sens. Environ.* 169, 139-149.

Lee, Z., Shang, S., Qi, L., Yan, J., Lin, G. 2016. A semi-analytical scheme to estimate Secchi disk depth from Landsat-8 measurements. *Remote Sens. Environ*. 177,101-106.

Lee, Z., Shang, S., Du, K., Wei, J. 2018. Resolving the long-standing puzzles about the observed Secchi depth relations. *Limnol. Oceanogr*. 63, 2321-2336

Lehner, B., Döll, P. 2004. Development and validation of a global database of lakes, reservoirs and wetlands. *J. Hydrol.* 296, 1-22.

Lillesand, T. M., Johnson, W. L., Deuell, R. L., Lindstrom, O. M., Meisner, D. E. 1983. Use of Landsat Data to Predict the Trophic State of Minnesota Lakes.

Loisel, H., Meriaux, X., Berthon, J. F., Poteau, A. 2007. Investigation of the optical backscattering to scattering ratio of marine particles in relation to their biogeochemical composition in the eastern English Channel and southern North Sea. *Limnol Oceanogr*. 52, 739-752.

Macuiane, M., Hecky, R., Guildford, S. 2016. Temporal and Spatial Changes in Water Quality in Lake Malawi/Niassa, Africa: Implications for Cage Aquaculture Management. *Ocean & fish. Open Access J.* 1, 555552.

Mamun, Md., An, K. G. 2017. Major nutrients and chlorophyll dynamics in Korean agricultural reservoirs along with an analysis of trophic state index deviation. *J. Asia-Pacific Biodi*. 10, 183-191.

Matthews, M.W., Bernard, S., Winter, K. 2010. Remote sensing of cyanobacteria-dominant algal blooms and water quality variables in Zeekoevlei, a small hypertrophic lake, using MERIS. *Remote Sens. Environ.* 114, 2070-2087.

Membrillo-Abad, A. S., Torres-Vera, M. A., Alcocer, J., Prol-Ledesma, R. M., Oseguera, L. A., Ruiz-Armenta, J. R. 2016. Trophic State Index estimation from remote sensing of lake Chapala, Mexico. *Revista Mexicana de Ciencias Geologicas*. 33, 183-191

MERCI. Available online: http://merisfrs-merci-ds.eo.esa.int/merci (accessed on 17 March 2016).

Mouw, C. B., Greb, S., Aurin, D., Digiacomo, P.M., Lee, Z., Twardowski, M., Binding, C., Hu, C., Ma, R., Moore, T., et al. 2015. Aquatic color radiometry remote sensing of coastal and inland waters: Challenges and recommendations for future satellite missions. *Remote. Sens. Environ.* 160, 15-30.

Munthali, M.S. 1997. Dwindling food-fish species and fishers' preference: problems of conserving Lake Malawi's biodiversity. *Biodiver. Conser*. 6, 253-261.

McCullough, G. K., Barber, D., Cooley, P. M. 2007. The Vertical Distribution of Runoff and its Suspended Load in Lake Malawi, Internat. *Assoc. Great Lakes Res*. 33, 449-465.

Nawrocka, L., Kobos, J. 2011. The trophic state of the Vistula Lagoon: an assessment based on selected biotic and abiotic variables according to the water frame-work directive, *Oceanologia,* 53: 3. 881-894.

Nechad, B., Ruddick, K. G., Park, Y. 2010. Calibration and validation of a generic multisensor algorithm for mapping of total suspended matter in turbid waters. *Remote Sens. Environ.* 114, 854-866.

Nicholson, S. E., Klotter, D., Chavula, G. 2014. A detailed rainfall climatology for Malawi, Southern Africa. *Int. J. Climatol.* 34, 315–325.

Ndungu, J., Augustijn, D. C. M., Hulscher, S. J. M. H., Kitaka, N., Mathooko, J. 2013. Spatio-temporal variations in the trophic status of Lake Naivasha, Kenya. *Lakes and Reservoirs: Res. Manag*, 18, 317-328.

Odermatt, D., Danne, O., Philipson, P., Brockmann, C. 2018. Diversity II water quality variables for 300 lakes worldwide from ENVISAT (2002-2012) *Earth Syst. Sci. Data*. 10, 1527-1549.

OECD. 1982. Eutrophication of waters: monitoring, assessment and control. Paris: Technical Report, Environmental Directorate, OECD: Paris, France, 147.

O'Reilly, J. E., Maritorena, S., Mitchell, B.G., Siegel, D.A., Carder, K.L., Garver, S.A., Kahru, M., Mcclain, C.1998. Ocean color chlorophyll algorithms for SeaWiFS. *J. Geophys. Res.* 103, 937-953.

Otu, M. K., Ramlal, P., Wilkinson, P., Hall, R.I., Hecky, R.E. 2011. Paleolimnological evidence of the effects of recent cultural eutrophication during the last 200 years in Lake Malawi, East Africa. *J. Great. Lakes. Res. 37*. 61-74.

Pomari, J., Kane, D. D., Nogueira, M. G. 2018. Application of multiple-use indices to assess reservoirs water quality and the use of plankton community data for biomonitoring purposes. *Int J Hydro*. 2(2):168–179.

Pope, R. M., Fry, E. S. 1997. Absorption spectrum (380-700 nm) of pure water. II. Integrating cavity measurements. *Applied optics*. *36*(33). 8710-8723.

Preisendorfer, R.W. 1986. Secchi disk science: Visual optics of natural waters. *Limnol. Oceanogr*. 31, 909-926.

Rawson, D. S. 1956. Algal indicator of trophic lake types, *Limnol. Oceanogr.* 1, 18-25

Rodrigues, T., Alcântara, E., Watanabe, F., Imai, N. 2017. Retrieval of Secchi disk depth from a reservoir using a semi-analytical scheme. *Remote Sens. Environ* .198, 213-228.

Salas, H. J., Martino, P. 1991. A simplified phosphorus trophic state model for warm-water tropical lakes. *Wat. Res.* 25,341-350.

Saluja, R., Garg, J. K. 2017. Trophic state assessment of Bhindawas Lake, Haryana, India. Environ. *Monit. Assess.* 189:32.

Secchi, P. A. 1864. Relazione delle esperienze fatte a bordo della pontificia pirocorvetta Imacolata Concezione per determinare la trasparenza del mare. In Il Nuovo Cimento Giornale de Fisica, Chimica e Storia Naturale. G. B. Paravia:Torino, Italy. 20, 205-237.

Schultheiß, R., Wilke, T., Jørgensen, A., Albrecht, C. 2011. The birth of an endemic species flock: demographic history of the Bellamya group (Gastropoda, Viviparidae) in Lake Malawi. *Biological Journal of the Linnean Society.* 102, 130-143.

Sheela, A. M., Letha, J., Joseph, S., Ramachandra, K.K., Sanalkumar, S.P. 2011. Trophic state index of a lake system using IRS (P6-LISS III) satellite imagery. *Environ. Monit. Assess.* 177, 575-592.

Sługocki, Ł., Czerniawski, R. 2018. Trophic state (TSI_{SD}) and mixing type significantly influence pelagic zooplankton biodiversity in temperate lakes (NW Poland). PeerJ. 6, e5731.

Snoeks, J. 2000. How well known is the ichthyodiversity of the large East African lakes? *Adv. Ecol. Res*. 31, 17-38.

Steissberg, T., Schladow, G., Hook, J.S. 2010. Monitoring Past, Present, and Future Water Quality Using Remote Sensing. Final Project Report Southern Nevada Public Lands Management Act Lake Tahoe Environmental

Improvement Program.

Stramska, M., Stramski, D., Mitchell, B. G., Mobley, C.D. 2000. Estimation of the absorption and backscattering coefficients from in-water radiometric measurements. *Limnol. Oceanogr*. 45, 628-641.

Thompson, B. A., Allison, H. E., Ngatunga P. Ben. 1996. Distribution and breeding biology of offshore cichlids in Lake Malawi/ Niassa. *Enviro. Biol. Fishes.* 41, 235-254.

Tyler, J. E. 1968. The secchi disc. *Limnol. Oceanogr.* 13, 1-6.

Twardowski, M. S., Boss, E., Macdonald, J. B., Pegau, W.S., Barnard, A. H., Zaneveld, J. R. V. 2001. A model for estimating bulk refractive index from the optical backscattering ratio and the implications for understanding particle composition in case I and case II waters. *J. Geophys. Res. Oceans* **.** 106, 14129-14142.

Wang, S., Li, J., Zhang, B., Spyrakos, E., Tyler, A. N., Shen, Q., Zhang, F., Kuster, T., Lehmann, M. K., Wu, Y., Peng, D. 2018. Trophic state assessment of global inland waters using a MODIS-derived Forel-Ule index. *Remote Sens. Environ.* 217. 444-460.

Watanabe, F. S. Y., Alcântara, E., Rodrigues, T. W. P., Imai, N. N., Barbosa, C. C. F., Rotta, L. H. da S. 2015. Estimation of Chlorophyll-a Concentration and the Trophic State of the Barra Bonita Hydroelectric Reservoir Using OLI/Landsat-8 Images. *Int. J. Environ. Res. Public Health.* 12, 10391-10417.

Wernand, M. 2010. On the history of the Secchi disc. *J. Eur.Opt. Soc. Rapid Publ*. 5, 10013.

Weyl, O. L. F., Ribbink, A. J., Tweddle, D. 2010. Lake Malawi: fishes, fisheries, biodiversity, health and habitat, *Aquat. Ecosyst. Health & Manag.*13, 241-254.

World Bank Climate Portal. Available online: http://sdwebx.worldbank.org/climateportal (accessed 19 June 2017)

Yang, W., Matsushita, B., Chen, J., Fukushima, T. 2011. Estimating constituent concentrations in case II waters from MERIS satellite data by semi-analytical model optimizing and look-up Tables. *Remote Sens. Environ. 115*, 1247-1259.

Yang, W., Matsushita, B., Chen, J., Yoshimura, K., Fukushima, T. 2013. Retrieval of Inherent Optical Properties for Turbid Inland Waters From Remote-Sensing Reflectance. *IEEE Transactions on Geoscience and Remote Sensing*, 51 (6) (June): 3761–3773.

Zhang, X., Hu, L., He, M. X. 2009. Scattering by pure seawater: effect of salinity. *Opt. Express*, 17, 5698-5710.